

**POSITION/FORCE CONTROL OF ROBOT
MANIPULATORS**

MEHMET İSMET CAN DEDE

APRIL 2003

POSITION/FORCE CONTROL OF ROBOT MANIPULATORS

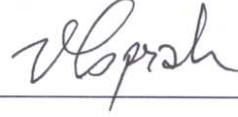
A THESIS SUBMITTED TO
THE GRADUATE SCHOOL OF NATURAL AND APPLIED SCIENCES
OF THE MIDDLE EAST TECHNICAL UNIVERSITY

BY
MEHMET İSMET CAN DEDE

IN PARTIAL FULFILLMENT OF THE REQUIREMENTS FOR THE DEGREE OF
MASTER OF SCIENCE
IN
THE DEPARTMENT OF MECHANICAL ENGINEERING

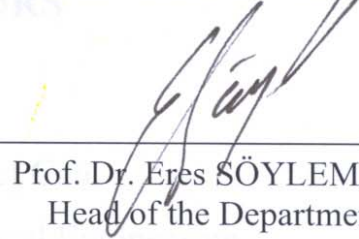
APRIL 2003

Approval of the Graduate School of Natural and Applied Sciences



Prof. Dr. Tayfur ÖZTÜRK
Director

I certify that this thesis satisfies all the requirement as a thesis for the degree of Master of Science.



Prof. Dr. Eres SÖYLEMEZ
Head of the Department

We certificate that we have read this thesis and that in our opinion it is fully adequate, in scope and quality, as a thesis for degree of Master of Science.



Prof. Dr. M. Kemal ÖZGÖREN
Supervisor

Examining Committee Member

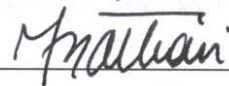
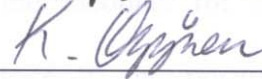
Prof. Dr. Reşit SOYLU

Prof. Dr. M. Kemal ÖZGÖREN

Prof. Dr. Tuna BALKAN

Prof. Dr. Kemal İDER

İlhan BAŞÇUHADAR, MSc. Mech. Eng.



ABSTRACT

POSITION/FORCE CONTROL OF ROBOT MANIPULATORS

DEDE, Mehmet İsmet Can
M.Sc., Department of Mechanical Engineering
Supervisor: Prof. Dr. M. Kemal ÖZGÖREN

April 2003, 112 Pages,

The purpose of this thesis is to investigate the existing position/force algorithms showing their differences, advantages and disadvantages by means of several simulations. Also, as a secondary purpose, inverse kinematics will be used to increase the efficiency of the algorithms for inverse of the Jacobian for the transformation from the Cartesian Space to the Joint Space in the position controllers.

The position/force control algorithms discussed in the thesis are stiffness control, impedance control, admittance control, hybrid position/force control, hybrid impedance control, explicit force control, implicit force control and their variations.

The existing algorithms are applied to a PUMA 560 (6R) manipulator with rigid joints developed in the Matlab[®] Simulink environment. Also, the constraint surface that the manipulator is to apply a force and/or a moment on, is developed in the same environment.

Selected tasks are performed using each algorithm. Utilizing the responses of each algorithm for the same task, a comparison between them can be done. Also by further investigation on the algorithms and using these algorithms on different tasks, certain control algorithms are addressed to certain tasks.

Keywords: Puma 560, Position/Force Control Algorithms, Stiffness Control, Impedance Control, Admittance Control, Hybrid Position/Force Control, Hybrid Impedance Control, Explicit Force Control, Implicit Force Control.

ÖZ

**ROBOT MANİPÜLATÖRLERİNİN KONUM/KUVVET
KONTROLU**

DEDE, Mehmet İsmet Can

Yüksek Lisans, Makine Mühendisliği Bölümü

Tez Yöneticisi : Prof. Dr. M. Kemal ÖZGÖREN

Nisan 2003, 112 Sayfa

Bu tezin amacı, kullanılagelen konum/kuvvet kontrolü algoritmalarının birbirlerine göre farklılıklarını, avantajlarını ve dezavantajlarını çeşitli benzetimler aracılığı ile göstererek incelemektir. Ayrıca, ikincil bir amaç olarak, konum denetimicisinde Kartezyen Uzaydan Eklem Uzayına dönüştürmelerde Jacobian'ın tersi yerine ters kinematik kullanılmasıyla algoritmaların daha iyi çalışması sağlanacaktır.

Bu tezde sertlik kontrolü, empedans kontrolü, admitans kontrolü, konum/kuvvet karma kontrolü, empedans karma kontrolü, açık kuvvet kontrolü, kapalı kuvvet kontrolü ve bu kontrollerin türevleri tartışılmıştır.

Kullanılagelen kontrol algoritmaları, Matlab® Simulink ortamında oluşturulan rijid eklemlili bir Puma 560 (6R) manipulatöründe uygulanmıştır. Ayrıca manipulatörün kuvvet ve/veya moment uygulayacağı kısıtlayıcı yüzey de aynı ortamda oluşturulmuştur.

Bütün kontrol algoritmaları seçilmiş görevler için kullanılmıştır. Aynı görevi yapan değişik kontrol algoritmalarının çıkardığı sonuçlar kullanılarak aralarında bir karşılaştırma yapılabilmektedir. Ayrıca bu algoritmalar üzerinde daha fazla incelemeler ve değişik görevlerde algoritmaların kullanımlarıyla adı geçen kontrol algoritmalarının hangisinin hangi görevler için en uygun olduğu önerilmiştir.

Anahtar Kelimeler: Konum/Kuvvet Kontrolü Algoritmaları, Sertlik Kontrolü, Empedans Kontrolü, Admitans Kontrolü, Konum/Kuvvet Karma Kontrolü, Empedans Karma Kontrolü, Kapalı Kuvvet Kontrolü, Açık Kuvvet Kontrolü.

ACKNOWLEDGEMENTS

I wish to express my deepest gratitude and appreciation to my supervisor Prof Dr. M. Kemal Özgören, for his never-ending faith in me, for his encouragement and guidance throughout this thesis.

I would also like to thank my parents and Miss Merve Kundakçı for their continuous support and help. Last but not the least, I would like to thank my colleagues in ASELSAN Inc. for always being understanding and always being ready for help.

TABLE OF CONTENTS

ABSTRACT.....	iii
ÖZET.....	v
ACKNOWLEDGMENT.....	vii
TABLE OF CONTENTS.....	viii
LIST OF FIGURES.....	x
LIST OF TABLES	xvi
NOMENCLATURE.....	xvii

CHAPTERS

1. INTRODUCTION.....	1
2. LITERATURE SURVEY.....	6
3. POSITION/FORCE CONTROL ALGORITHMS.....	10
3.1 Stiffness control.....	10
3.2 Impedance control.....	13
3.3 Admittance control.....	17
3.4 Hybrid position/force control.....	19
3.5 Hybrid impedance control.....	23
4. SYSTEM MODELING.....	25
4.1 Manipulator model	25

4.1.1 Kinematic equations of the manipulator.....	26
4.1.2 Dynamic properties of the manipulator.....	31
4.1.3 Modeling the manipulator with Simmechanics blockset.....	34
4.2 Compliant environment modeling.....	44
5. SIMULATION RESULTS.....	46
5.1 Stiffness control simulation results.....	49
5.2 Impedance control simulation results... ..	65
5.3 Admittance control simulation results.....	76
5.4 Hybrid position/force control simulation results.....	87
6. DISCUSSIONS AND CONCLUSIONS.....	96
REFERENCES.....	99
APPENDICES	
A. DYNAMIC PROPERTIES OF THE LINKS.....	103
B. FEEDFORWARD COMPENSATION AND MASS MATRIX EQUATIONS.....	109

LIST OF FIGURES

FIGURES

3.1 Basic principle of active stiffness control.....	11
3.2 Basic impedance control.....	14
3.3 Position-based second order impedance control.....	16
3.4 Admittance control.....	18
3.5 Conceptional organization of hybrid position/force control.....	20
3.6 Explicit force control.....	22
3.7 Implicit force control.....	22
3.8 Hybrid impedance control.....	23
4.1 General sketch of the PUMA 560.....	25
4.2 PUMA manipulator with its assigned coordinate frames.....	26
4.3 A detailed schematical representation of the PUMA 560.....	33
4.4 A link composition of the manipulator created in Simmechanics.....	34
4.5 “Body” block parameter window.....	35
4.6 “Revolute Joint” block parameter window.....	36
4.7 “Joint Actuator” block parameter window.....	37
4.8 “Joint Sensor” block parameter window.....	38
4.9 “Body Sensor” block parameter window.....	39
4.10 “Joint Initial Condition” block parameter window.....	40

4.11 “Goto” block parameter window.....	41
4.12 “From” block parameter window.....	42
4.13 “PMC_port” block parameter window.....	42
4.14 “Ground” block parameter window.....	43
5.1 Continuous planar surface.....	47
5.2 Discontinuous planar surface.....	47
5.3 Modified stiffness control algorithm.....	49
5.4 End-effector position in \vec{u}_1^0 axis following a straight line on a planar surface.....	52
5.5 End-effector position in \vec{u}_2^0 axis following a straight line on a planar surface.....	53
5.6 End-effector position in \vec{u}_3^0 axis following a straight line on a planar surface.....	54
5.7 Force applied by the end-effector to the environment along \vec{u}_1^0 axis following a straight line on a planar surface.....	55
5.8 End-effector position in \vec{u}_1^0 axis following a circle path on a planar surface.....	56
5.9 End-effector position in \vec{u}_2^0 axis following a circle path on a planar surface.....	56
5.10 End-effector position in \vec{u}_3^0 axis following a circle path on a planar surface.....	57
5.11 Force applied by the end-effector to the environment along \vec{u}_1^0 axis following a circle path on a planar surface.....	57
5.12 Circle path followed by the end-effector on the surface ($k_F = 0.0001$).....	58
5.13 Circle drawn by the end-effector on the surface ($k_F = 0.0001$).....	59

5.14 End-effector position in \vec{u}_1^0 axis following a circle path on a discontinuous surface.....	60
5.15 End-effector position in \vec{u}_2^0 axis following a circle path on a discontinuous surface.....	61
5.16 End-effector position in \vec{u}_3^0 axis following a circle path on a discontinuous surface.....	62
5.17 Force applied by the end-effector to the environment along \vec{u}_1^0 axis following a circle path on a discontinuous surface.....	63
5.18 Force applied by the end-effector to the environment along \vec{u}_2^0 axis following a circle path on a discontinuous surface.....	64
5.19 End-effector position in \vec{u}_1^0 axis following a straight line on a planar surface.....	66
5.20 End-effector position in \vec{u}_2^0 axis following a straight line on a planar surface.....	67
5.21 End-effector position in \vec{u}_3^0 axis following a straight line on a planar surface.....	68
5.22 Force applied by the end-effector to the environment along \vec{u}_1^0 axis following a straight line on a planar surface.....	68
5.23 End-effector position in \vec{u}_1^0 axis following a circle path on a planar surface.....	69
5.24 End-effector position in \vec{u}_2^0 axis following a circle path on a planar surface.....	70
5.25 End-effector position in \vec{u}_3^0 axis following a circle path on a planar surface.....	70
5.26 Force applied by the end-effector to the environment along \vec{u}_1^0 axis following a circle path on a planar surface.....	71
5.27 Circle path followed by the end-effector on the surface ($k_F = 0.0001$).....	71

5.28 Circle drawn by the end-effector on the surface ($k_F = 0.0001$).....	72
5.29 End-effector position in \bar{u}_1^0 axis following a circle path on a discontinuous surface.....	73
5.30 End-effector position in \bar{u}_2^0 axis following a circle path on a discontinuous surface.....	74
5.31 End-effector position in \bar{u}_3^0 axis following a circle path on a discontinuous surface.....	74
5.32 Force applied by the end-effector to the environment along \bar{u}_1^0 axis following a circle path on a discontinuous surface.....	75
5.33 Force applied by the end-effector to the environment along \bar{u}_2^0 axis following a circle path on a discontinuous surface.....	75
5.34 End-effector position in \bar{u}_1^0 axis following a straight line on a planar surface.....	76
5.35 End-effector position in \bar{u}_2^0 axis following a straight line on a planar surface.....	77
5.36 End-effector position in \bar{u}_3^0 axis following a straight line on a planar surface.....	78
5.37 Force applied by the end-effector to the environment along \bar{u}_1^0 axis following a straight line on a planar surface.....	78
5.38 End-effector position in \bar{u}_1^0 axis following a circle path on a planar surface.....	79
5.39 End-effector position in \bar{u}_2^0 axis following a circle path on a planar surface.....	79
5.40 End-effector position in \bar{u}_3^0 axis following a circle path on a planar surface.....	80

5.41 Force applied by the end-effector to the environment along \vec{u}_1^0 axis following a circle path on a planar surface.....	80
5.42 Circle path followed by the end-effector on the surface ($k_F = 0.0001$).....	81
5.43 Circle drawn by the end-effector on the surface ($k_F = 0.0001$).....	82
5.44 End-effector position in \vec{u}_1^0 axis following a circle path on a discontinuous surface.....	83
5.45 End-effector position in \vec{u}_2^0 axis following a circle path on a discontinuous surface.....	84
5.46 End-effector position in \vec{u}_3^0 axis following a circle path on a discontinuous surface.....	84
5.47 Force applied by the end-effector to the environment along \vec{u}_1^0 axis following a circle path on a discontinuous surface.....	85
5.48 Force applied by the end-effector to the environment along \vec{u}_2^0 axis following a circle path on a discontinuous surface.....	86
5.49 Modified hybrid position/force control algorithm.....	87
5.50 End-effector position in \vec{u}_1^0 axis following a straight line on a planar surface.....	89
5.51 End-effector position in \vec{u}_2^0 axis following a straight line on a planar surface.....	90
5.52 End-effector position in \vec{u}_3^0 axis following a straight line on a planar surface.....	91
5.53 Force applied by the end-effector to the environment along \vec{u}_1^0 axis following a straight line on a planar surface.....	91
5.54 End-effector position in \vec{u}_1^0 axis following a circle path on a planar surface.....	92

5.55 End-effector position in \bar{u}_2^0 axis following a circle path on a planar surface.....	93
5.56 End-effector position in \bar{u}_3^0 axis following a circle path on a planar surface.....	93
5.57 Force applied by the end-effector to the environment along \bar{u}_1^0 axis following a circle path on a planar surface.....	94
5.58 Circle path followed by the end-effector on the surface ($k_F = 0.0001$).....	94
5.59 Circle drawn by the end-effector on the surface ($k_F = 0.0001$).....	95
A.1 3D representation of the Link 1.....	103
A.2 3D representation of the Link 2.....	104
A.3 3D representation of the Link 3.....	105
A.4 3D representation of the Link 4.....	106
A.5 3D representation of the Link 5.....	107
A.6 3D representation of the Link 6.....	108

LIST OF TABLES

TABLES

4.1 Link coordinate parameters of the PUMA 560 manipulator.....	31
A.1 Dynamic properties of the Link 1.....	103
A.2 Dynamic properties of the Link 2.....	104
A.3 Dynamic properties of the Link 3.....	105
A.4 Dynamic properties of the Link 4.....	106
A.5 Dynamic properties of the Link 5.....	107
A.6 Dynamic properties of the Link 6.....	108

NOMENCLATURE

J	: Jacobian matrix
X_D	: Desired position vector in the task space
\dot{X}_D	: Desired velocity vector in the task space
\ddot{X}_D	: Desired acceleration vector in the task space
X	: End-effector's position vector in the task space
\dot{X}	: End-effector's velocity vector in the task space
ΔX	: End-effector's position error vector
$\Delta\theta$: Joint angle displacement error
τ_p	: Command input vector to joints associated with stiffness control
N	: Nonlinear feedforward compensation vector for gravity, centrifugal and coriolis forces
τ	: Total joint torque/force input vector
X_E	: Position vector of the contacted environment
K_E	: Net stiffness of the sensors and the environment
F	: Resulting contact force/torque vector in the world space
K_p, k_p	: Proportional control gain
k_i	: Integral control gain
K_v, k_v	: Derivative control gain
K_F	: Compliance matrix for modifying the position command

Z_m	: Mechanical impedance
M	: Desired inertia matrix
D	: Desired damping matrix
K	: Desired stiffness matrix
K_{F1}	: Compliance matrix for modifying the position command
K_{F2}	: Compliance matrix for modifying the velocity command
X_F	: Equivalent force-feedback trajectory
X_I	: Modified desired position
\dot{X}_I	: Modified desired velocity
\ddot{X}_I	: Modified desired acceleration
A	: Mechanical admittance matrix
K	: Force compensator
E	: Force error vector
F_D	: Desired force/torque vector
X_c	: Command trajectory in admittance control
S	: Compliance selection matrix
s_j	: Compliance selection matrix variable
τ_{pf}	: Force subspace command torque in hybrid position/force control
τ_{pp}	: Position subspace command torque in hybrid position/force control
Z_{mp}	: Desired impedance for the position subspace of hybrid impedance control
Z_{mf}	: Desired impedance for the force subspace of hybrid impedance control
X_i	: Modified desired trajectory in hybrid impedance control

X_{pi}	: Modified position trajectory expressed in position subspace of hybrid impedance control
X_{fi}	: Modified force trajectory expressed in force subspace of hybrid impedance control
$\{P\}$: Position subspace
$\{F\}$: Force subspace
O_i	: Origin of the coordinate frame i
β_i, α_i	: Twist angle between the axes of the joints i and i+1
d_i, s_i	: Axial offset along the axis of the joint i
b_i, a_i	: Common normal distance between the axes of the joint i and i+1
\bar{u}_i	: i^{th} unit vector
\bar{u}_i	: 3x1 matrix representation corresponding to \bar{u}_i
\tilde{u}_i	: 3x3 cross-product matrix corresponding to \bar{u}_i
$\hat{C}^{(i,i+1)}$: 3x3 transformation matrix representing the orientation of the frame i+1 with respect to the frame i
$e^{\bar{u}_i, \theta}$: 3x3 transformation matrix representing an orientation θ about the axis \bar{u}_i
θ_i	: Angular position of the i^{th} link with respect to the $(i-1)^{\text{th}}$ link
$\bar{p}^{(0)}$: Tip position vector with respect to the world coordinate frame
$\bar{r}^{(0)}$: Wrist position vector with respect to the world coordinate frame
d_p	: Tip point's location with respect to the wrist point along the vector $\bar{u}_3^{(6)}$
$\dot{\bar{q}}$: 6x1 matrix representation corresponding to joint velocities
\hat{J}_p	: 6x6 tip point Jacobian matrix
\hat{J}_r	: 6x6 wrist point Jacobian matrix
\bar{V}_p	: 6x1 matrix representation corresponding to tip point velocity with respect to world coordinate frame
\bar{V}_r	: 6x1 matrix representation corresponding to wrist point velocity with respect to world coordinate frame

- \bar{V}_{pp} : 3x1 matrix representation corresponding to tip point linear velocities with respect to world coordinate frame
 $\bar{\omega}_n$: 3x1 matrix representation corresponding to tip and wrist point angular velocities with respect to world coordinate frame
 \bar{J}_{p_k} : k^{th} link tip point velocity influence coefficient
 \bar{J}_{r_k} : k^{th} link wrist point velocity influence coefficient
 \bar{J}_{a_k} : k^{th} link tip point angular velocity influence coefficient
 O_i^* : Center of the joint between the links i and $i+1$
 C_i : Center of mass of the link i
 \vec{q}_i : Position vector of O_i^* with respect to C_i
 \bar{q}_i : 3x1 matrix representation of \vec{q}_i in the frame i
 \vec{q}_i^* : Position vector of C_i with respect to O_{i-1}^*
 \bar{q}_i^* : 3x1 matrix representation of \vec{q}_i^* in the frame i

CHAPTER 1

INTRODUCTION

Industrial robots, in past years, were used widely in tasks, which required only positional control (point to point control) of the end-effector. The most striking example is in automobile spot-welding where it is important only to ensure that the welding tool is placed correctly. It is not of primary importance to control the path taken by the tool as it passes from weld point to weld point-provided if it does not violate any workspace constraints.

The next most straightforward area of application of robots is those jobs which do require a continuous position control of the end-effector, but which do not require at the same time, the application of any forces to the environment. Typical task of this kind of robot is arc-welding application. In arc-welding, the torch must be controlled accurately in position and orientation but no significant forces exist between the torch and the work-piece.

In recent years, more interest has been focused on a third class of jobs to which robots might effectively be applied. These are jobs in which the robot control system must be capable of accurately positioning and orienting the tool, while at the same time using it to apply a given force/moment pattern to the work-piece.

Applying robot manipulators to a wider class of tasks, it will be necessary to control not only the position of a manipulator but also the force exerted by the end-effector to the environment. Whereas many tasks performed by a robot manipulator require the robot to interact with its environment such as pushing, scraping, deburring, grinding, pounding, polishing, twisting, cutting, excavating, etc. Implementation of all these tasks necessitates that a robot, besides realizing the predisposed position, provides the necessary force to either overcome the resistance from the environment, or comply with environment.

Also the addition of force information in the control of robots increases their adaptability to uncertain environments, such as are found in deburring, grinding, and assembly tasks and provides safety against breakage due to excessive contact forces. Precise control of manipulators in the presence of uncertainties and variations in their environments is a must for feasible application of robot manipulators to complex handling and assembly problems in industry and space. An important step to achieve such control can be possible by providing manipulator hands with sensors that provide information about the progress of interactions with the environment, force/torque sensors.

Most of the automated assembly tasks require the control of contact forces rather than pure position control. Position control is sufficient only in case of exactly positioned work-pieces of well-known shape, a robot of high positioning accuracy and perfect tools. In practical applications, it is often impossible or uneconomic to satisfy these conditions. A force-controlled robot in contrast can cope with uncertainties, tolerances, etc.

Automating assembly tasks reveal a number of difficulties including misalignments and geometric uncertainties, instability, convergence, friction, and the prevention of damage to the robot and its environment. Any time a manipulator contacts with its environment deviations of the positions of objects from their expected locations risks damaging, high interaction forces due to forcing a motion upon a misaligned system. Using force feedback for programmed compliance or a passive compliant device can minimize the risk of damage.

The use of manipulators for assembly tasks requires that the precision with which parts are positioned with respect to one another be quite higher in fact than that available from joint-mounted position sensors attached to imperfectly rigid manipulators driven by imperfectly meshed gears. Manipulators of greater precision can be achieved only at the expense of size, weight, and cost. Measuring and controlling contact forces generated at the hand, offers a low cost alternative for extending effective precision. Since small variations in the relative position generate large contact forces when parts of moderate stiffness interact, knowledge and control of these forces can achieve a tremendous increase in effective positional accuracy.

Another example to the tasks that require position and force control is automated excavation. The task of a backhoe excavator is to free and remove material from its original location and to transfer it to another location by lowering the bucket, digging by dragging the bucket through the soil, then lifting, slewing and dumping the bucket. In automatic excavation, there is a need for the development of a controller that is robust to uncertainties associated with these operations. Excavators are, however, subject to a wide variation of soil-tool interaction forces. When digging, the bucket tip motion is effectively force-constrained by the non-linear constitutive equations of the environment and by the hydraulic forces, where other than pure position control, force regulation is needed.

Currently, the rapid development of scientific technology offers two power tools to improve control performance. The first one is the development of hardware, such as new sensors, more powerful microprocessors, and high performance servo systems. The other one is the development of control techniques and theories.

At the end, robust and reliable operation of manipulators in contact with objects in their environment is the basic requirement for successful execution of many robotic tasks. Stable control of robot environment interaction poses a technically challenging problem and has attracted the attention of several robot control specialists for almost two decades.

In recent years, theoretical research on position/force control has been well studied. Based on the application of the relationship between position/applied force or between velocity/applied force, the control method can be as stiffness control, admittance control, impedance control, explicit force control and hybrid position/force control. Also, to improve the performance of the mentioned basic position/force controls, adaptive, robust and learning algorithms are applied.

The scope of this thesis is to apply the position/force algorithms to a PUMA 560 manipulator performing a certain task where the manipulator exerts forces to the environment. Performing the same tasks, with each control algorithm, the advantages and disadvantages of each control algorithm with respect to one to another will be determined. The tasks that will be performed in the simulation differs significantly to simulate different kinds of real-time tasks. Utilizing these simulation results, certain tasks will be able to be addressed to certain control algorithms in practical robot position/force control. Also, inverse kinematics will be used in transformation from the Cartesian Space to Joint Space instead of inverse of

the Jacobian, as advised in all the algorithms found in the literature, to increase the efficiency of the algorithms.

Following this Introduction Chapter, in Chapter 2, history and brief explanation of the position/force control algorithms are given. In Chapter 3, the formulations of the control algorithms to be applied to the PUMA 560 manipulator are exposed. In Chapter 4, the PUMA 560 manipulator to be used in the simulations is presented and also the modeling of the manipulator in Matlab Simulink environment is explained. In Chapter 5, the results of the simulation of each control algorithm are examined and discussed. In Chapter 6, further and final discussions are made on the control algorithms and future works to be carried out are proposed.

CHAPTER 2

LITERATURE SURVEY

Ganwen ZENG and Ahmad HEMAMI [1], classified the robot force control algorithms into 2 main groups as fundamental and advanced force control in “An Overview of Robot Force Control” paper. Fundamental force control algorithms can be categorized based on application of the relationship between position and applied force or between velocity and applied force, or the application of direct force feedback, or their combinations.

Methods involving the relation between position and applied force are the stiffness control by only position feedback and the stiffness control by force feedback corrections as it is stated in [1]. There are mainly two kinds of stiffness control found in the literature of force control. Stiffness control can be either passive or active. Passive stiffness control does not have a control algorithm to control the interaction forces that form between the environment and the end-effector but it has spring and damper compositions on the end-effector to compensate the interaction forces. Passive stiffness control can only be used in very specific tasks where the stiffness of the environment is known and the way of the contact is known for example, handling a peg with a known length and orientation with respect to the hand. Utilizing the knowledge of the stiffness of the environment, suitable mechanical (passive) spring-damper systems can be developed for the end-effector.

Stiffness of the end-effector is controlled in different directions due to the specific task in the active stiffness control. The stiffness of the end-effector depends on the stiffness of the joint servos. Adjusting the stiffness of the servos in the robot joints, desired stiffness of the end-effector can be achieved [2]. Providing the desired stiffness in the selected directions, desired forces can be applied while following the desired position trajectory.

Methods employing the relation between velocity and applied force are impedance control and admittance control (or accommodation control). According to Hogan [3], manipulator control system should be designed not to track a motion trajectory alone, but rather regulate the mechanical impedance of the manipulator where the relationship between the velocity and applied force is referred to as mechanical impedance. Impedance control has been implemented in various forms depending on how the measured signals (velocity, position or force) are used. Basically in the impedance control, sensed forces are multiplied with a gain matrix depending on the mechanical impedance to give rise to the modifications to be made for the position and velocity [1].

Admittance control as impedance control uses the relationship between the velocity and the applied force. But in contrast to impedance control, admittance control focuses more on the force tracking control. Force feedback is main feedback signal for this control [4].

Admittance, impedance and the selected stiffness can vary due to the change in the stiffness of the environment. Stabilizing these controls in the face of changing environments can be possible with adaptive algorithms applied to these controls.

Methods employing the relation directly between position and applied force are hybrid position/force control and hybrid impedance control. Hybrid position/force control combines force and torque information with positional data based on two complementary orthogonal workspaces on displacement and force. These workspaces can be defined as position and force sub-spaces. Due to the task, some of the joints are position controlled which means they form the position sub-space and the others are force controlled which means they form the force sub-space [5]. Different control algorithms can be applied to each sub-space. Utilizing different control algorithms for the sub-spaces, various hybrid position/force control algorithms can be formed.

Hybrid impedance control was proposed by Anderson and Spong [6], who combined impedance control and hybrid position/force control into one strategy. This allows a designer to obtain more flexibility in choosing the desired impedance of the controlled robotic system, which means the impedances in force-controlled and position-controlled subspaces can be chosen independently.

Robots used in complex tasks face many challenging problems, such as unknown parameters, unstructured environments and external disturbances, etc. To achieve a good control performance in the presence of unmodelled dynamics, sensor noise and external disturbances for robot force control more advanced force control algorithms are needed. An advanced method must provide accurate force tracking or perfect task accomplishment in the presence of unknown parameters and uncertainties regarding the robot and environment. Based on the fundamental force control methods, there are many advanced force control techniques, which are classified as adaptive control, robust control and learning control.

The basic objective of adaptive control is to maintain consistent performance of a control system in the presence of unknown parameters in robot and environment [7]. Based on the existing definitions of the fundamental force control methods, a robot adaptive force controller incorporates certain adaptive strategy into a controller in order to maintain the proper desired stiffness, impedance, admittance and so forth when unknown parameters of robot and contact environment exist.

The objective of robust force control is to achieve the target dynamics such as the target impedance, etc, and to preserve the stability robustness in the presence of modeling errors in the robot and in the environment[8]. The design concept of sliding mode is widely used to overcome the difficulty to achieve a robust control. Robust control law is usually built by employing Lyapunov's direct method. Finally, the designed robust control guarantees the achievement of the predefined target dynamics, while preserving stability in the presence of modeling errors.

Learning algorithm is applied to the hybrid position/force control when the robot performs the same task repeatedly, in the literature of robot position and force control [9]. The algorithm utilizes position, velocity and acceleration errors or force error for learning the command input required to perform tasks. It guarantees the convergence of both position and force tracking errors, as well as robustness, for sufficiently small parameter uncertainties and disturbances.

CHAPTER 3

POSITION/FORCE CONTROL ALGORITHMS

3.1 STIFFNESS CONTROL

The stiffness of the end-effector depends on the stiffness of the joints. Adjusting the stiffness of the servos in the robot joints, desired stiffness of the end-effector can be achieved. Therefore, desired force can be applied to the environment while following the desired position trajectory.

Accurate position control of the end-effector needs very stiff servo controllers to be applied around the joints of the manipulator where the servos reject all the disturbances (dynamic forces of the robot itself, external forces, etc.) that may act upon them with the high stiffness of the controllers. Stiffness of the servo depends on the feedback gain. Although, accurate position control requires high stiffness, it is limited by the condition that the servo must not excite unmodelled structural modes of the system. Therefore, a finite stiffness of the servo can be ensured leading to finite stiffness of the robot hand [2].

In conflict with the position control, the force control requires that the system stiffness be as low as possible. This concludes that in order to realize force control, the stiffness of the servo should be decreased. Decreasing the stiffness of the joint servo systems, the end-effector will also behave as having low stiffness, which will enable appropriate force control.

Realizing control tasks which require that the end-effector position has to be controlled in some directions and the force applied by the end-effector must be controlled in other directions, maximal stiffness must be achieved in some directions (those in which its position should be controlled) and minimal stiffness in other directions (those in which force applied by the end-effector has to be controlled). The idea of the stiffness control is to try to control the end-effector stiffness in various directions depending on the specific task. The stiffness of the servos (by adjusting control gains) should be adjusted in order to obtain desired stiffness of the end-effector where the change in the stiffness of the joint servos results as a change in the stiffness of the end-effector. At the end, the stiffness of the end-effector determines the forces to be exerted to the environment by the end-effector. Figure 3.1 shows the basic principle of an active stiffness control.

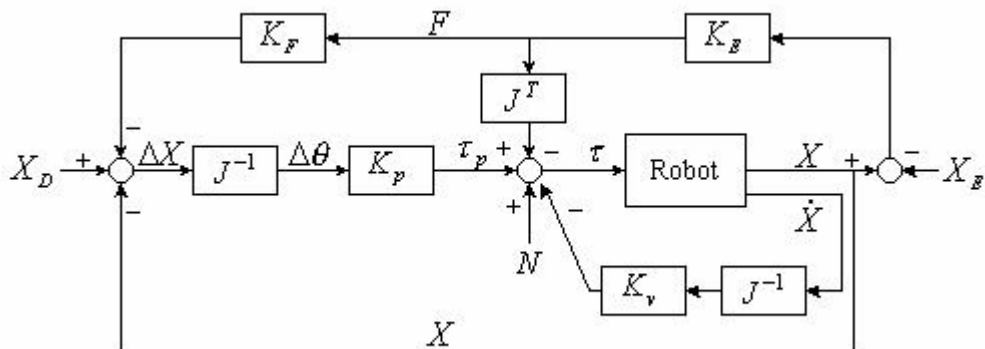


Figure 3.1 Basic principle of active stiffness control

In the figure and in what follows, J is the robot's Jacobian matrix, X_D is the desired position vector in the task space, X and \dot{X} are position and velocity vectors in the task space, ΔX is the position vector error, $\Delta\theta$ is the joint angle displacement vector, τ_p is the vector of command input to joints associated with stiffness control, N is a vector of nonlinear feedforward compensation for gravity and centrifugal and Coriolis forces, τ is the vector of total joint torque/force input, X_E is the position vector of the contacted environment, K_E is the net stiffness of the sensors and environment, and F is the resulting contact force (or torque) vector in the world space. K_p and K_v are the control gains, usually chosen as diagonal matrices, K_F is the compliance matrix for modifying position command. A non-redundant robot in the 3-D space, a PUMA 560 is considered; therefore, the dimension of all the vectors are 6, and that of the matrices are 6 X 6.

The basic system includes a robot and its environment, velocity feedback and nonlinear compensation for linearizing the robot dynamic system. The stiffness control loop comprising a proportional feedback of force and position defines joint torque τ_p of the total joint torque τ due to the contact force. τ_p is thus defined by the following equation

$$\tau_p = K_p \Delta\theta \quad (3.1)$$

The unit of K_F in Figure 3.1 is displacement/force, which is stiffness. Therefore, active stiffness control allows the user to specify arbitrarily the mechanical stiffness of the manipulator by choosing different values for the matrix K_F . As the environment changes, the value of K_F should change to exert the same force on different environments. This could be achieved with an adaptive algorithm.

3.2 IMPEDANCE CONTROL

The objective of impedance control is to establish a desired dynamical relationship between the end-effector position and the applied force. The relationship between the velocity \dot{X} and the applied force F is referred to as the mechanical impedance Z_m . In the frequency domain, this is represented by

$$F(s) = Z_m(s)\dot{X}(s) \quad (3.2)$$

In terms of position $X(s)$, we may write,

$$F(s) = sZ_m(s)X(s) \quad (3.3)$$

Desired impedance can be specified as;

$$sZ_m(s) = Ms^2 + Ds + K \quad (3.4)$$

The constant matrices M , D and K represents the desired inertia, damping and stiffness values, respectively. Typically, as in this case, the target impedance is chosen as a linear second-order system to mimic mass-spring-damper dynamics [10]. It is task of impedance control to guarantee the behavior of the controlled system to be as dictated by equation (3.4). Impedance control has been implemented in various forms, depending on how the measured signals, i.e. velocity, position or force are used. Figure 3.2 shows the structure of a basic impedance control loop, which determines an appropriate value for $Z_m(s)$.

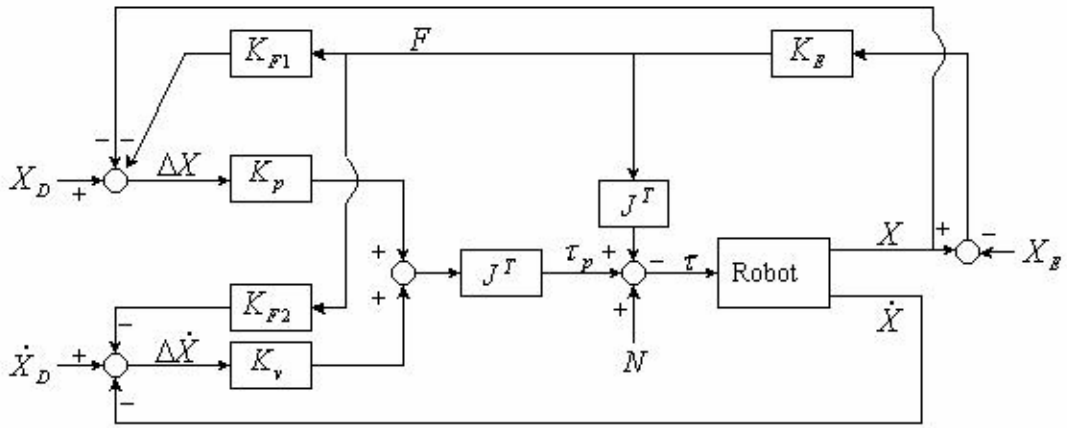


Figure 3.2 Basic impedance control

The position modification results from multiplying the sensed forces by matrix K_{F1} that has the same role as in the stiffness control. The velocity modification results from multiplying the sensed forces by matrix K_{F2} . In the joint space the command force for error correction, thus, is defined by

$$\tau_p = J^T (K_p \Delta X + K_v \Delta \dot{X}) \quad (3.5)$$

In Figure 3.2, the control loop has the effect of modifying the damping constant of the manipulator when it is in contact with the environment. This kind of impedance is called the first order impedance. In the first order impedance control, damping and stiffness of the manipulator are taken into consideration. Stiffness and damping values of the manipulator can be adjusted by changing the K_p and K_v control gains. Zeroth order impedance deals only with the stiffness of the manipulator [11]. This is actually called the stiffness control as discussed before.

Second order impedance control is applied to a position based control system in Figure 3.3, in which X_f represents the equivalent force-feedback trajectory, X_I is the modified desired trajectory defined as the solution to the differential equation

$$M\ddot{X}_I + D\dot{X}_I + KX_I = -F + M\ddot{X}_D + D\dot{X}_D + KX_D \quad (3.6)$$

where $X_I(0) = X_D(0)$, $\dot{X}_I(0) = \dot{X}_D(0)$. M , D and K are as defined before. Equation (3.6) can be obtained by inspection from Figure 3.3. It implies the same impedance definition as in equations (3.3) and (3.4). It is noted that in the impedance control formulation X_I is a function of both the input X_D and the measured contact force F . Since the position-controlled subsystem ensures that the end-effector position X closely tracks X_I defined in equation (3.6), therefore the target impedance of the manipulator is obtained [12].

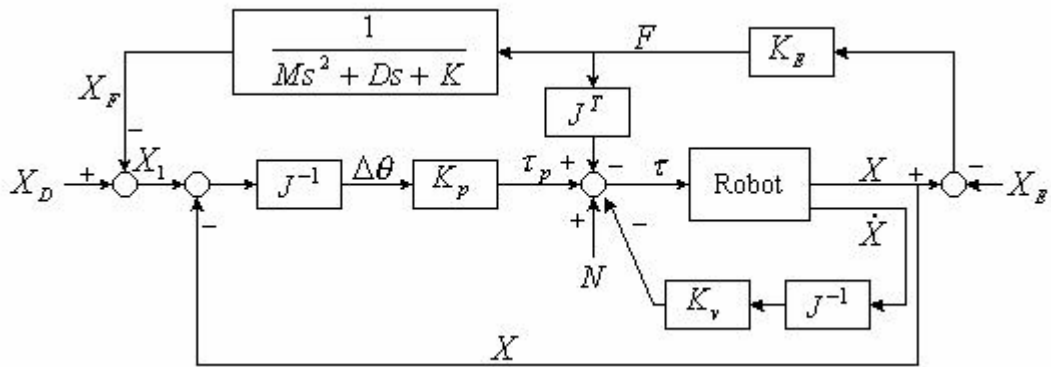


Figure 3.3 Position-based second order impedance control

Sensor based, feedback controlled interaction with the environment requires the impedance to be of second order at most. This is for two reasons as explained in [11]. First, the dynamics of a second order system are well understood and familiar. Second, for higher order systems, it is difficult to obtain measurements corresponding to the higher order state variables.

The selected impedance value for a certain environment should be reconsidered when the manipulator is used in a significantly different environment for the sake of the precise control of the force exerted on the environment. This could be achieved by employing adaptive algorithms to the impedance control.

3.3 ADMITTANCE CONTROL

Admittance control specifies a force setpoint and the setpoint is tracked by a force compensator. In contrast with a pure position control which rejects disturbance forces in order to track a given reference motion trajectory, the force compensator attempts to comply with the environmental interaction and react quickly to contact forces by rapidly modifying the reference motion trajectory [4]. The mechanical admittance is defined as;

$$\dot{X} = AF \quad (3.7)$$

where the force compensator is defined as in s domain;

$$X(s) = K(s)F(s) \quad (3.8)$$

$$K(s) = \frac{1}{s} A(s) \quad (3.9)$$

As it can be observed from equation (3.7), mechanical admittance is the inverse of impedance definition in equation (3.2). Figure 3.4 shows the structure of a common admittance control.

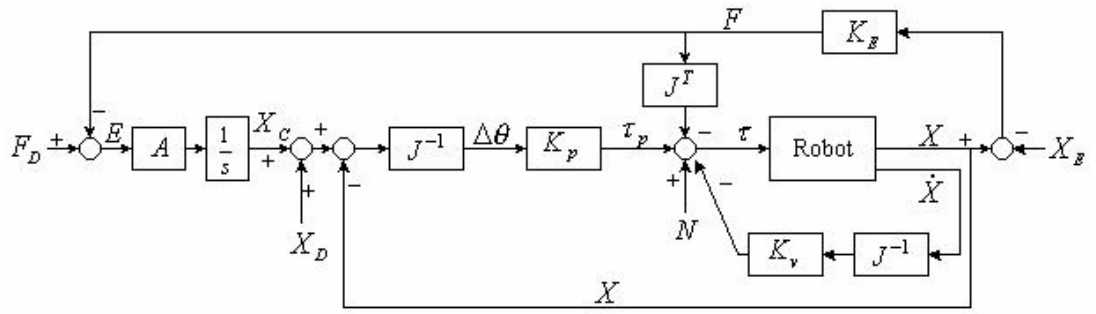


Figure 3.4 Admittance control

In Figure 3.4, admittance matrix A relates the force error vector E ($E = F_D - F$) to the end-effector velocity perturbation. Effective and precise admittance control can be achieved by choosing a suitable A matrix for the known stiffness of the environment. As the working environment is changed to a significantly different environment, A matrix should be recalculated in order to adapt the new environment. Changing the admittance value due to the change in environment is possible with adaptive algorithms. The command trajectory X_c is defined as;

$$X_c = \int A(F_D - F)dt \quad (3.10)$$

Considering a second-order admittance for this control scheme, the admittance is defined as;

$$A(s) = k_d s^2 + k_p s + k_i \quad (3.11)$$

which results in the PID force compensator;

$$K(s) = \frac{1}{s} \cdot A(s) = k_d s + k_p + \frac{k_i}{s} \quad (3.12)$$

3.4 HYBRID POSITION/FORCE CONTROL

Combining position and force information into one control scheme for moving the end-effector in nondeterministic environments is called the hybrid position/force control. The advantage of hybrid position/force control with respect to others is that the position and force information are analyzed independently to take advantage of well-known control techniques for each and are combined only at the final stage when both have been converted to joint torques [13]. This means that there is not a constant relationship between the applied force and the position of the end-effector. Figure 3.5 shows the hybrid position/force control scheme.

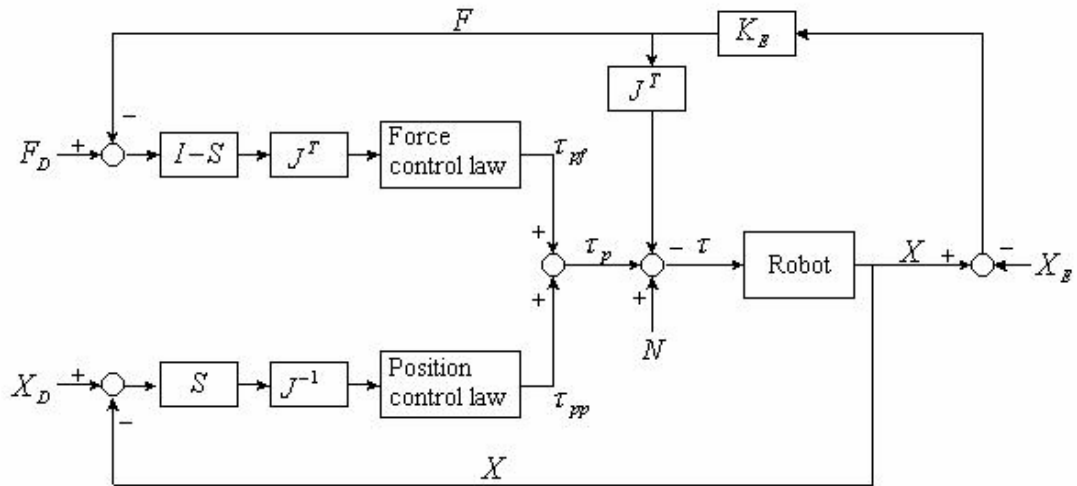


Figure 3.5 Conceptual organization of hybrid position/force control

In figure 3.5, $S = \text{diag}(s_j)$ ($j=1\dots n$) is called the compliance selection matrix, n is the degree of freedom. The matrix S determines the subspaces for which force or position are to be controlled, and s_j is selected as 1 or 0. When $s_j = 0$, the j th DOF must be force controlled, otherwise it must be position controlled. S matrix can be constant, can change with the configuration or can continuously change in time [14].

For each task configuration, a generalized surface can be defined in a constraint space with position constraints along the normals to this surface and force constraints along the tangents, which means, the end-effector can not move along the normals into the surface and can not exert forces along the tangents of the surface. These two types of constraints partition the degrees of freedom of possible end-effector motions into two orthogonal sets that must be either position or force controlled [5]. Utilizing this partition, S matrix is formed.

The command torque is

$$\tau_p = \tau_{pp} + \tau_{pf} \quad (3.13)$$

τ_{pp} and τ_{pf} are the command torques acting in position and force subspaces, respectively. In this way, position control and force control are decoupled. The control laws for each can be designed independently, so that the different control performance requirements for the desired position and force trajectory trackings are simultaneously realized. Normally, the position control law in Figure 3.5 consists of a PD action, and the force control law consists of a PI action. This is because for the position control, a faster response is more desirable, and for the force control a smaller error is more preferable. Though, in some applications of hybrid position/force control, different force control algorithms are used for the force-controlled subspace as explicit and implicit force control.

Robot explicit force control includes two categories. One is force-based and the other is position-based explicit force control [1]. But, the second category consists of the same structure as the admittance control explained earlier and illustrated in Figure 3.4. In figure 3.6, explicit force control is shown.

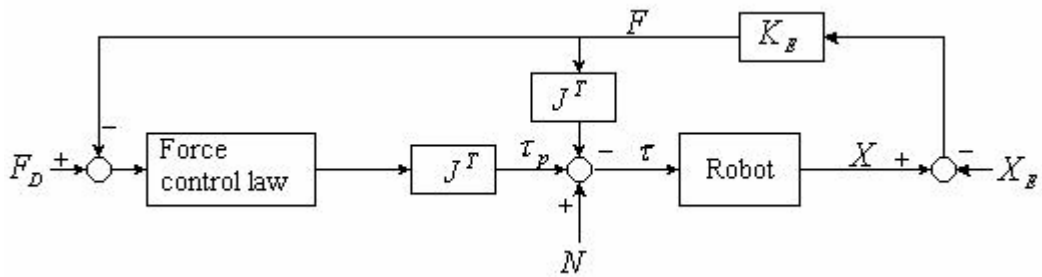


Figure 3.6 Explicit force control

In Figure 3.6, the measured force is directly used for feedback in order to form the force error vector. The force control law is normally chosen as PID. Obviously, the design of force control law in explicit force control is the key to successful force tracking.

Figure 3.7 shows the implicit force control where there is no force feedback. Instead, the position is controlled based on the predefinition of position for a desired force. For this, the proportional control gain K_p is determined such that the robot arm can obtain a particular stiffness.

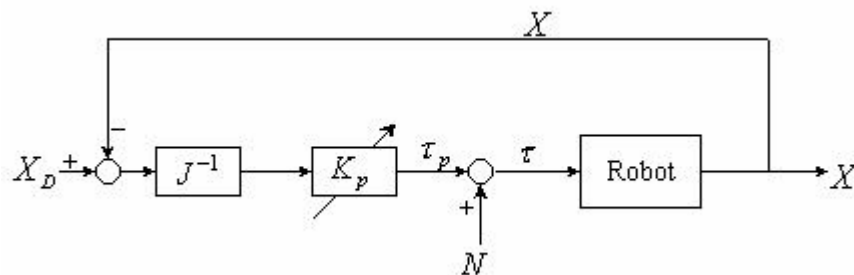


Figure 3.7 Implicit force control

3.5 HYBRID IMPEDANCE CONTROL

Combining impedance control and hybrid position/force control into one strategy allows a designer to obtain more flexibility in choosing the desired impedance of the controlled robotic system. A distinction of impedances in force-controlled and position-controlled subspaces thus can be made [6]. This means that different impedances for each subspace can be chosen. Hybrid impedance control is a more sophisticated algorithm than the hybrid position/force control but in contrast, impedance values of the manipulator should be reiterated as the manipulator encounters different environments. This also could be achieved by using adaptive algorithms [6]. Figure 3.8 shows the hybrid impedance control block diagram.

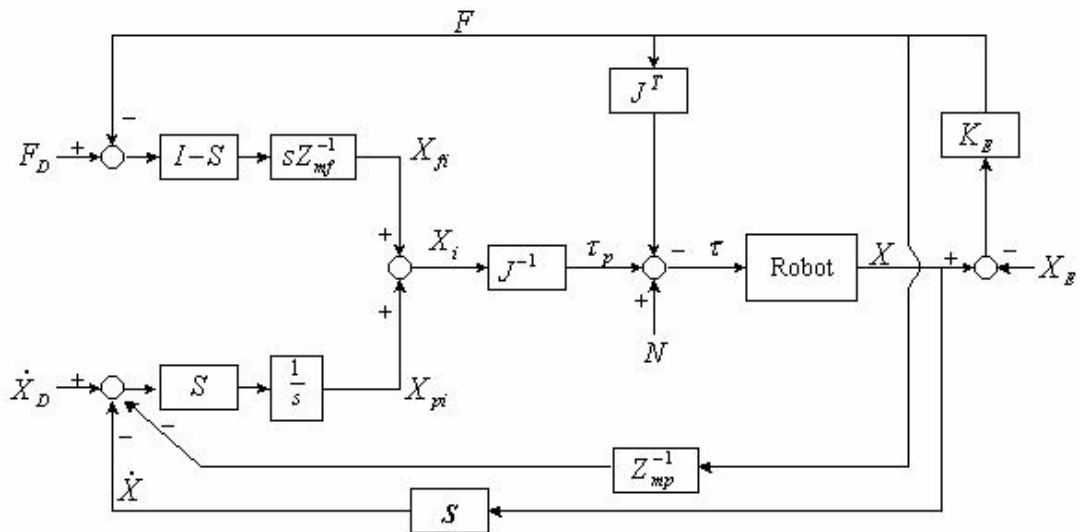


Figure 3.8 Hybrid impedance control

In Figure 3.8, Z_{mp} and Z_{mf} are the desired impedance terms that are selected by the user. If they are chosen as diagonal matrices, their elements represent the impedance along each degree of freedom. S is the compliance selection matrix, same as the one in the hybrid position/force control. The modified desired trajectory X_i is

$$X_i = X_{pi} + X_{fi} \quad (3.14)$$

where X_{pi} and X_{fi} are the modified position and force trajectories expressed in position and force subspace, respectively.

CHAPTER 4

SYSTEM MODELING

4.1 MANIPULATOR MODEL

Position/Force control algorithms described in Chapter 3 will be performed on a six degree-of-freedom, well-known type of manipulator, PUMA 560. The specific PUMA 560 manipulator to be used in the simulations is the PUMA 560 manipulator described in Başçuhadar's master's thesis [15]. Figure 4.1 shows a general sketch of the manipulator.

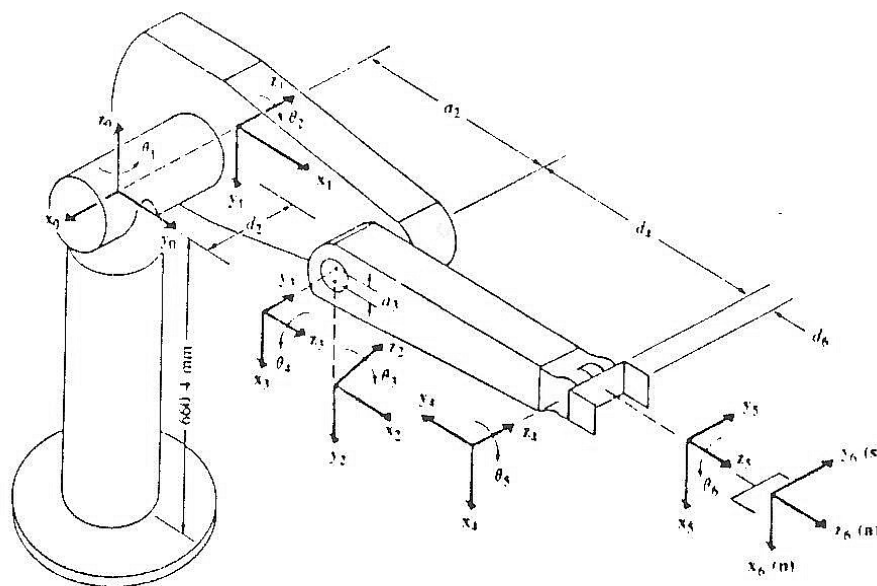


Figure 4.1 General sketch of the PUMA 560

4.1.1 Kinematic equations of the manipulator

Inverse kinematics of the manipulator is required to transform cartesian space motions to joint space motions. For the solution of inverse kinematics problem, forward kinematic equations are required as expressed in [16, 17, 18]. Link coordinate parameters of the manipulator are given in Table 4.1 calculated from the joint coordinate frames presented in Figure 4.2 according to the Denavit-Hartenberg convention. In the Figure 4.3 and in what follows, $\beta_k = \alpha_k$, $d_k = s_k$, $b_k = a_k$. For the sake of simplicity in deriving the kinematic equations, origin of Joint 3 (O_2) is moved along the $\vec{u}_3^{(2)}$ vector for d_3 mm. to be aligned with the origin of Joint 2 (O_1) along the $\vec{u}_1^{(2)}$. As a result of this, in Denavit-Hartenberg parameters of the manipulator presented below, the value of d_3 , which was 93.5 mm., came out to be 0 mm. and d_2 which was 175 mm. became 81.5 mm.

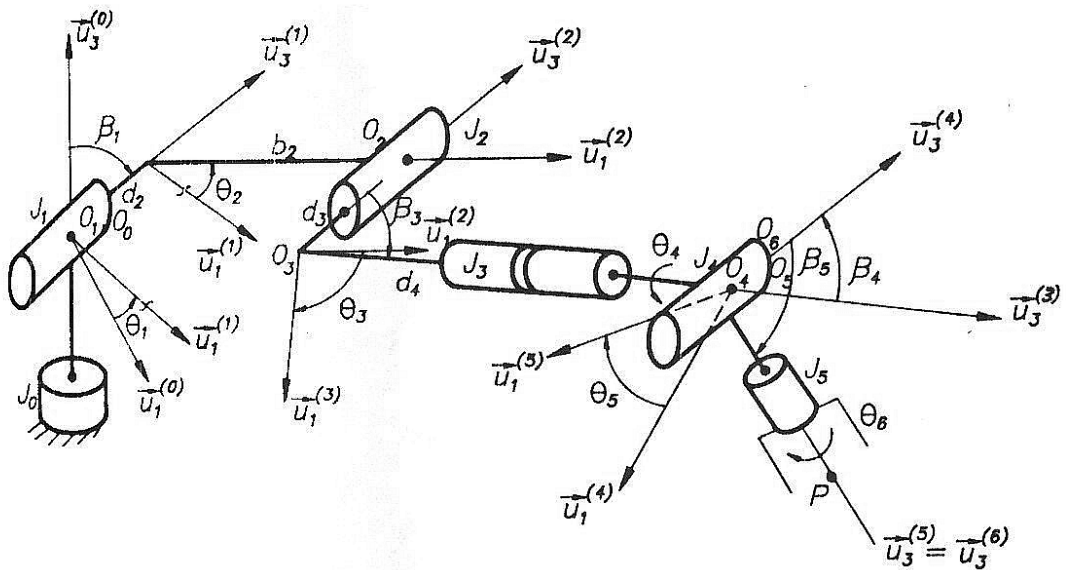


Figure 4.2 PUMA manipulator with its assigned coordinate frames

Using link coordinate parameters, link-to-link rotational transformation matrices are calculated;

$$\hat{C}^{(0,1)} = e^{\tilde{u}_3 \theta_1} e^{-\tilde{u}_1 \pi / 2} \quad (4.1)$$

$$\hat{C}^{(1,2)} = e^{\tilde{u}_3 \theta_2} \quad (4.2)$$

$$\hat{C}^{(2,3)} = e^{\tilde{u}_3 \theta_3} e^{\tilde{u}_1 \pi / 2} \quad (4.3)$$

$$\hat{C}^{(3,4)} = e^{\tilde{u}_3 \theta_4} e^{-\tilde{u}_1 \pi / 2} \quad (4.4)$$

$$\hat{C}^{(4,5)} = e^{\tilde{u}_3 \theta_5} e^{\tilde{u}_1 \pi / 2} \quad (4.5)$$

$$\hat{C}^{(5,6)} = e^{\tilde{u}_3 \theta_6} \quad (4.6)$$

Table 4.1 Link coordinate parameters of the PUMA 560 manipulator

Joints	α_k (deg.)	s_k (mm.)	a_k (mm.)	θ_k (deg.)
1	-90°	0	0	θ_1
2	0	81.5	300	θ_2
3	90°	0	0	θ_3
4	-90°	304.5	0	θ_4
5	90°	0	0	θ_5
6	0	0	0	θ_6

Using these link-to-link rotational transformation matrices and the method mentioned in [17, 18], the base-to-hand transformation matrix $\hat{C}^{(0,6)}$ is obtained with the following simplified expression:

$$\hat{C}^{(0,6)} = \hat{C}^{(0,1)} \hat{C}^{(1,2)} \hat{C}^{(2,3)} \hat{C}^{(3,4)} \hat{C}^{(4,5)} \hat{C}^{(5,6)} = e^{\tilde{u}_3 \theta_1} e^{\tilde{u}_2 \theta_2} e^{\tilde{u}_3 \theta_3} e^{\tilde{u}_2 \theta_4} e^{\tilde{u}_3 \theta_5} e^{\tilde{u}_3 \theta_6} \quad (4.7)$$

where

$$\theta_{23} = \theta_2 + \theta_3 \quad (4.8)$$

Tip point position vector $\bar{p}^{(0)}$ is calculated from the wrist point position vector $\bar{r}^{(0)}$. Wrist point position is calculated using the link coordinate parameters.

$$\bar{p}^{(0)} = \bar{r}^{(0)} + d_p \hat{C}^{(0,6)} \bar{u}_3 \quad (4.9)$$

where d_p is the end-effector's location with respect to the wrist point along the vector $\bar{u}_3^{(6)}$, described as $d_p = O_6P$ which is 120 mm for the PUMA 560 manipulator considered in this thesis. Again using the method mentioned in [17, 18], the wrist point position is obtained as expressed below:

$$\bar{r}^{(0)} = e^{\tilde{u}_3 \theta_1} [\bar{u}_1 (d_4 s \theta_{23} + a_2 c \theta_2) + \bar{u}_2 d_2] + \bar{u}_3 (d_4 c \theta_{23} - a_2 s \theta_2) \quad (4.10)$$

In what follows, $s \theta_k = \sin \theta_k$ and $c \theta_k = \cos \theta_k$. Solving equations (4.7) and (4.9) for known values of $\hat{C}^{(0,6)}$ and $\bar{p}^{(0)}$, joint angles, θ_k , are calculated by the method presented in [17].

To transform end-effector's velocity in Cartesian space to joint velocities $\dot{\bar{q}}$ in the joint space, Jacobian matrix is required. Jacobian matrix can be formed for the tip point \hat{J}_p or for the wrist point \hat{J}_r .

$$\bar{V}_p = \hat{J}_p \dot{\bar{q}} \quad \text{and} \quad \bar{V}_r = \hat{J}_r \dot{\bar{q}} \quad (4.11)$$

Hand velocity state referring to the tip point is indicated below;

$$\bar{V}_p = \begin{bmatrix} \bar{V}_{pp} \\ \bar{\omega}_n \end{bmatrix} \quad (4.12)$$

where \bar{V}_{pp} is the tip point linear velocity and $\bar{\omega}_n$ is the angular velocities of these points.

Jacobian matrix is a 6x6 matrix composed of tip or wrist point velocity influence coefficients (\bar{J}_{p_k} or \bar{J}_{r_k}) and angular velocity influence coefficients (\bar{J}_{a_k}).

$$\hat{J}_p = \begin{bmatrix} \bar{J}_{p_1} & \dots & \bar{J}_{p_n} \\ \bar{J}_{a_1} & \dots & \bar{J}_{a_n} \end{bmatrix} \quad \text{or} \quad \hat{J}_r = \begin{bmatrix} \bar{J}_{r_1} & \dots & \bar{J}_{r_n} \\ \bar{J}_{a_1} & \dots & \bar{J}_{a_n} \end{bmatrix} \quad (4.12)$$

$$\bar{J}_{p_k} = \partial \bar{p} / \partial q_k \quad \text{or} \quad \bar{J}_{r_k} = \partial \bar{r} / \partial q_k \quad (4.13)$$

$$\bar{J}_{a_k} = \text{col} \left[\frac{\partial \hat{C}}{\partial q_k} \hat{C}^t \right] \quad (4.14)$$

Tip point velocity influence coefficient can be calculated in terms of wrist point velocity influence coefficient.

$$\bar{J}_{p_k} = \bar{J}_{r_k} + d_p \tilde{J}_{a_k} \hat{C}^{(0,6)} \bar{u}_3 \quad (4.15)$$

4.1.2 Dynamic properties of the manipulator

The masses, the moments of inertia and the mass centers of the links obtained from Başçuhadar's thesis [15] are given as dynamic properties of Başçuhadar's PUMA 560. Dynamic properties are used for the dynamics of the robot developed for the simulation using Matlab[®] Simulink Simmechanics blockset.

Moments of inertia of all links are about the center of mass and their unit is kg.mm². in the tables that are given in the Appendix A. Moments of inertia are calculated with respect to the world axis at an initial position of the manipulator when all links except Link 1 are parallel to the $\bar{u}_1^{(0)}$ vector. This is because the body-blocks of the robot in the simulation use the inertia parameters with respect to the world axes. Mass unit of all links are in kg. in the tables of Appendix A.

Figure 4.3 shows the detailed representation of the PUMA 560 manipulator considered in this thesis. In [15], the numerical values of the link vectors describing the center of mass location are calculated with respect to the coordinate frame of the link that its center of mass locations are given. In this thesis, the numerical values of the link vectors are given with respect to the world coordinate frame at an initial position of the manipulator when all links except Link 1 are parallel to the $\bar{u}_1^{(0)}$ vector because the body-blocks, that is used to represent the links in the simulation, requires all the dimensions of the manipulator to be given with respect to the world coordinate frame. In the Figure 4.3 and in what follows, O_i^* is the center of the joint between the links i and $i+1$; C_i is the center of mass of the link i ; \bar{q}_i is the position vector of O_i^* with respect to C_i ; \bar{q}_i^* is the position vector of C_i with respect to O_i^* . Numerical values of the link vectors describing the center of mass locations with respect to the world coordinate frame are as follows (dimensions are in m):

$$\begin{aligned}
\bar{q}_1^t &= [0.0430 \quad 0.0460 \quad 0.0150] \\
\bar{q}_2^t &= [0.3400 \quad 0.0330 \quad 0.0010] \\
\bar{q}_3^t &= [0.2645 \quad -0.0080 \quad -0.0010] \\
\bar{q}_4^t &= [0.0540 \quad 0 \quad 0] \\
\bar{q}_5^t &= [-0.0050 \quad -0.0010 \quad 0] \\
\bar{q}_6^t &= [0.0040 \quad 0 \quad 0] \\
\bar{q}_1^{*t} &= [-0.0430 \quad -0.0460 \quad 0.5850] \\
\bar{q}_2^{*t} &= [-0.0400 \quad 0.1420 \quad -0.0010] \\
\bar{q}_3^{*t} &= [-0.0160 \quad -0.0855 \quad 0.0010] \\
\bar{q}_4^{*t} &= [0.0020 \quad 0 \quad 0] \\
\bar{q}_5^{*t} &= [0.0050 \quad 0.0010 \quad 0] \\
\bar{q}_6^{*t} &= [0.1160 \quad 0 \quad 0]
\end{aligned}$$

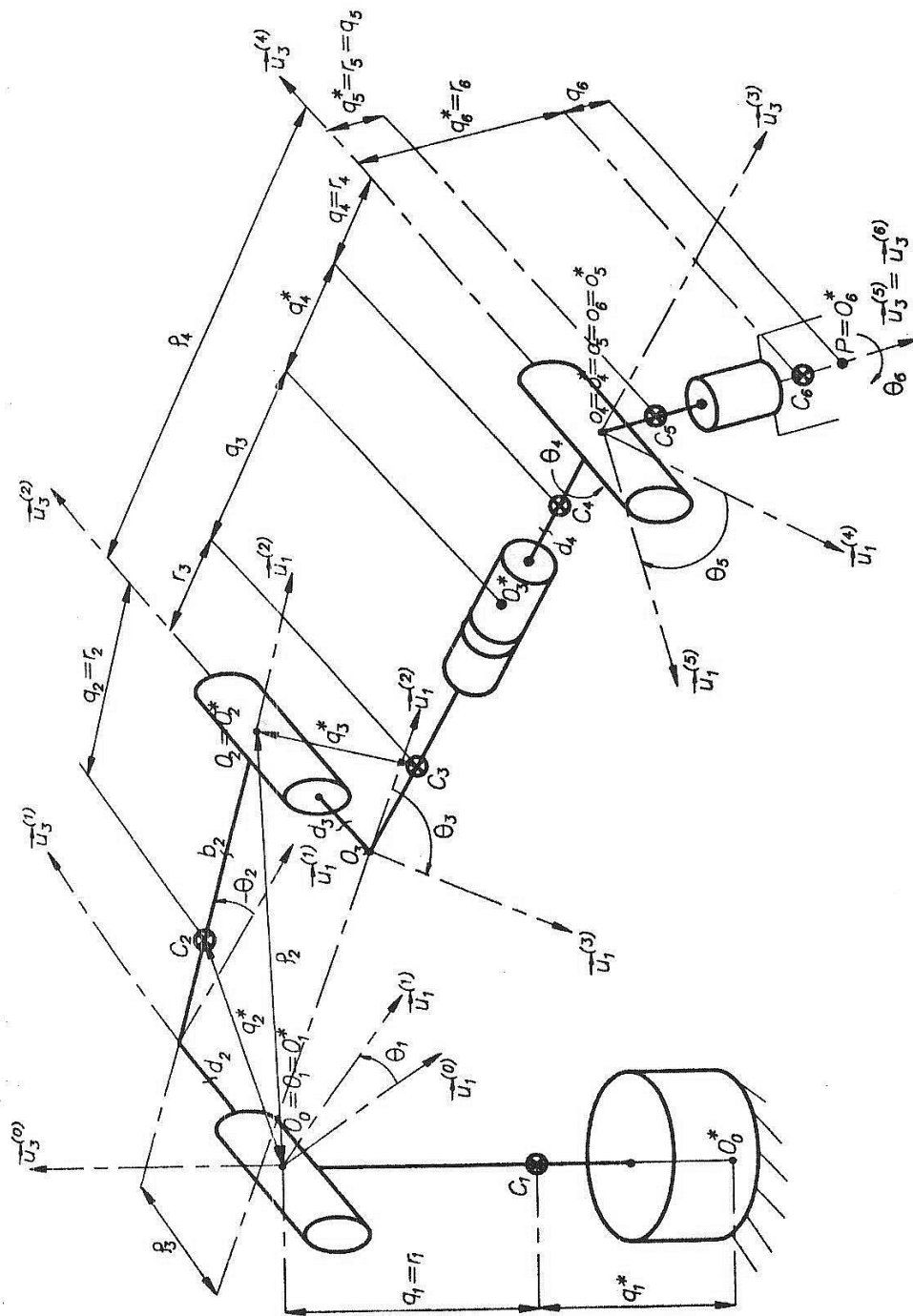


Figure 4.3 A detailed schematical representation of the PUMA 560

4.1.3 Modeling the manipulator with Simmechanics blockset

Simmechanics blockset is a tool, created by Mathworks that can operate with the other Matlab[®] Simulink blocks, used to build mechanical systems. The PUMA 560 manipulator model that the kinematic and dynamic properties given before is build in the simulation using Simmechanics blockset.

Figure 4.4 shows the blocks of a link of the manipulator. A link is composed of “Body”, “Revolute Joint”, “Joint Actuator”, “Joint Sensor”, “Body Sensor”, “Joint Initial Condition”, “Goto”, “From” and “PMC Port” blocks.

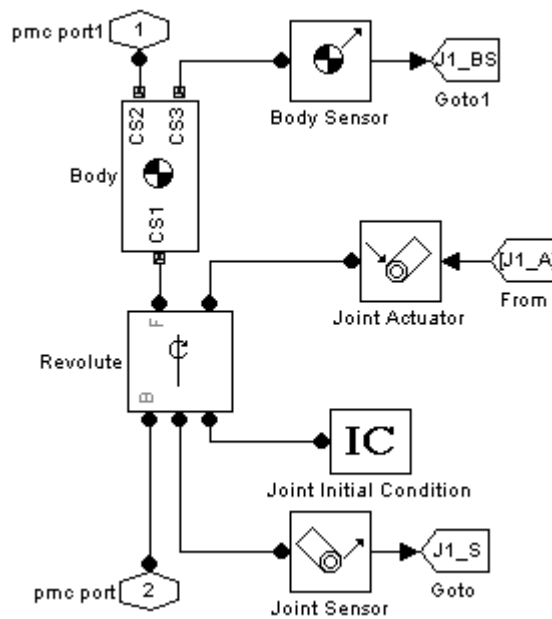


Figure 4.4 A link composition of the manipulator created in Simmechanics

Dynamic properties of a link of the manipulator are entered in the “Body” block as shown in Figure 4.5. Mass and inertia information of the links are entered to the spaces indicated as “Mass” and “Inertia”. Link start, end and mass center positions are entered in the spaces indicated as “CS1”, “CS2” and “CG” respectively. Position of the center of mass is translated from the origin of world O_o with respect to the world coordinate frame. Positions of the start and end of the links are translated from the origin of the mass center and with respect to the world coordinate frame. “CS1” port must be either connected to a ground block if the link is the first link or connected to the joint before it. “CS2” port must be either connected to a joint after the link or not connected to anything if it is the last link body. “CS3” must be connected to a body sensor block.

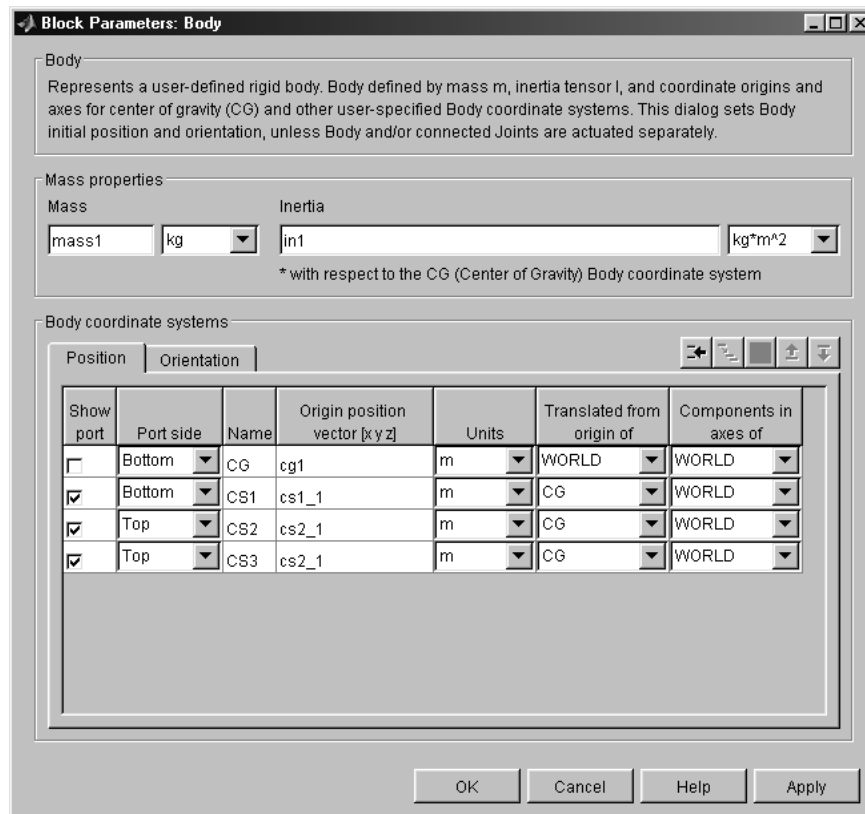


Figure 4.5 “Body” block parameter window

Rotation axes of the joints are entered in the “Revolute Joint” block shown in Figure 4.6. Axis of rotation of the joint is entered in the space indicated as “Axis of rotation” with respect to the world coordinate frame. To drive the joint, to get feedbacks from the joint and to enter the initial positions of the joints, sensor/actuator ports are used. The amount of these ports are entered in the space indicated as “Number of sensor/actuator ports”.

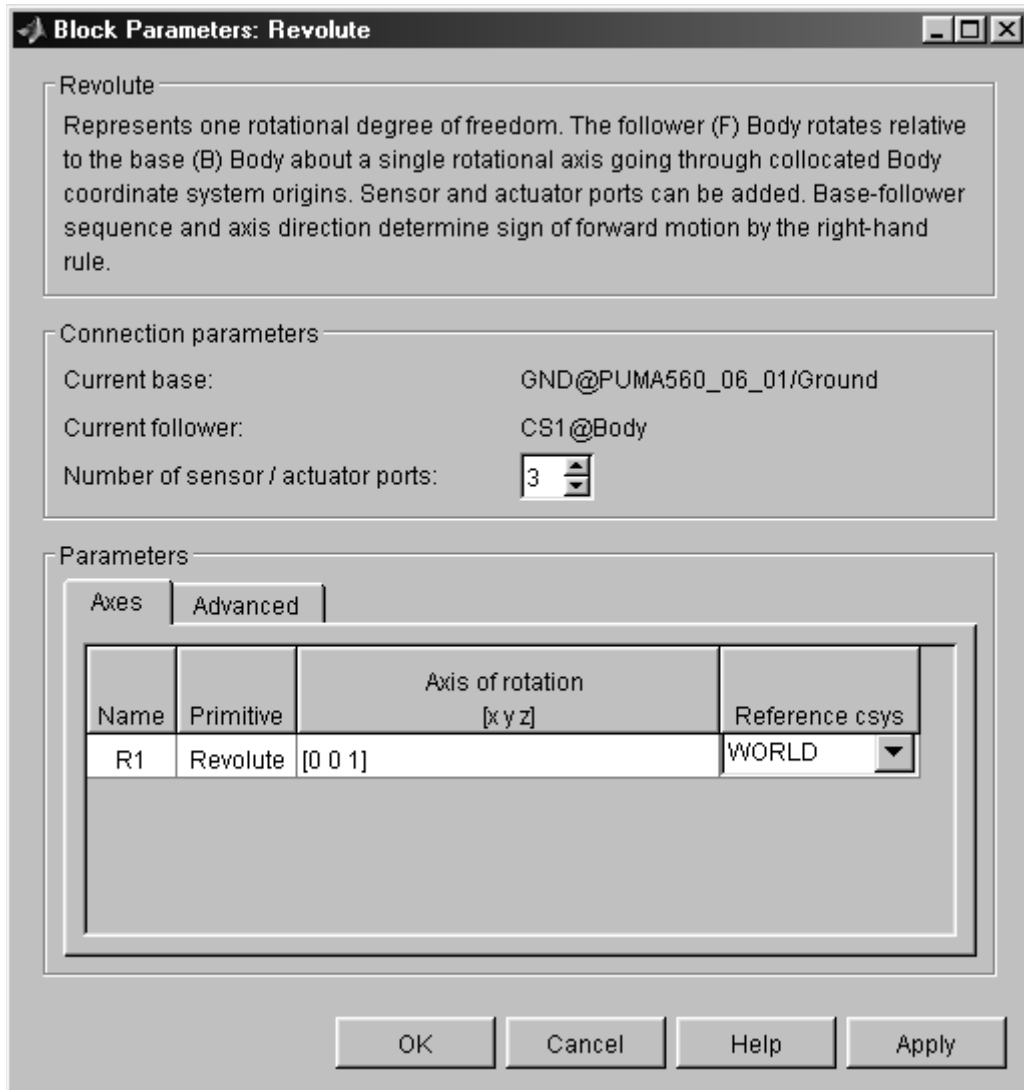


Figure 4.6 “Revolute Joint” block parameter window

Actuation of the joints are achieved by “Joint Actuator” blocks. In the actuator block parameter window shown in Figure 4.7, the type of actuation is selected. Selecting the “Generalized Forces” for actuation the block applies torque to the revolute joint. In the space indicated as “Apply torque (revolute only)”, unit of torque is entered. One port of this block must be connected to an actuation signal created by the control system and the other port must be connected to the “joint” block it actuates.

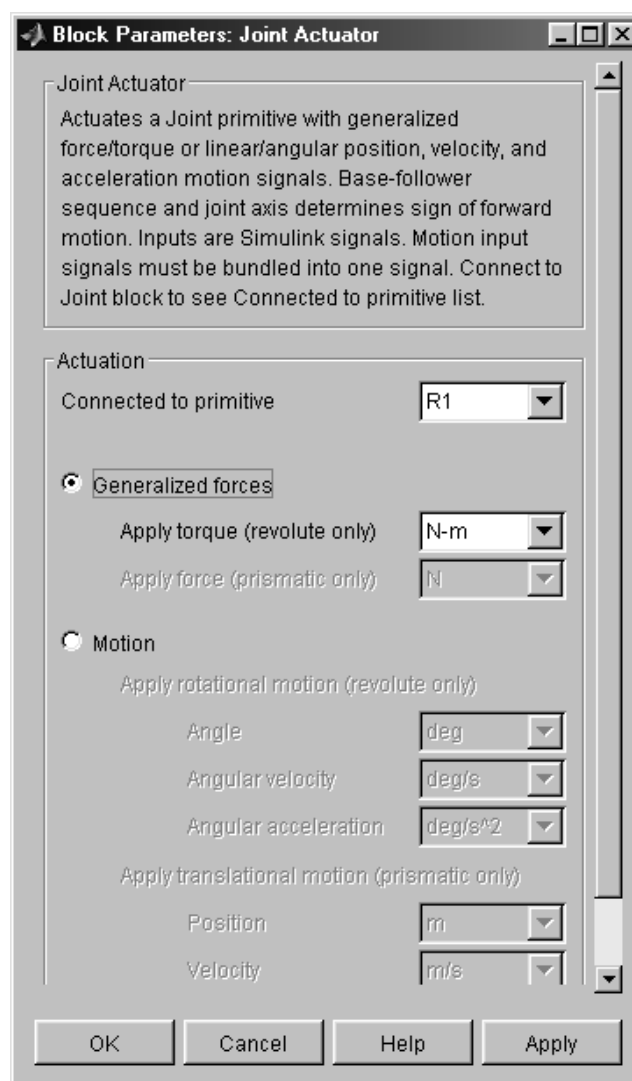


Figure 4.7 “Joint Actuator” block parameter window

“Joint Sensor” block is used to feedback the joint angular position, velocity, acceleration, computed torque and reaction force. In the parameter window of this block shown in Figure 4.8 the feedback signal to be measured are selected by ticking the required feedback signal’s box. The units of the feedback signals are selected from the space on the right of the feedback signal name. One port of this block must be connected to the “Joint” block that the feedback signals to be calculated from and the other port must be connected to the control system as feedback signals.

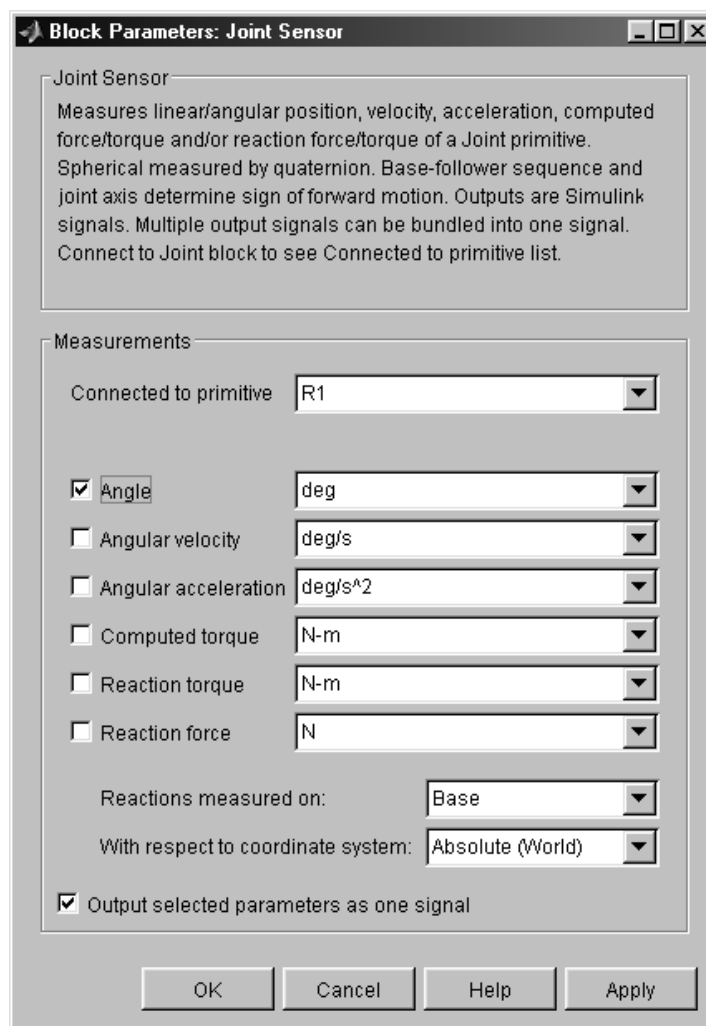


Figure 4.8 “Joint Sensor” block parameter window

“Body Sensor” block is used to get feedback from a selected port of the body that it is connected to. Figure 4.9 shows the parameter window of a body sensor block. In this block, linear/angular position, velocity and acceleration of the point of the body that it is connected to are calculated as feedback signals. Feedback signal to be measured are selected by ticking the required feedback signal’s box. The units of the feedback signals are selected from the space on the right of the feedback signal name. One port of this block must be connected to the body that the feedback signals to be calculated from and the other port must be connected to the control system as feedback signals.

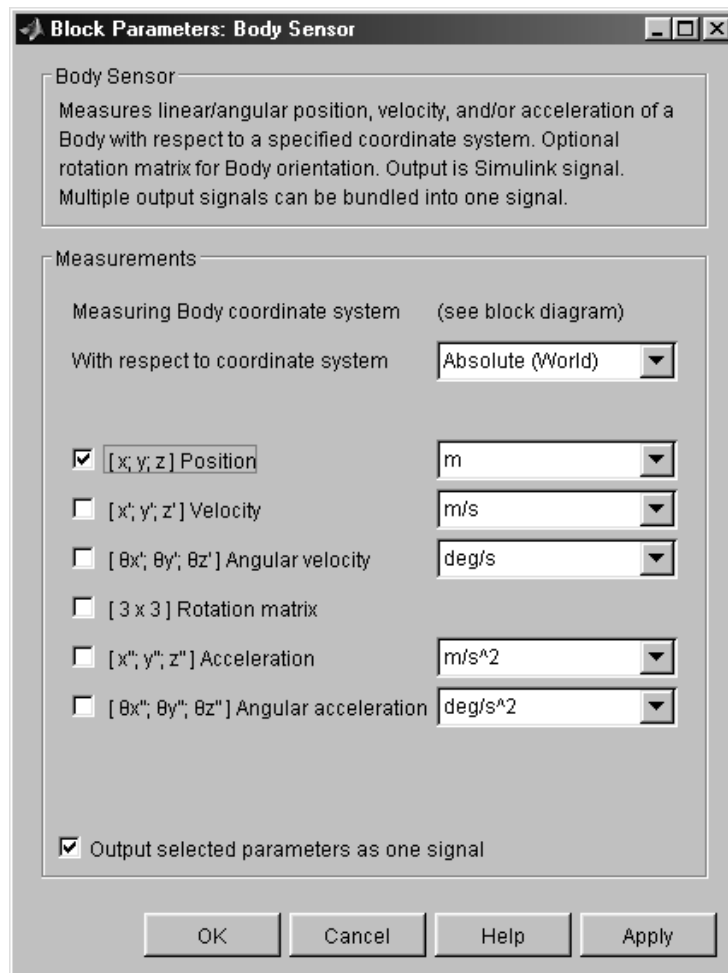


Figure 4.9 “Body Sensor” block parameter window

“Joint Initial Condition” block is used to input initial condition to the joint for the simulation start position of the joint. Parameter window of this block is shown in Figure 4.10. Initial position and velocity are entered in the space indicated as “Position” and “Velocity” respectively. The units of these can be selected from the spaces indicated as “Units”. The one and only port of this block must be connected to the “Joint” block that its initial condition is given.

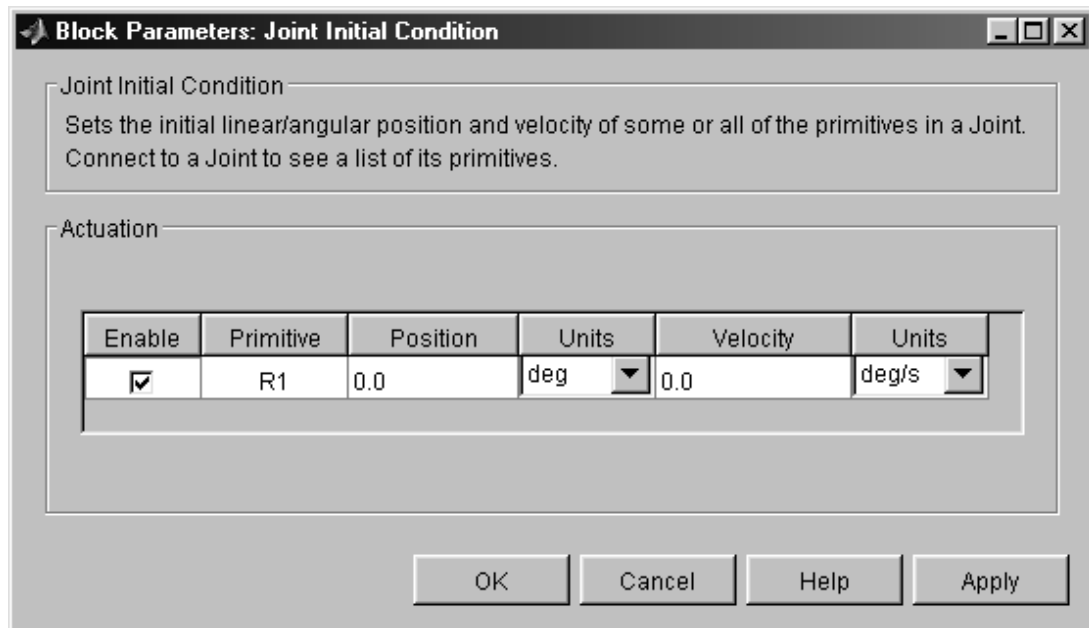


Figure 4.10 “Joint Initial Condition” parameter window

“Goto” blocks are used to send signals in or out the current simulation window to the “From” block. Parameter window of this block is shown in Figure 4.11. Tag name is given in the space indicated as tag. This tag name must be the same as the tag name of the “From” block which the signal is obtained from. Selecting the tag visibility as global enables the signal to be active outside the current simulation window. This block must be connected to signal source to that its signal to be transferred.

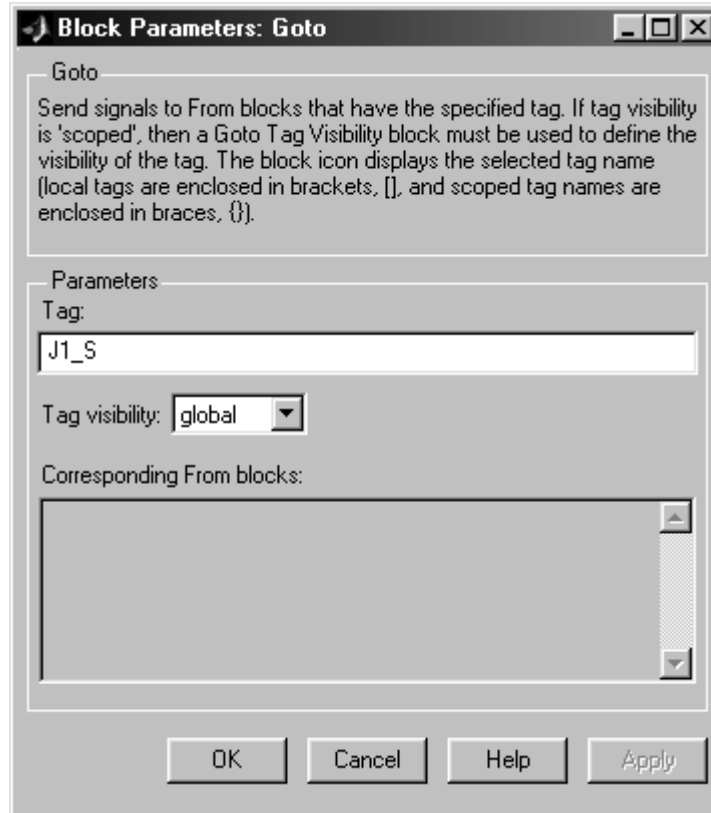


Figure 4.11 “Goto” block parameter window

“From” block is used to receive signals from the “Goto” block. Parameter window of this block is shown in figure 4.12. The only parameter to change in this block’s parameter window is the “Goto” blocks tag name that the signal is required to be received from the space indicated as “Goto tag”. This block must be connected to a block that the signal it is carrying must be input.



Figure 4.12 “From” block parameter window

“PMC_port” block is used to connect Simmechanics blocks that are in different simulation windows to each other. Figure 4.13 shows the parameter window of this block. This block must be connected to a Simmechanics block.

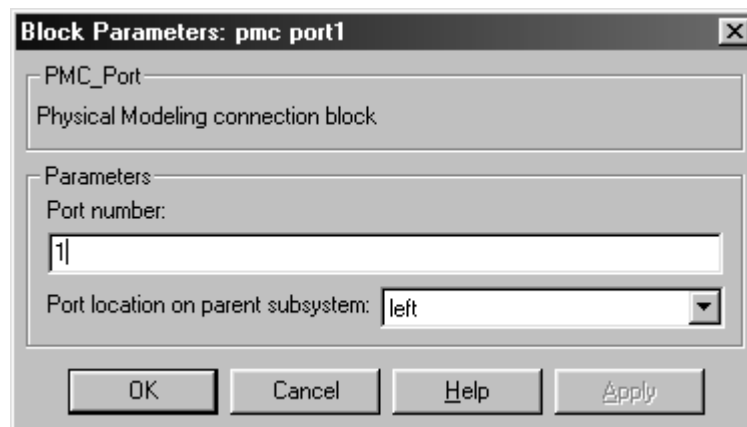


Figure 4.13 “PMC_port” block parameter window

All the mechanical systems created using Simmechanics blockset must be fixed to the ground from the first “Joint” block with the “Ground” block. The parameter window of the “Ground” block is shown in Figure 4.14. Location of the ground point is entered in the space indicated as “Location[x y z]”.

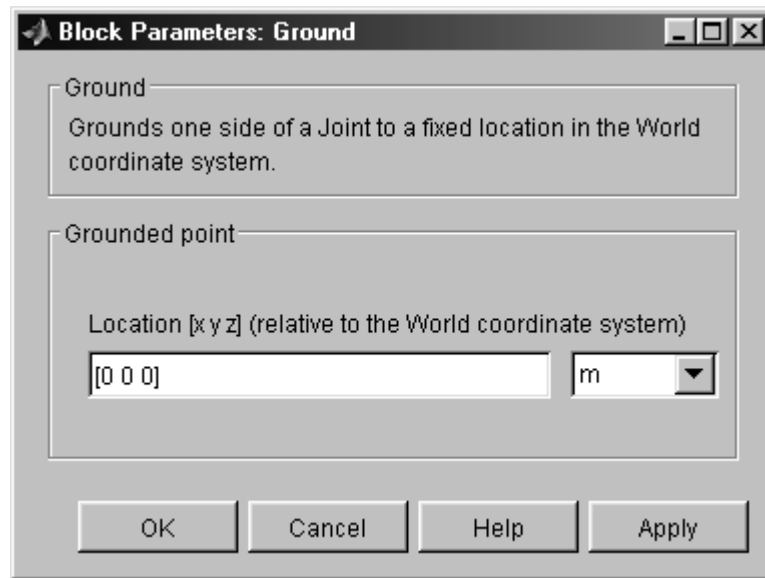


Figure 4.14 “Ground” block parameter window

4.2 COMPLIANT ENVIRONMENT MODELING

Different tasks performed by the manipulator are dependent on the parameters of the environment and the force and position trajectories. Changing the parameters of the compliant environment, tasks to be performed are changed. One of these parameters is the compliant surface's material, which is the stiffness of the compliant surface. Using different materials for the compliant surface, different environments can be simulated. On the other hand, the manipulator to be used in these simulations is not a manipulator to exert large amounts of forces on the surface due to its size. This causes the stiffness of the force sensor to be rather small for measuring small amounts of forces with precision. As a result of this fact, the affect of stiffness of the environment, k_E , which is much higher than the stiffness of the force sensor, k_S , in determining the stiffness of the sensor and environment, k_{SE} , can be neglected.

$$k_{ES} = \frac{1}{\frac{1}{k_E} + \frac{1}{k_S}} \approx k_S \quad (4.16)$$

The other parameter is the form of the compliant surface. Compliant surface can be a continuous one or can have sharp edges. Position trajectory can be selected to follow a straight line or a curve. Force trajectory can be selected as applying the same amount of force or can be selected to apply variational force throughout the simulation.

Compliant environment models are created with the Simulink blocks. The force applied to the surface is calculated using the amount of interference into the surface and the known surface stiffness.

CHAPTER 5

SIMULATION RESULTS

Results of the simulations done with different position/force control algorithms with different tasks will be presented in this chapter. As it is stated in Chapter 4, change in the stiffness of the environment will not be considered as different tasks. Since the change in the stiffness of the environments will not be considered, adaptive algorithms need not to be applied to stiffness, impedance and admittance controls. Also no dry friction is considered for the simulations. Change in the shape of the environment will rather be considered as different tasks. One of the surfaces is a continuous planar surface. This surface is located 0.6 meters away from the O_0 in \vec{u}_1^0 axis. The other surface is a discontinuous surface where it is composed of two planar surfaces connected at 90° with respect to each other. One of the planar surfaces forms a plane in \vec{u}_2^0 and \vec{u}_3^0 axes.

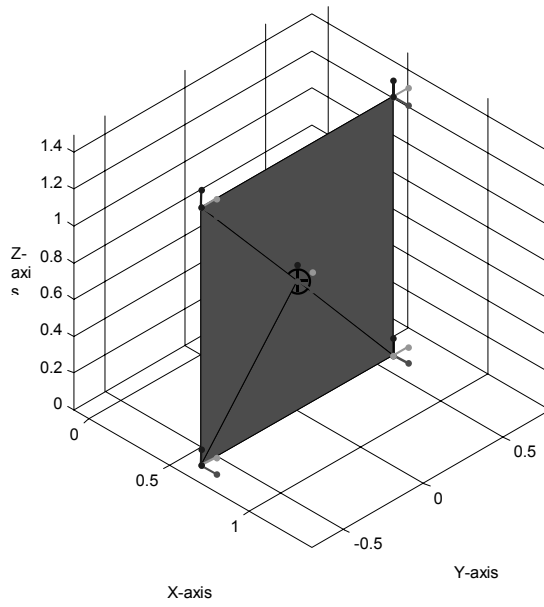


Figure 5.1 Continuous planar surface

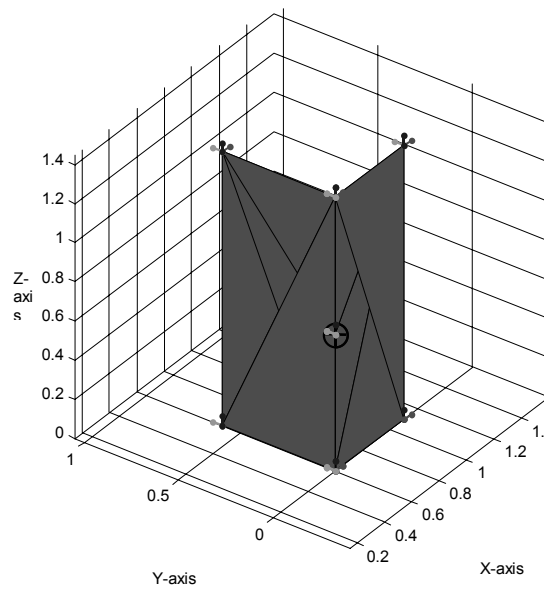


Figure 5.2 Discontinuous planar surface

Position trajectories are selected as a straight line and a circle to be followed by the manipulator. The force to be applied to the surface is selected as 15 N. The contact type of the manipulators end-effector is a point type of contact where five DOF are not constrained but only the motion along the normal of the surface is constrained.

5.1 STIFFNESS CONTROL SIMULATION RESULTS

Stiffness control architecture presented in Chapter 3 is changed to the algorithm shown below. “IK” in below figure and in the following figures represents the Inverse Kinematics.

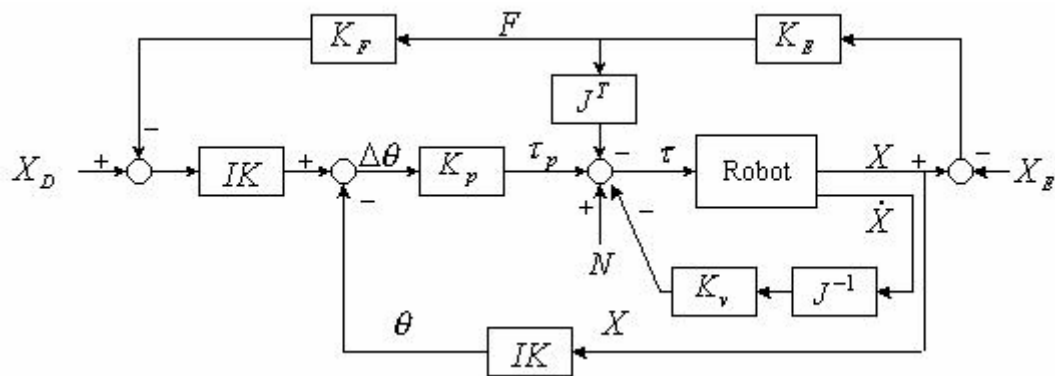


Figure 5.3 Modified stiffness control algorithm

Equation of motion is shown below considering the block diagram above;

$$M\ddot{\theta} + C(\theta, \dot{\theta}) + G(\theta) = T_{FB} + N - K_v J^{-1} \dot{X} - J^T F \quad (5.1)$$

$J^T F$ term represents the effect of the environment, when the manipulator exerts a force of F to the environment, on the joints. As it can be observed from the block diagram modified desired positional trajectory is transformed from task space to joint space by using the inverse kinematics equations before comparing it with the positional feedback calculated in task space. Instead, in the modified algorithm, modified desired trajectory is compared with the positional feedback in the joint space as stated in the equation below.

$$T_{FB} = K_p (\theta_D^* - \theta) \quad (5.2)$$

Where,

$$\theta_D^* = IK(X_D - k_F F) \quad \text{and} \quad \theta = IK(X) \quad (5.3)$$

Since the nonlinear feedforward compensation term N cancels out the coriolis and centrifugal terms, $C(\theta, \dot{\theta})$, and gravitational forces, $G(\theta)$, equation 5.1 changes into equation 5.4 as shown below.

$$M\ddot{\theta} + K_v \dot{\theta} + K_p \theta = K_p \theta_D^* - J^T F \quad (5.4)$$

Equation 5.4 can be re-written as;

$$\ddot{\theta} + (M^{-1}K_v)\dot{\theta} + (M^{-1}K_p)\theta = (M^{-1}K_p)\theta_D^* - M^{-1}J^T F \quad (5.5)$$

Control gains K_p and K_v can be determined by thinking of the equation 5.5 as a second order systems equation.

$$K_v = 2\zeta\omega_n M \quad (5.6)$$

$$K_p = \omega_n^2 M \quad (5.7)$$

For the sake of simplicity in control parameters determination, mass matrix M is taken as a diagonal matrix. ζ is selected as 0.8 and ω_n is selected as 50 rad/s. Usually ω_n is selected between 5-15 rad/s, but to make the response of the manipulator faster it is selected higher. This was required to make the simulations faster.

As it can be seen from the block diagram, there is no desired force/moment specified. As a result of this, stiffness control algorithm's aim is to decrease magnitude of the interaction forces/moments. In the simulations K_F parameter is adjusted in order to decrease the amount of interaction forces.

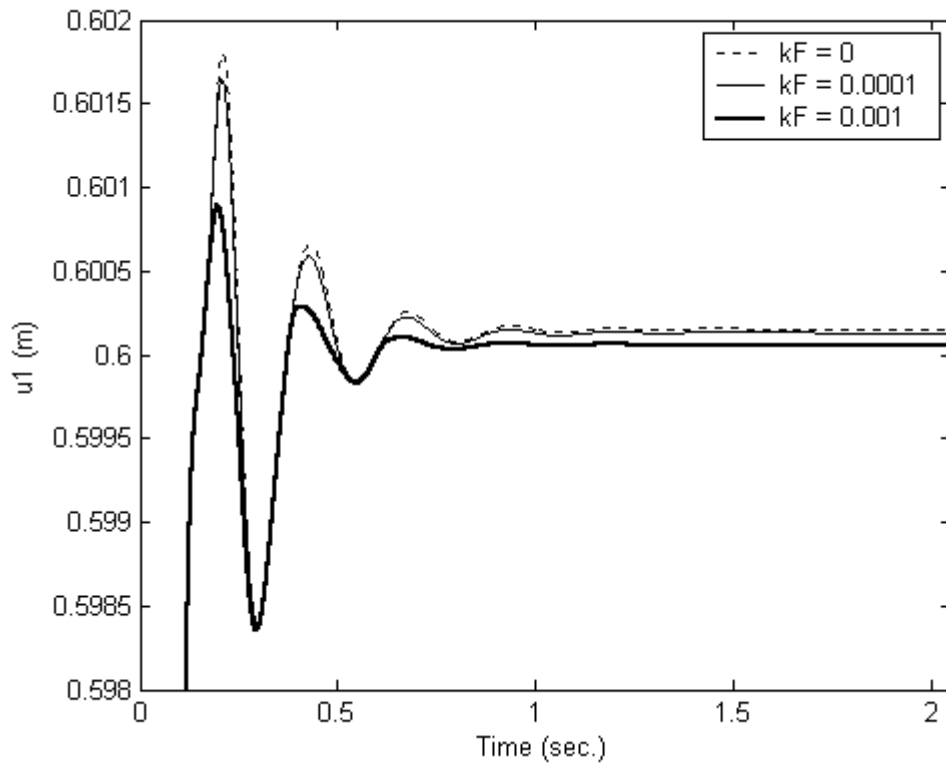


Figure 5.4 End-effector position in \bar{u}_1^0 axis following a straight line on a planar surface

The effect of the change in K_F parameter can be observed from the Figure 5.4. Stiffness control is only active when there is contact with the environment. This can also be observed from the Figure 5.4. The overrun into the surface is limited as K_F parameter rises but this parameter is not active when the contact is lost. This causes the same response in all simulation for no contact cases.

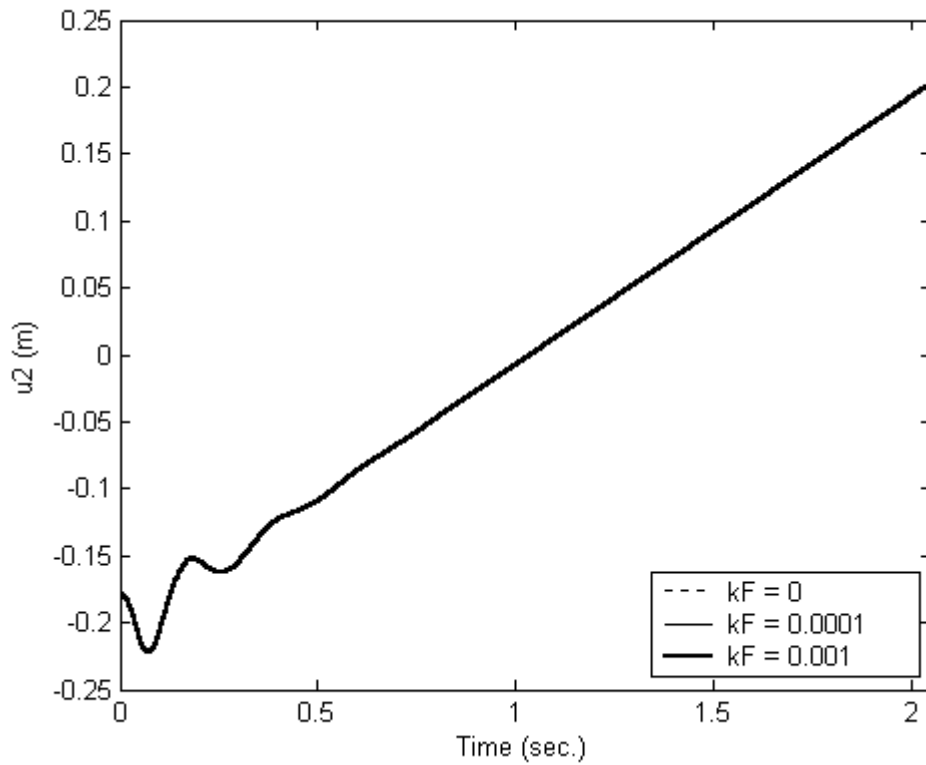


Figure 5.5 End-effector position in \bar{u}_2^0 axis following a straight line on a planar surface

As it can be observed from the Figure 5.5, the change in K_F does not have an effect on the motion along the \bar{u}_2^0 . This is the expected case because the applied force is along the normal of the surface \bar{u}_1^0 and not along the vector \bar{u}_2^0 . For this reason K_F does not have an effect on the motions along \bar{u}_2^0 .

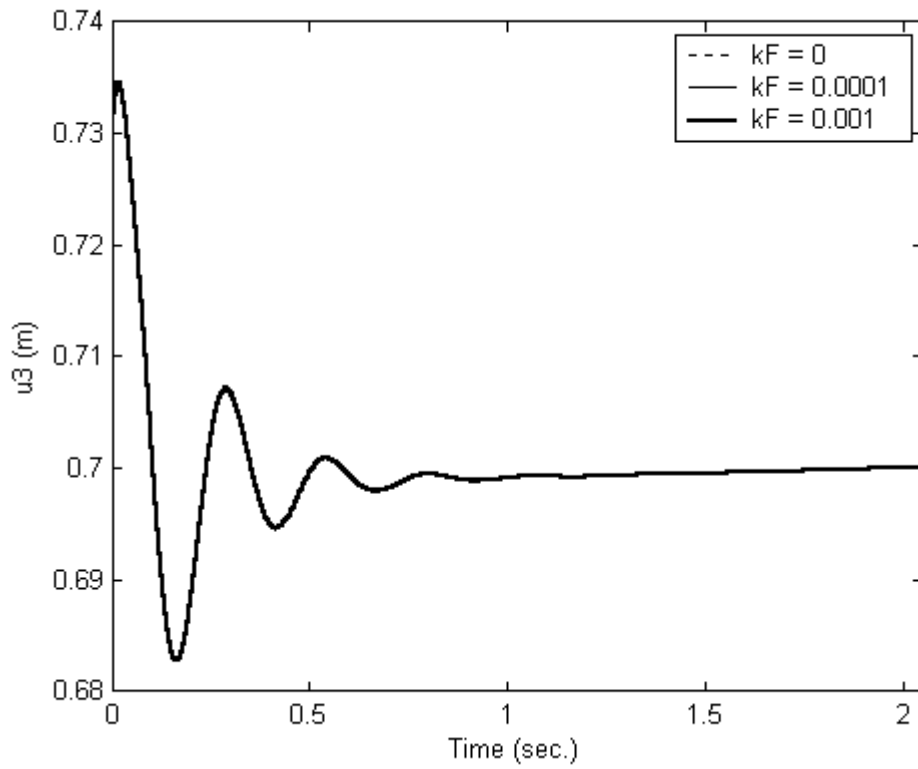


Figure 5.6 End-effector position in \bar{u}_3^0 axis following a straight line on a planar surface

As it is stated for the motions along \bar{u}_2^0 , motions along the \bar{u}_3^0 are not affected by the forces applied along the normal of the surface \bar{u}_1^0 .

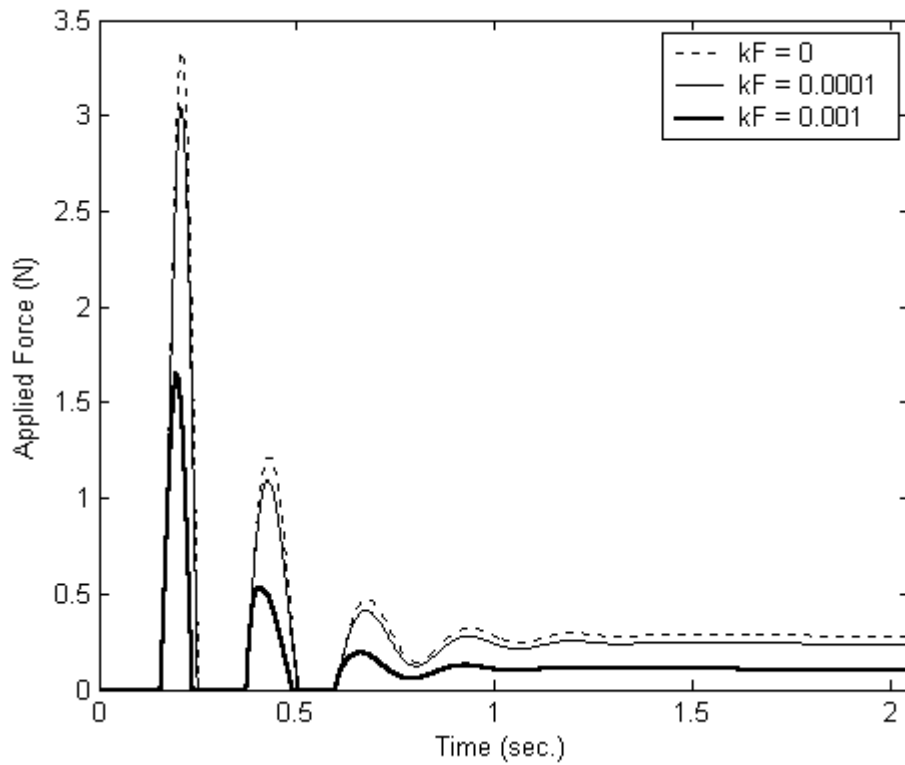


Figure 5.7 Force applied by the end-effector to the environment along \vec{u}_1^0 axis following a straight line on a planar surface

Applied force is decreased by a respectable amount by increasing the K_F parameter. As the K_F parameter increased over 0.01 for this simulation system becomes unstable. Although the applied force seems to reach steady state at a positive value of force from the Figure 5.7, it has a trend to converge to zero force in time. This can be seen clearly in the circle trajectory following case.

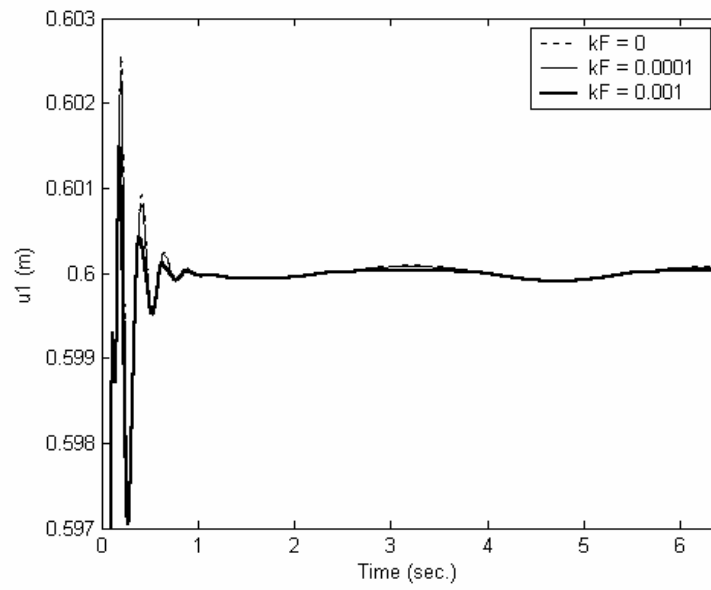


Figure 5.8 End-effector position in \vec{u}_1^0 axis following a circle path on a planar surface

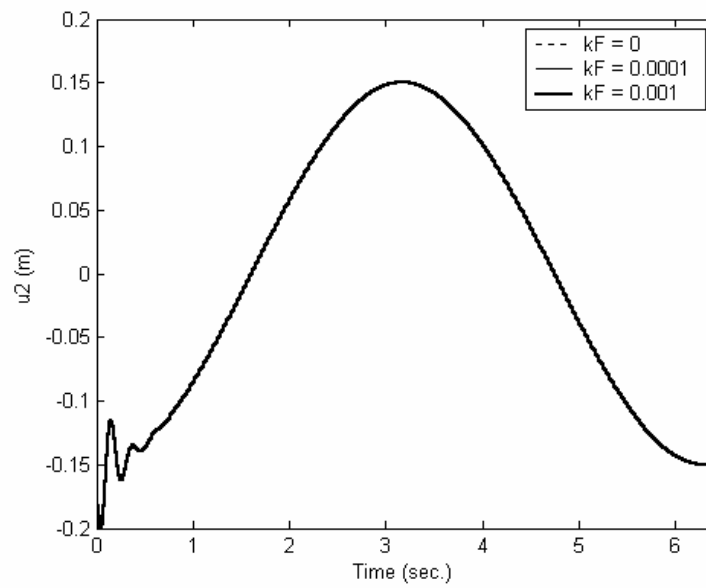


Figure 5.9 End-effector position in \vec{u}_2^0 axis following a circle path on a planar surface

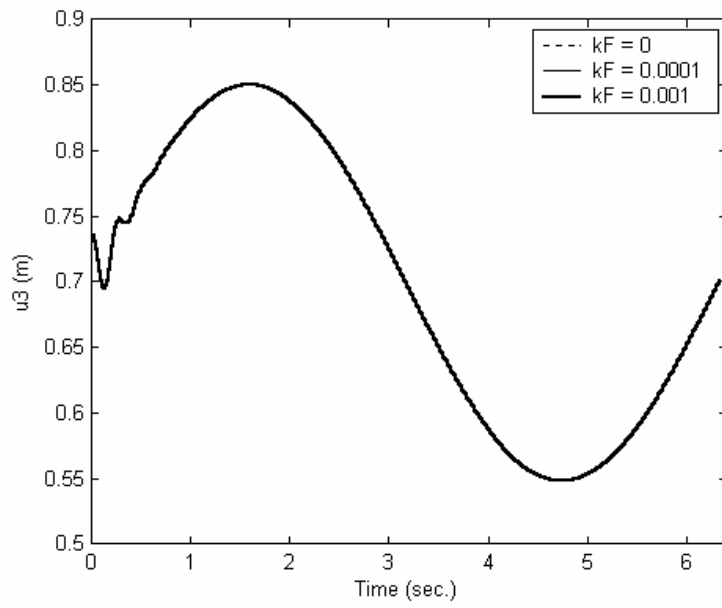


Figure 5.10 End-effector position in \bar{u}_3^0 axis following a circle path on a planar surface

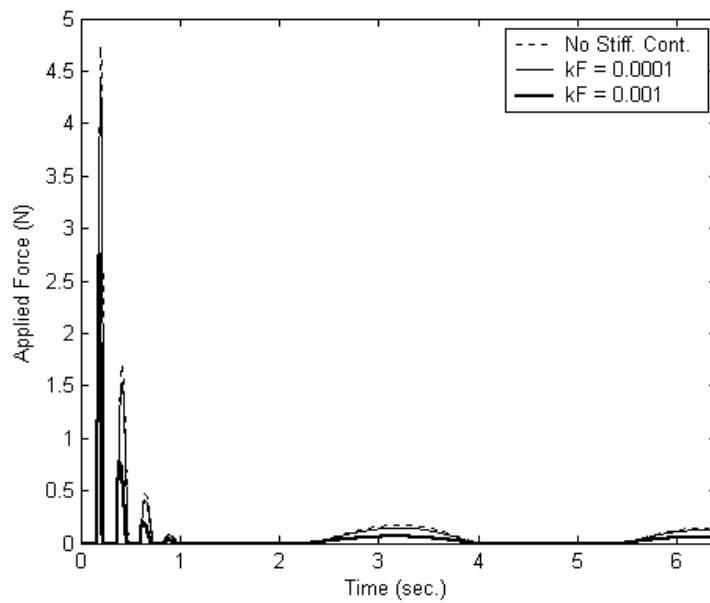


Figure 5.11 Force applied by the end-effector to the environment along \bar{u}_1^0 axis following a circle path on a planar surface

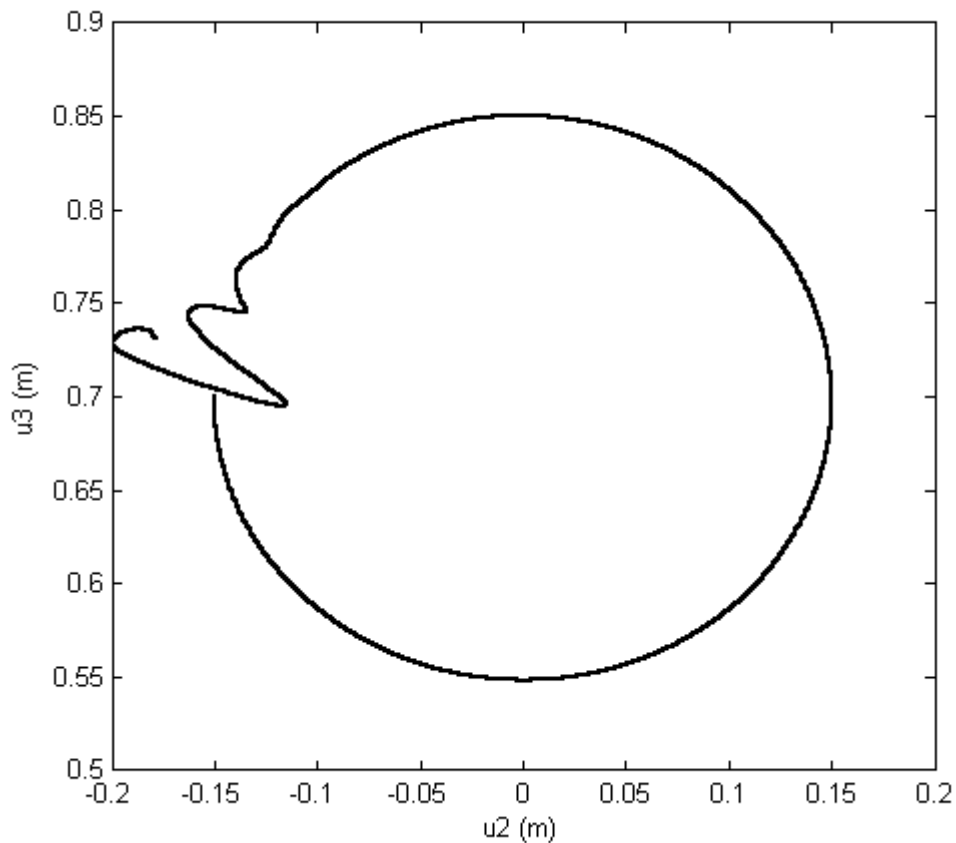


Figure 5.12 Circle path followed by the end-effector on the surface ($k_F = 0.0001$)

At the start of the motion of the manipulator, end-effector has a trend to move in the opposite direction of the circle path that it has to follow. Initial condition of the end-effector orientation is not set along the surface normal. Because of this, manipulator tries to correct the orientation of the end-effector while it tries to follow the demanded trajectory. The joints on the wrist have a better reaction time than the joints before the wrist, so the motion to correct the orientation dominates the motion to follow the trajectory at the start. This results as the motion in the opposite direction of the circle path at the start. This kind of response also true for the impedance and admittance controls.

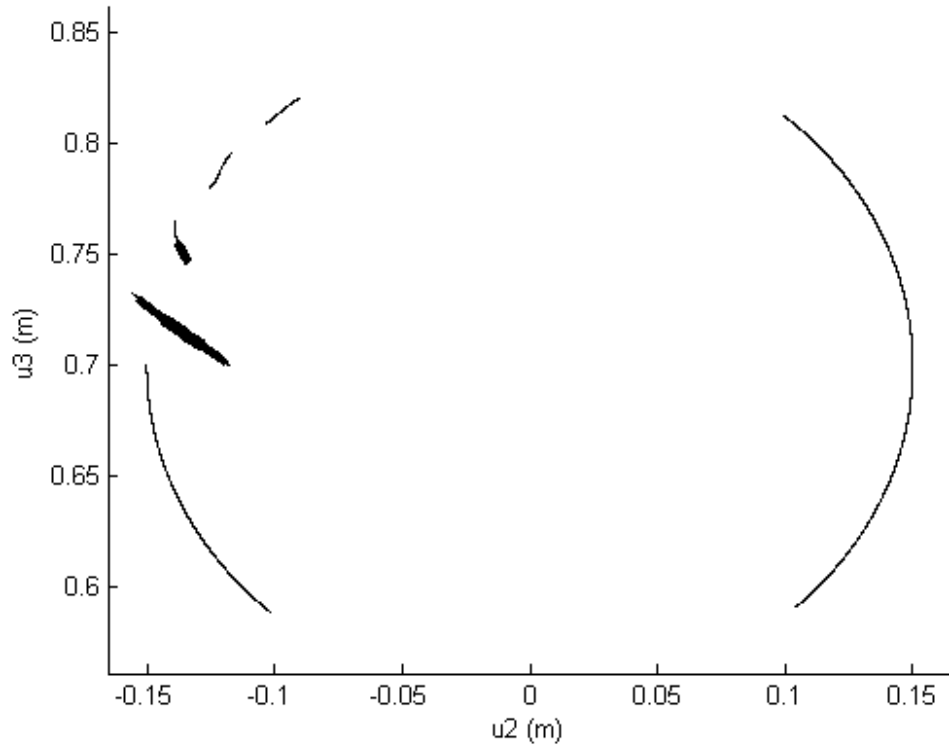


Figure 5.13 Circle drawn by the end-effector on the surface ($k_F = 0.0001$)

Figure 5.13 shows the line drawn by the end-effector on the surface with varying line width due to the magnitude of force exerted on the surface. The drawn circle is shown for only one of the changing parameters because the parameters changed to control the force exerted does not affect the motion along the other directions where no force is exerted.

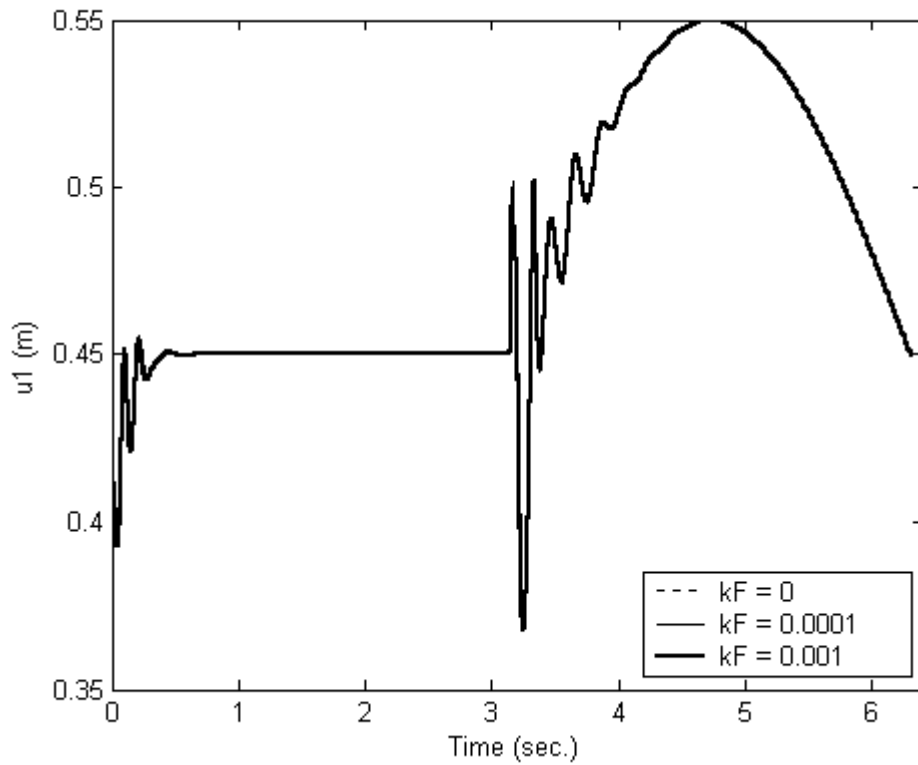


Figure 5.14 End-effector position in \bar{u}_1^0 axis following a circle path on a discontinuous surface

Half of the circle is followed on the plane formed by \bar{u}_2^0 and \bar{u}_3^0 axes, and the other half of the circle is followed on the plane formed by \bar{u}_1^0 and \bar{u}_3^0 axes. In the first half circle, the normal of the surface is along the \bar{u}_1^0 axis and in the second half of the circle the normal of the surface is along \bar{u}_2^0 axis. This means the forces will be applied along the \bar{u}_1^0 axis for the first half and along the \bar{u}_2^0 axis for the second half.

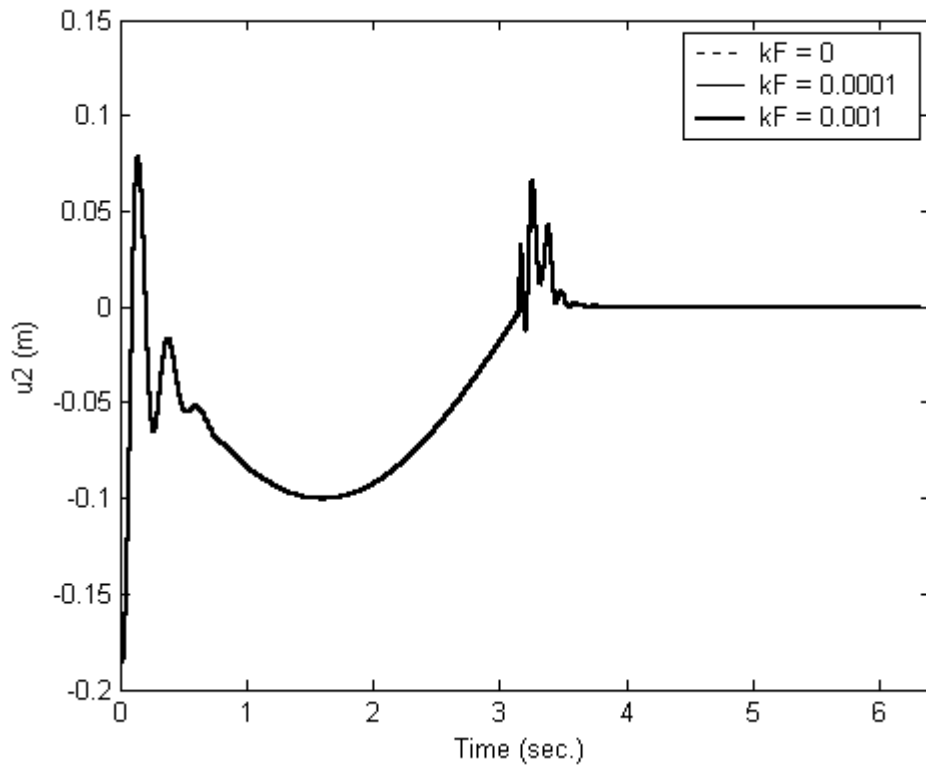


Figure 5.15 End-effector position in \vec{u}_2^0 axis following a circle path on a discontinuous surface

As it can be observed from the Figure 5.15, as the surface changes after 3 seconds, transient state is seen like the transient state at the start of the motion.

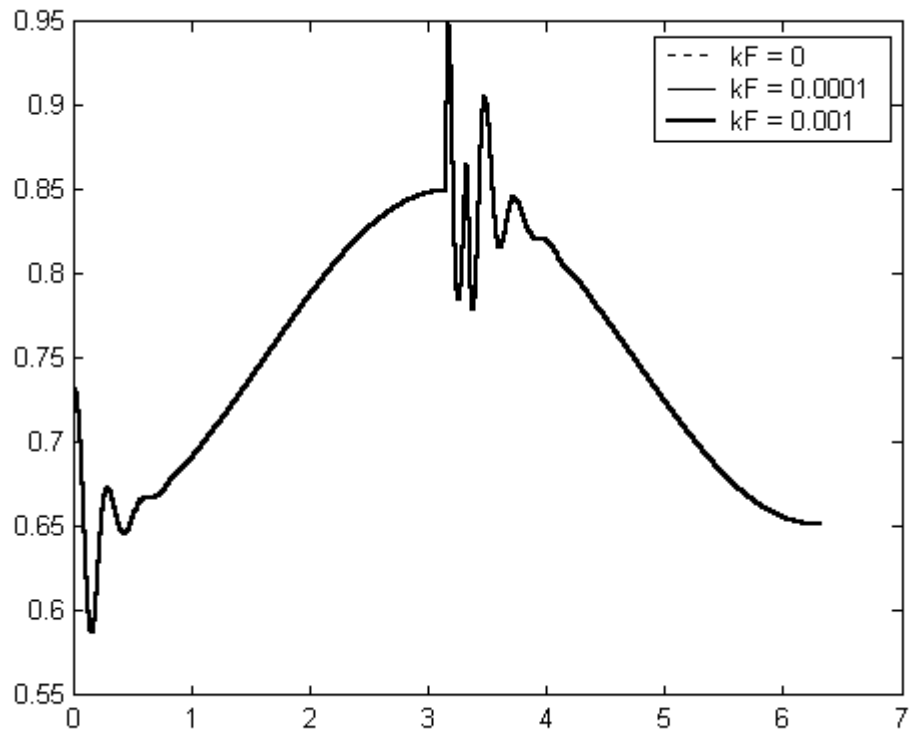


Figure 5.16 End-effector position in \bar{u}_3^0 axis following a circle path on a discontinuous surface

The transient state after 3 seconds can also be observed from the Figure 5.16 due to the change in the sudden change in the normal of the surface.

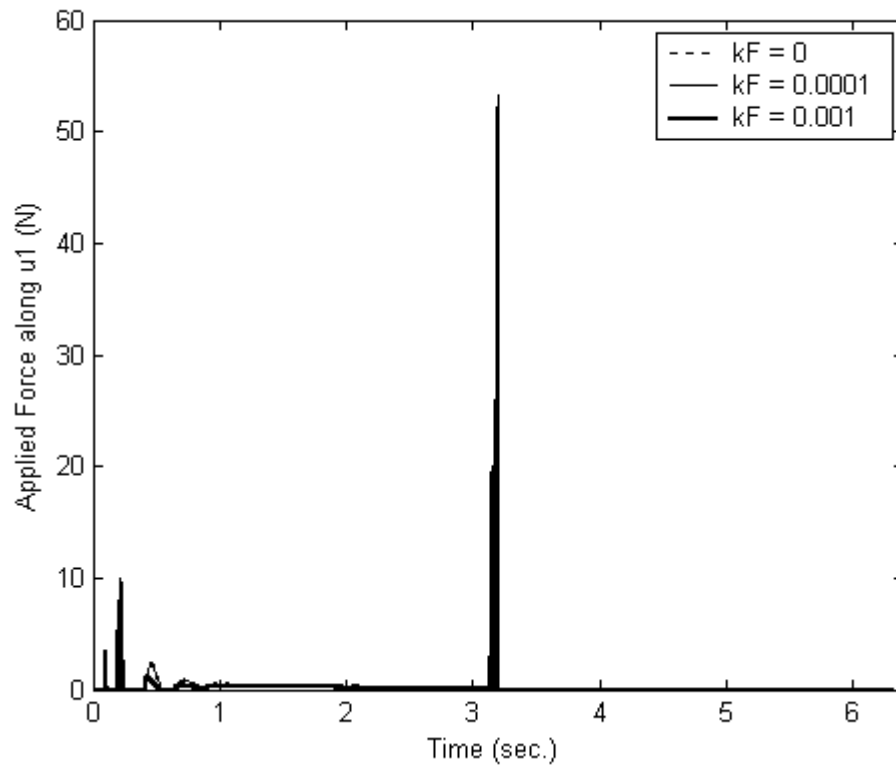


Figure 5.17 Force applied by the end-effector to the environment along \bar{u}_1^0 axis following a circle path on a discontinuous surface

The large amount of contact force that occurred after 3 seconds is caused because of the unstable transient state.

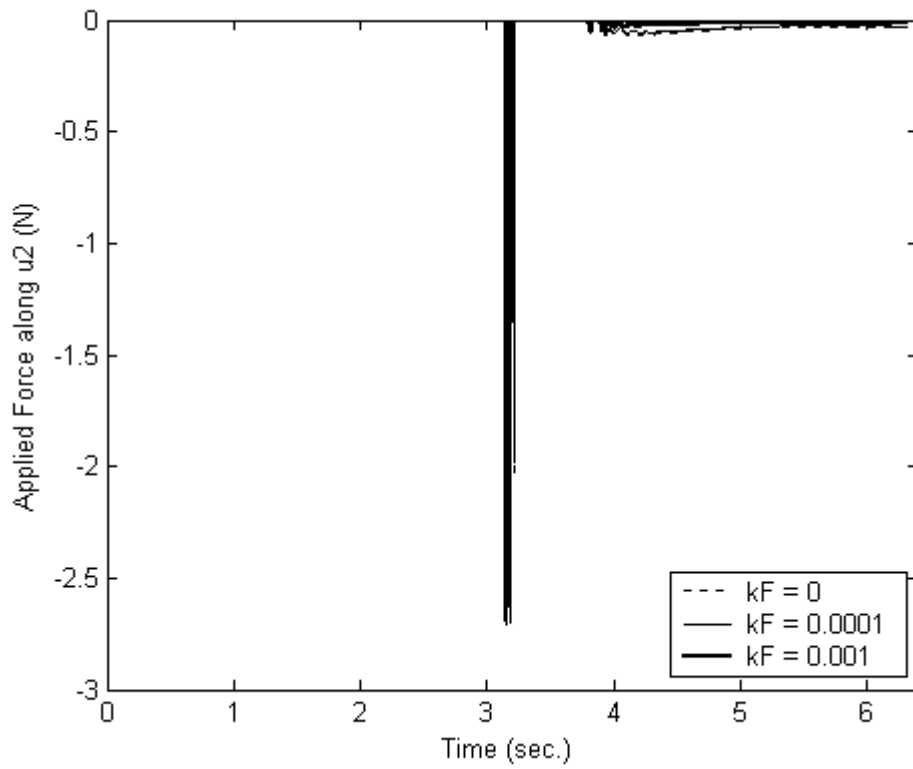


Figure 5.18 Force applied by the end-effector to the environment along \bar{u}_2^0 axis following a circle path on a discontinuous surface

The effect of the transient state when changing surface can be also seen from the Figure 5.18.

5.2 IMPEDANCE CONTROL SIMULATION RESULTS

Equation of motion for the position based second order impedance control is just like the equation of motion of the stiffness controlled manipulator. The only difference is in the modified desired trajectory term where instead of K_F , $(Ms^2 + Ds + K)^{-1}$ is used.

The position control parameters are determined as it is determined for the stiffness control. There is no desired force trajectory specified in the control algorithm of the impedance control. This concludes that the impedance control is used to minimize the interaction forces occurred while manipulation. For this reason as the $(Ms^2 + Ds + K)^{-1}$ term increases, the limit of the interaction forces is decreased.

$(Ms^2 + Ds + K)^{-1}$ term is considered as an second order system and the parameters of this term are determined within this assumption. ζ is selected as 0.8 and ω_n is selected as 15, 6 rad/s respectively.

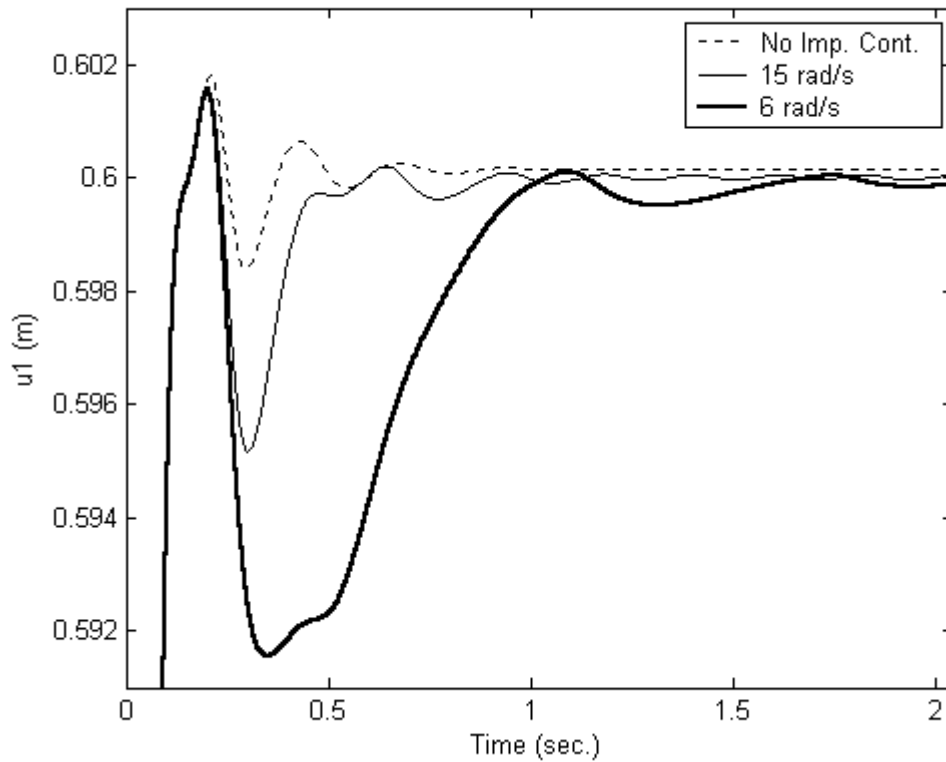


Figure 5.19 End-effector position in \bar{u}_1^0 axis following a straight line on a planar surface

Decreasing the ω_n in determining the parameters of the $(Ms^2 + Ds + K)^{-1}$ term, increases the overshoot in the only unconstrained motion but on the other hand decreases the magnitude of interaction forces. Optimal parameters can be selected differently due to the specification of different tasks. Whereas if smooth motions are required higher ω_n can be selected and if the decrease of interaction forces is the dominant factor lower ω_n can be selected.

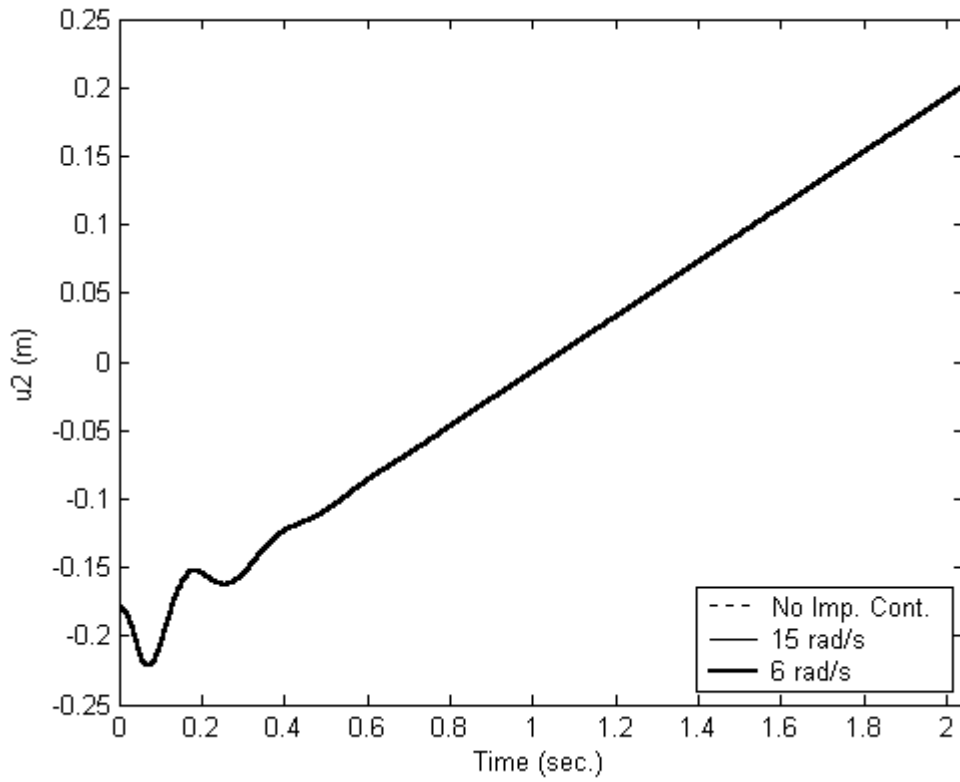


Figure 5.20 End-effector position in \vec{u}_2^0 axis following a straight line on a planar surface

The motion along the \vec{u}_2^0 and \vec{u}_3^0 axes are not affected while changing the impedance value along the \vec{u}_1^0 axis where the force is exerted along.

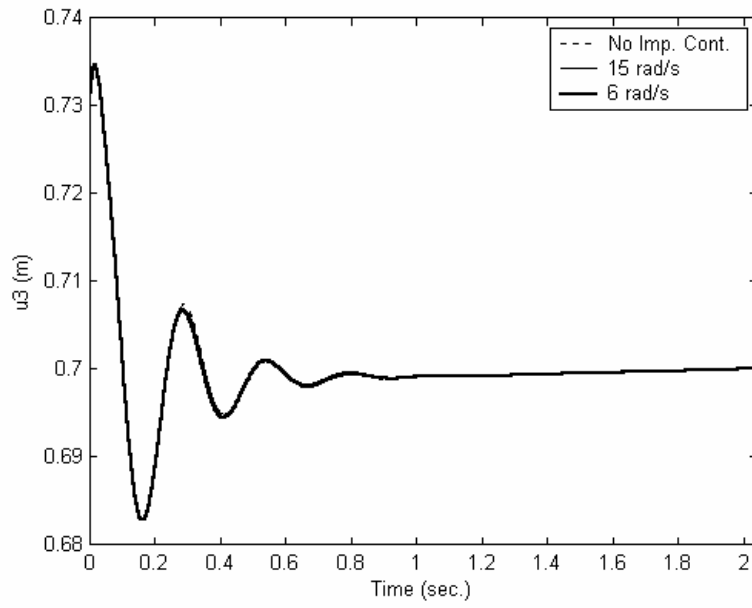


Figure 5.21 End-effector position in \vec{u}_3^0 axis following a straight line on a planar surface

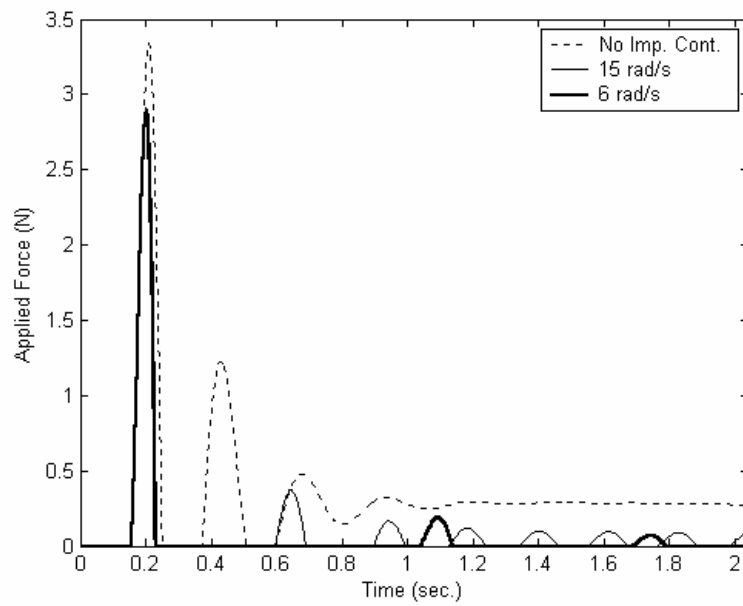


Figure 5.22 Force applied by the end-effector to the environment along \vec{u}_1^0 axis following a straight line on a planar surface

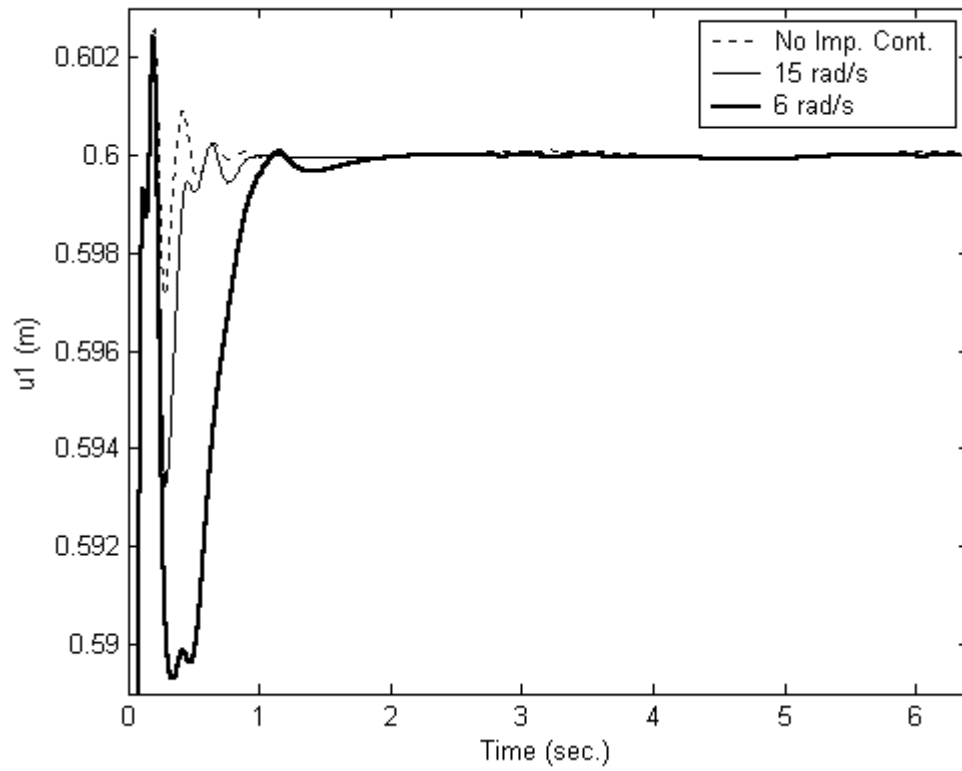


Figure 5.23 End-effector position in \vec{u}_1^0 axis following a circle path on a planar surface

Same kind of response is achieved for the circle trajectory task.

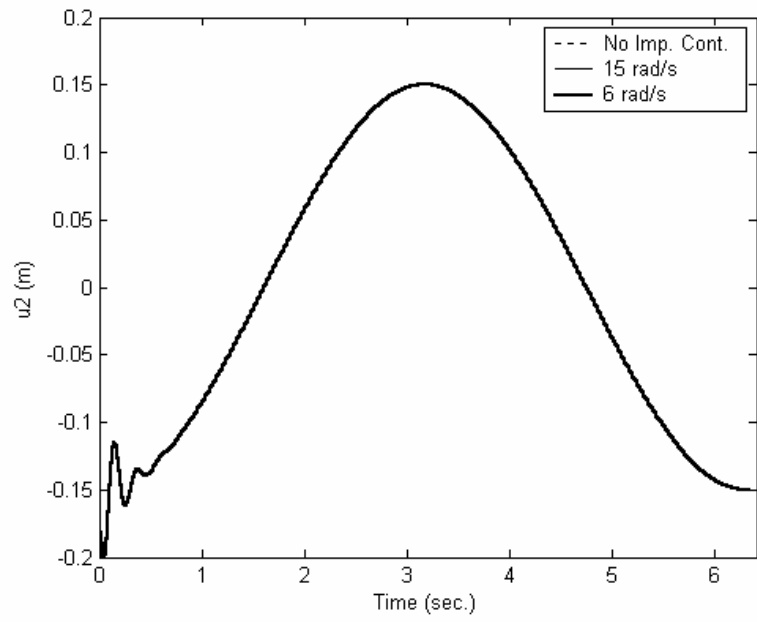


Figure 5.24 End-effector position in \bar{u}_2^0 axis following a circle path on a planar surface

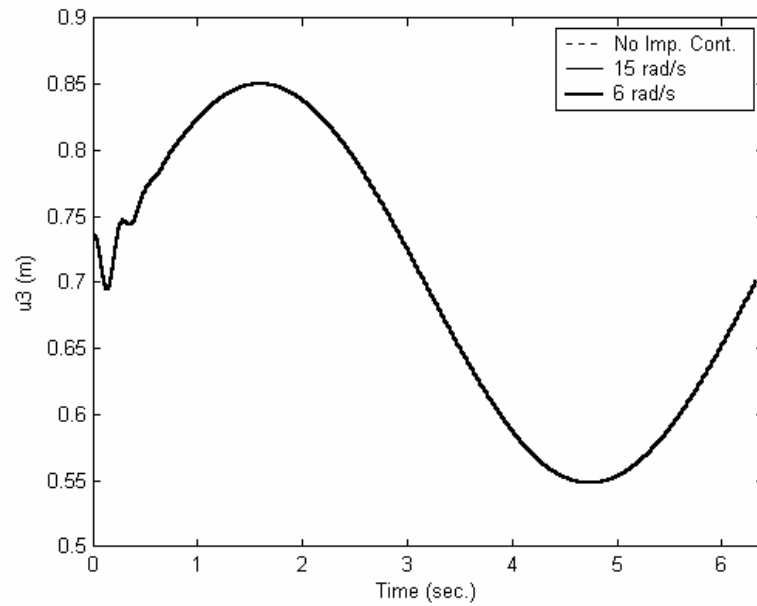


Figure 5.25 End-effector position in \bar{u}_3^0 axis following a circle path on a planar surface

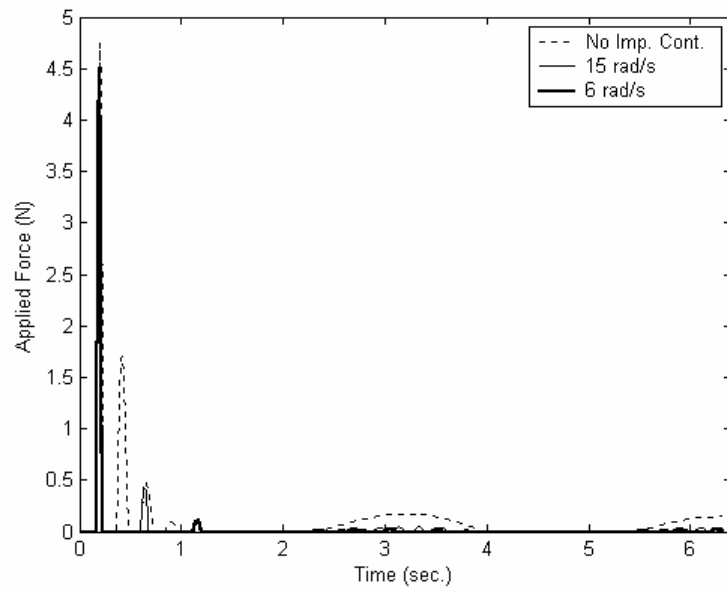


Figure 5.26 Force applied by the end-effector to the environment along \vec{u}_1^0 axis following a circle path on a planar surface

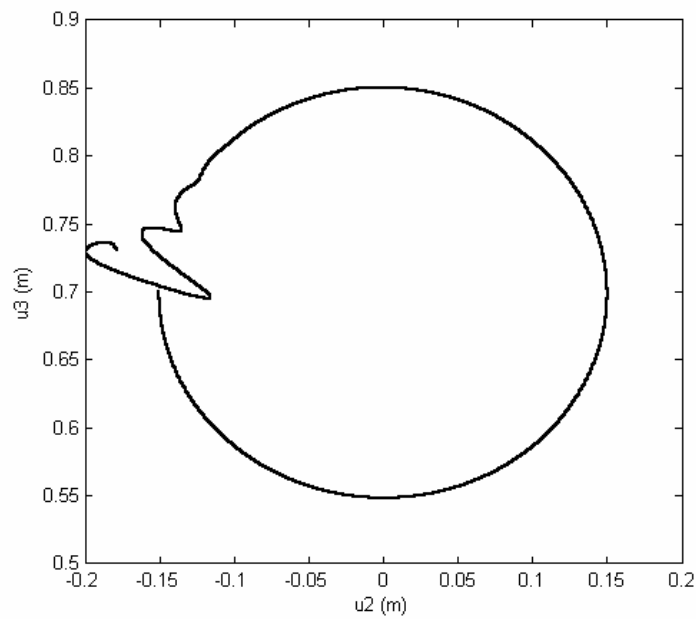


Figure 5.27 Circle path followed by the end-effector on the surface ($\omega_n = 15$ rad/sec.)

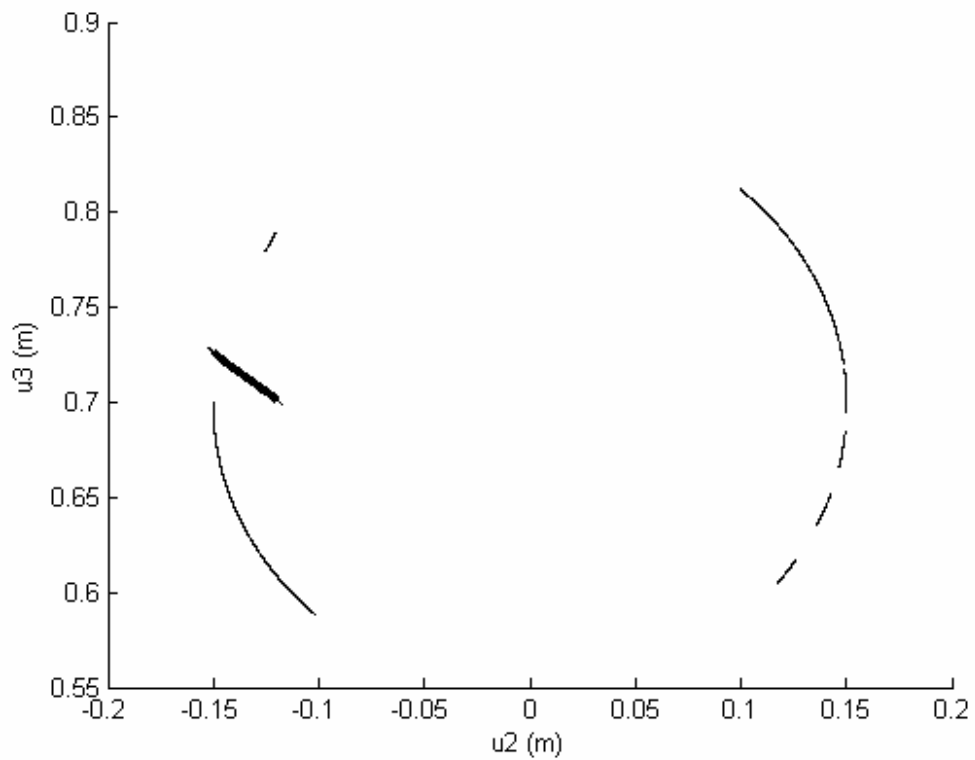


Figure 5.28 Circle drawn by the end-effector on the surface ($\omega_n = 15$ rad/sec.)

Figure 5.28 shows the line drawn by the end-effector on the surface with varying line width due to the magnitude of force exerted on the surface. The drawn circle is shown for only one of the changing parameters because the parameters changed to control the force exerted does not affect the motion along the other directions where no force is exerted.

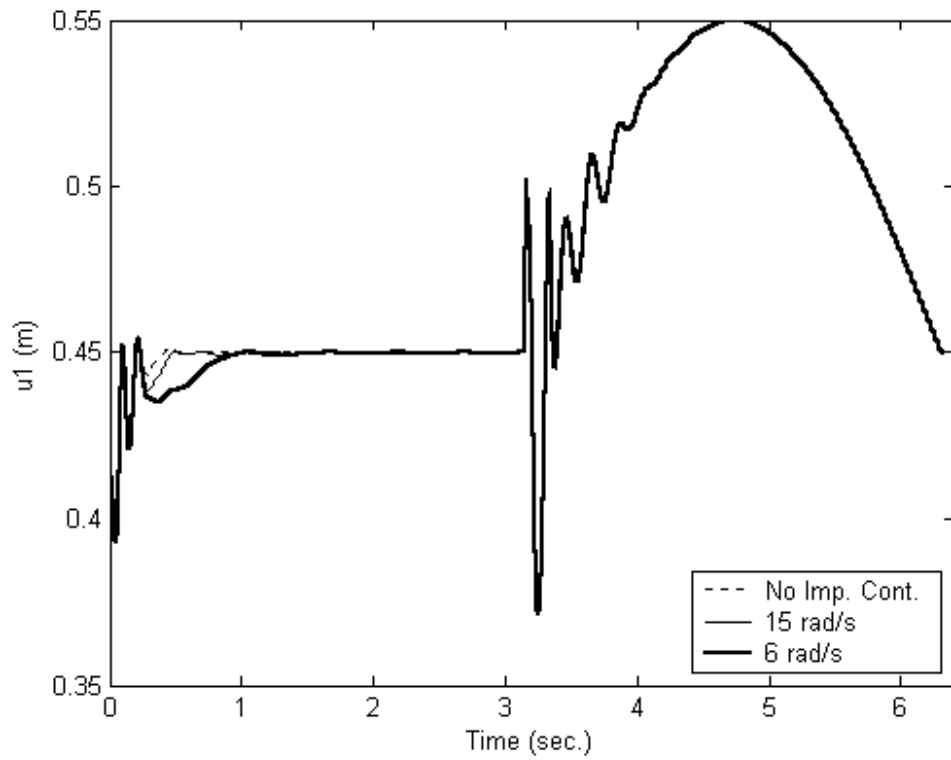


Figure 5.29 End-effector position in \vec{u}_1^0 axis following a circle path on a discontinuous surface

Same task as described in stiffness control is achieved with the impedance control for the circle trajectory following on a discontinuous surface. Transient state is visible just like in the stiffness control when moving from one surface to the other.

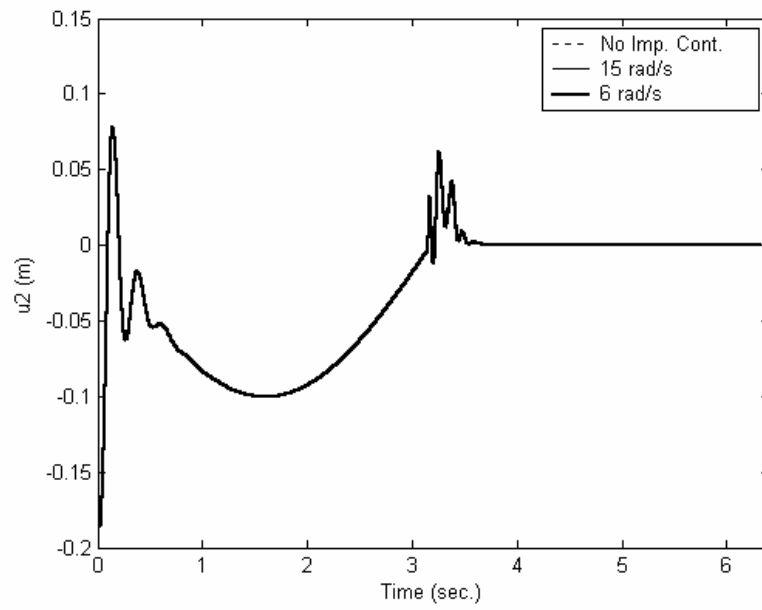


Figure 5.30 End-effector position in \vec{u}_2^0 axis following a circle path on a discontinuous surface

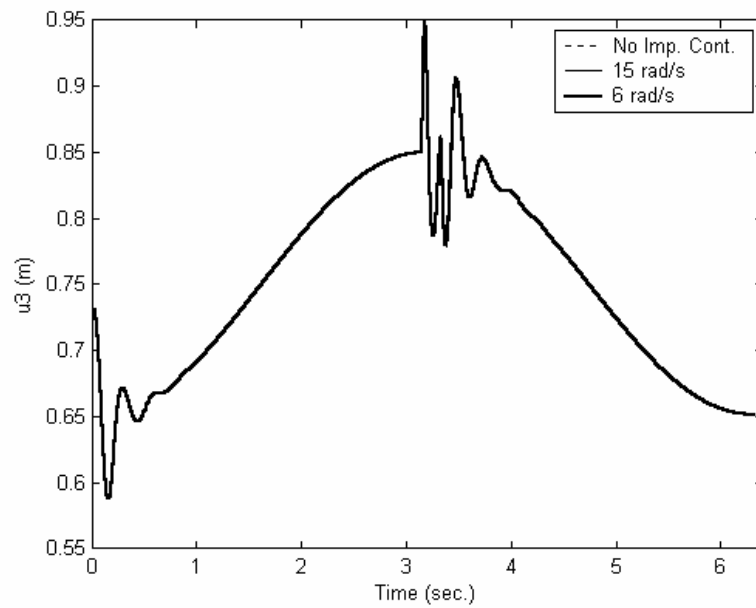


Figure 5.31 End-effector position in \vec{u}_3^0 axis following a circle path on a discontinuous surface

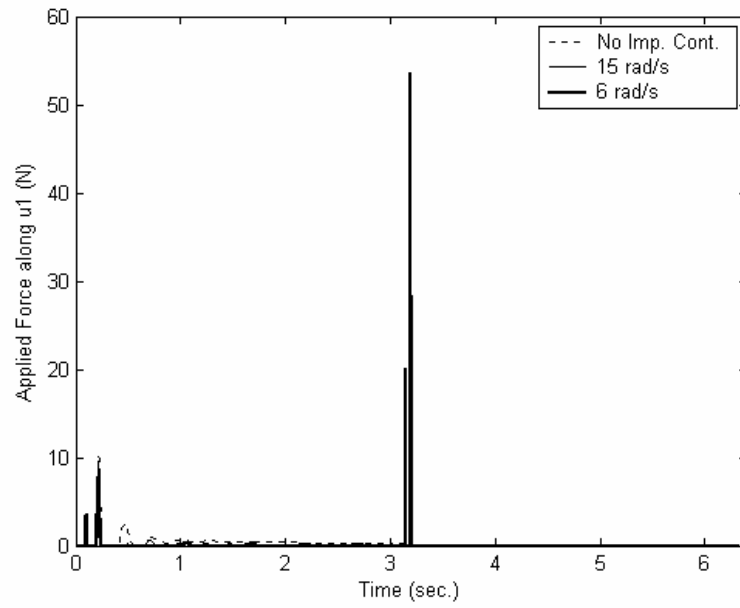


Figure 5.32 Force applied by the end-effector to the environment along \vec{u}_1^0 axis following a circle on a discontinuous surface

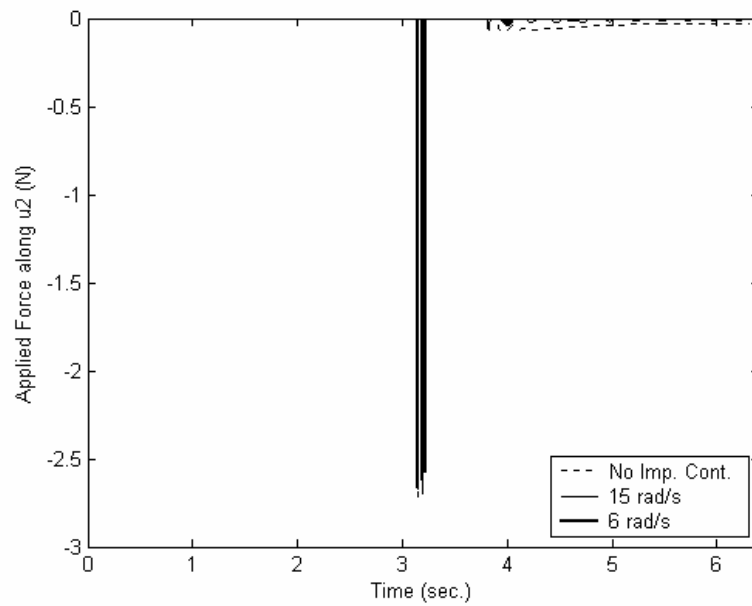


Figure 5.33 Force applied by the end-effector to the environment along \vec{u}_2^0 axis following a circle path on a discontinuous surface

5.3 ADMITTANCE CONTROL SIMULATION RESULTS

Admittance control modifies the desired position in order to achieve the desired force on the surface. Second order admittance term modifies to a PID controller as shown in Chapter 3. The parameters of the position controller is selected as it is selected in stiffness control and impedance control. Different values are tried for the PID parameters of the force controller which the results are shown in the below diagrams. The force to be applied to the surface is specified as 15 N.

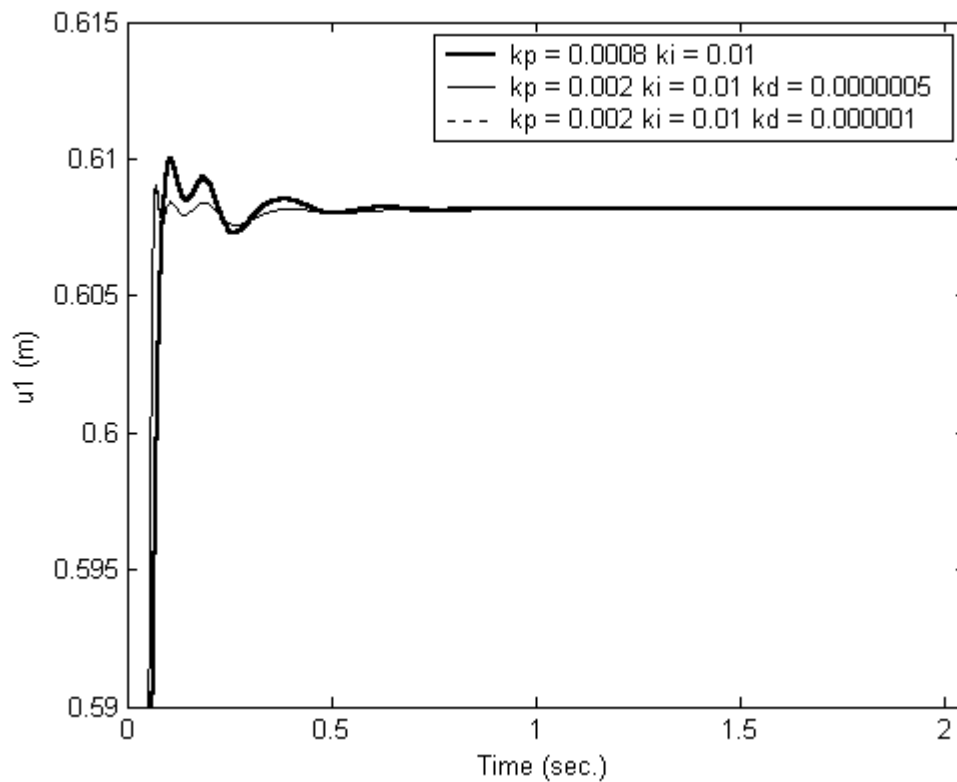


Figure 5.34 End-effector position in \vec{u}_1^0 axis following a straight line on a planar surface

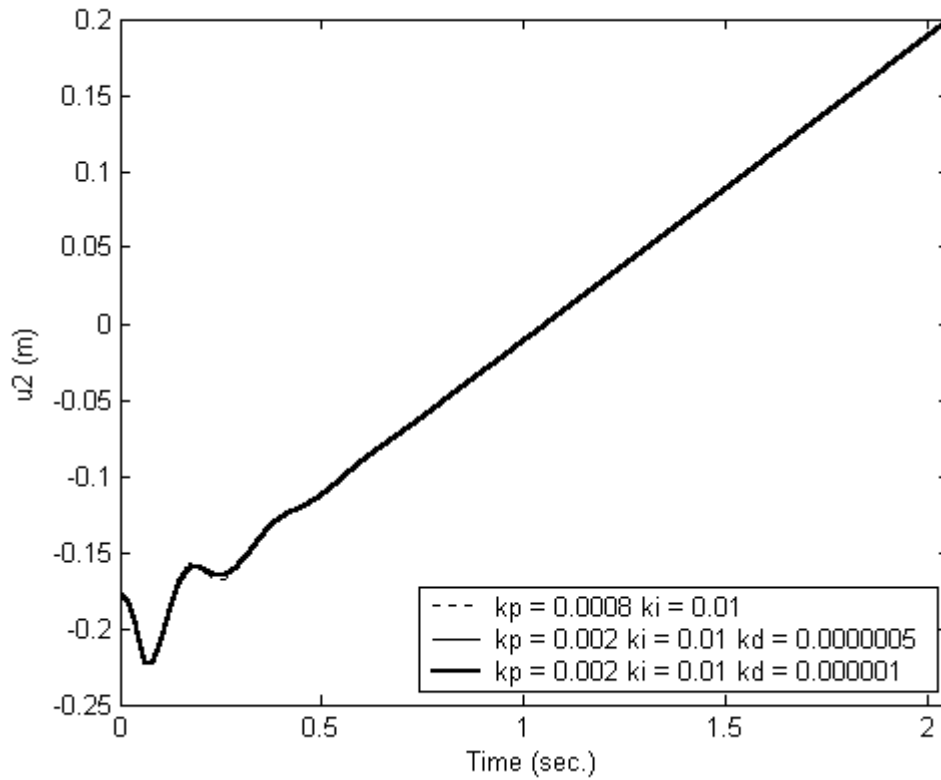


Figure 5.35 End-effector position in \vec{u}_2^0 axis following a straight line on a planar surface

The modification made by the force controller on the desired position does not affect the motions that are not aligned with the force to be exerted. This can be seen clearly from Figures 5.35 and 5.36.

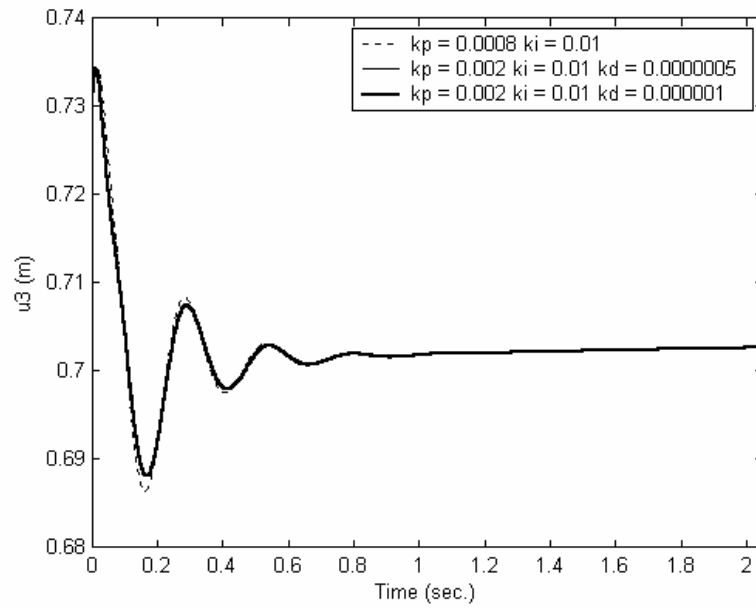


Figure 5.36 End-effector position in \vec{u}_3^0 axis following a straight line on a planar surface

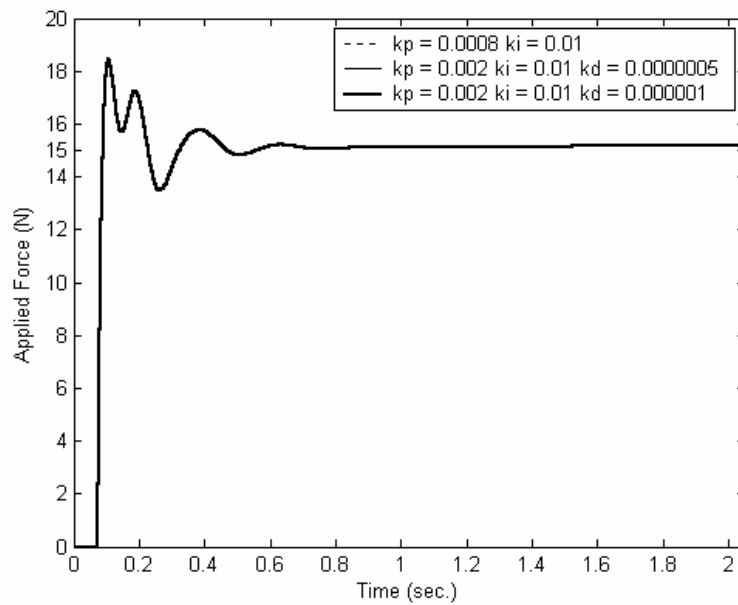


Figure 5.37 Force applied by the end-effector to the environment along \vec{u}_1^0 axis following a straight line on a planar surface

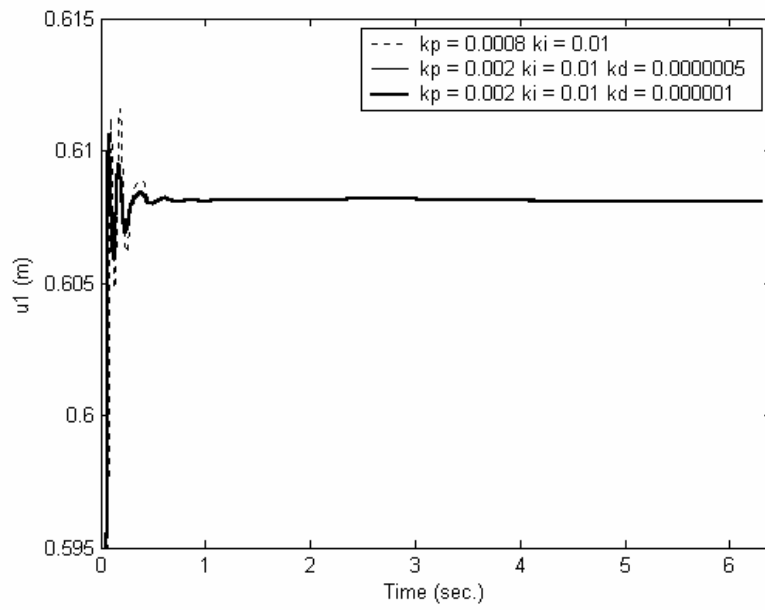


Figure 5.38 End-effector position in \bar{u}_1^0 axis following a circle path on a planar surface

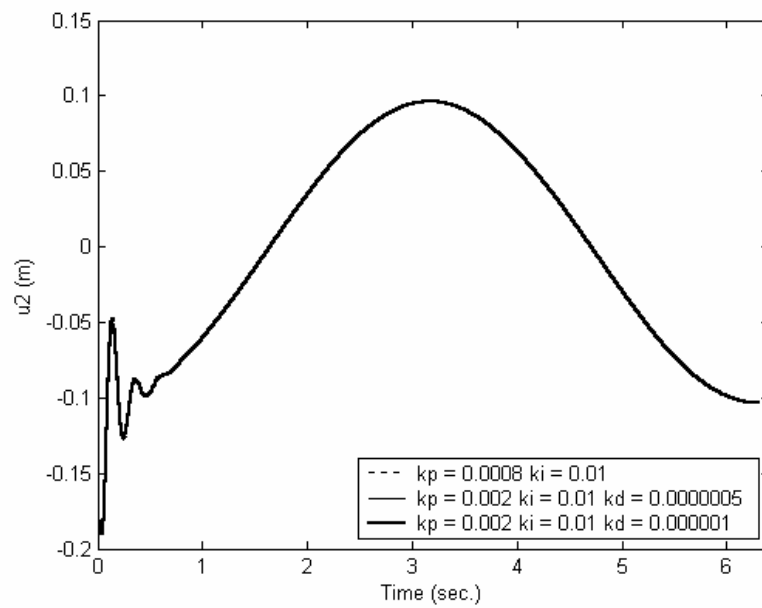


Figure 5.39 End-effector position in \bar{u}_2^0 axis following a circle path on a planar surface

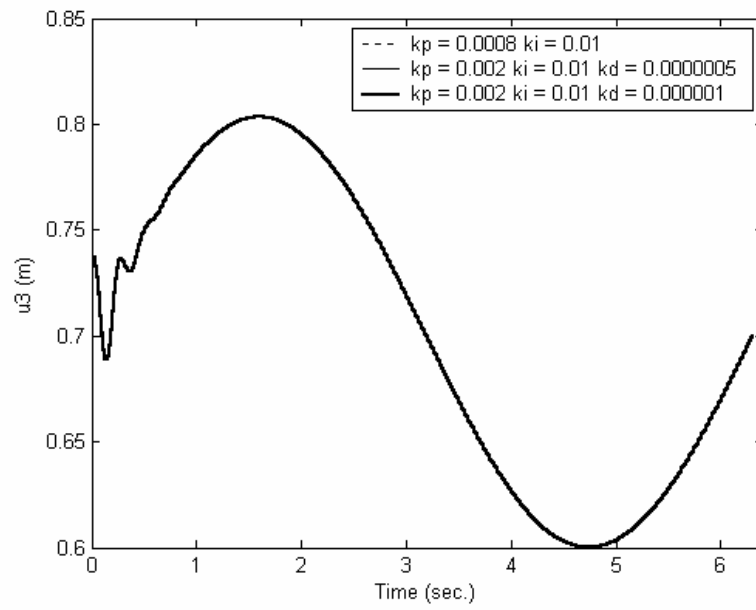


Figure 5.40 End-effector position in \vec{u}_3^0 axis following a circle path on a planar surface

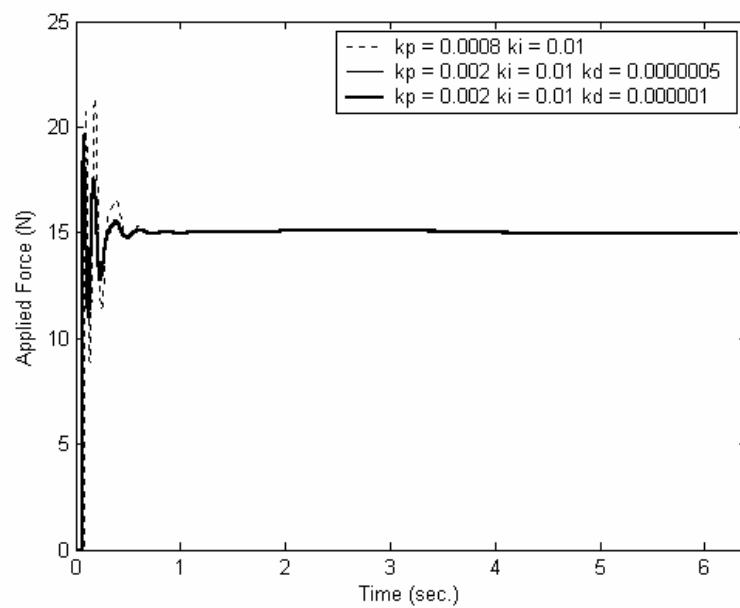


Figure 5.41 Force applied by the end-effector to the environment along \vec{u}_1^0 axis following a circle path on a planar surface

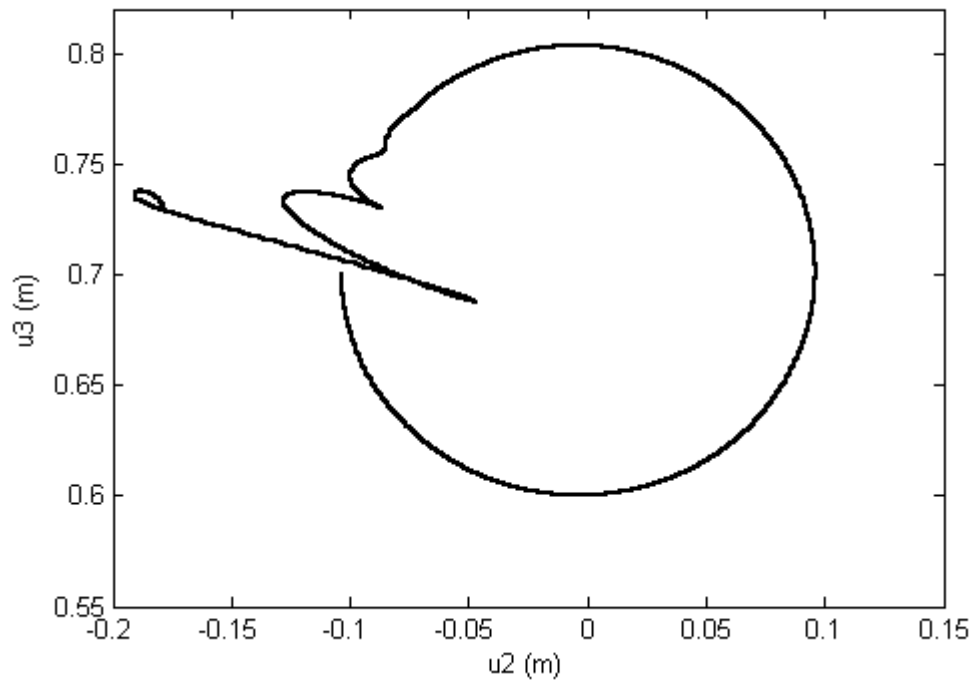


Figure 5.42 Circle path followed by the end-effector on the surface ($k_p = 0.0008$,
 $k_i = 0.01$)

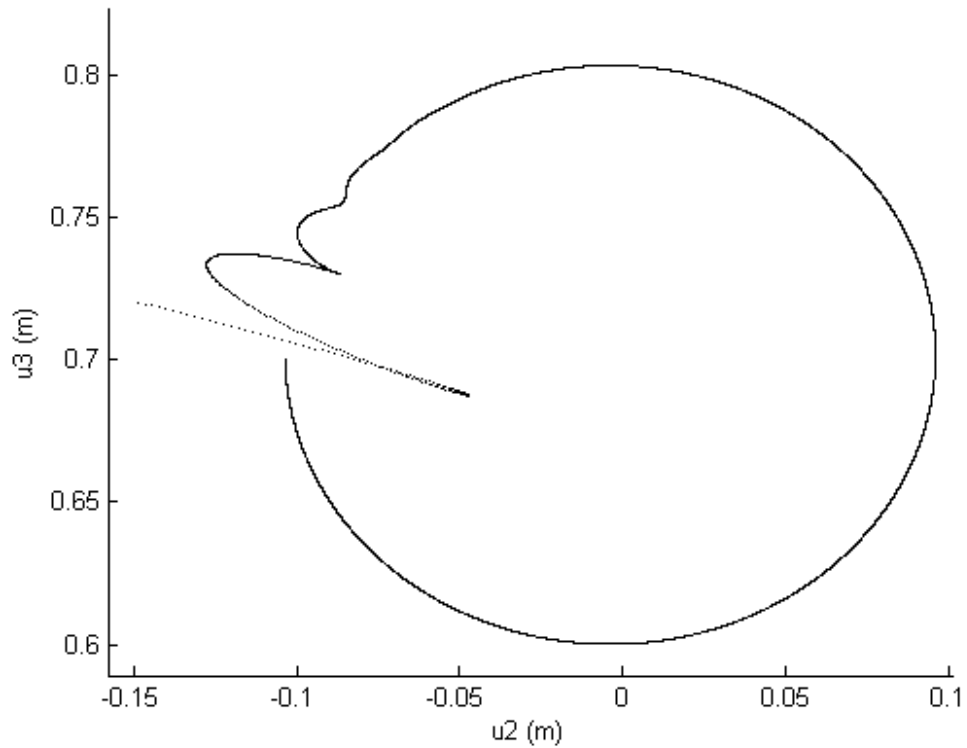


Figure 5.43 Circle drawn by the end-effector on the surface ($k_p = 0.0008$,
 $k_i = 0.01$)

Figure 5.43 shows the line drawn by the end-effector on the surface with varying line width due to the magnitude of force exerted on the surface. The drawn circle is shown for only one of the changing parameters because the parameters changed to control the force exerted does not affect the motion along the other directions where no force is exerted.

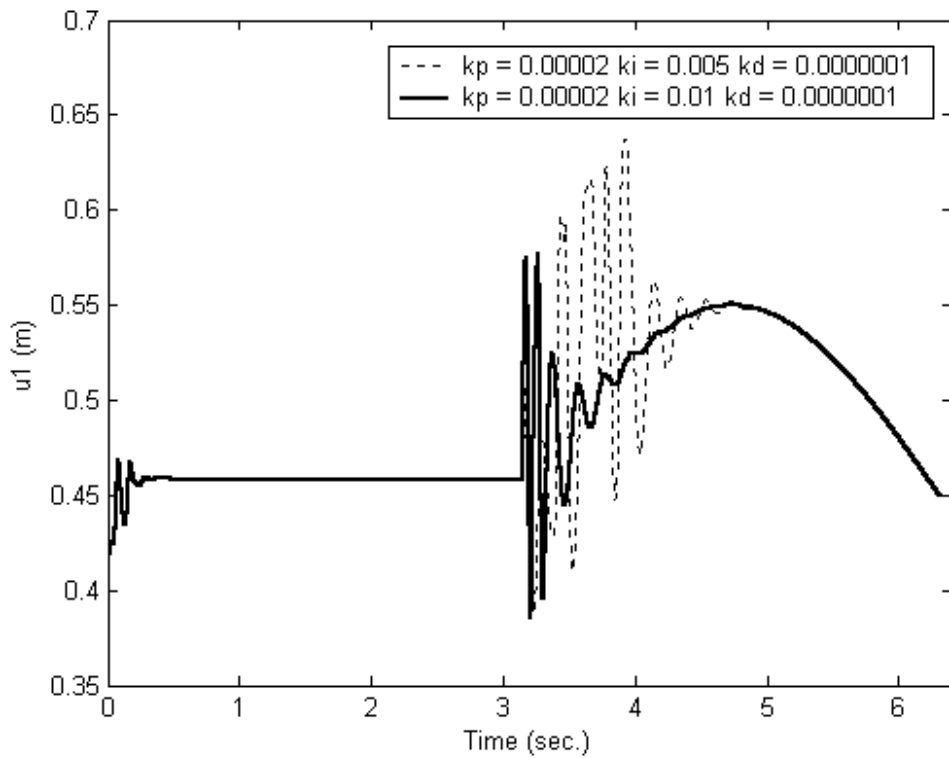


Figure 5.44 End-effector position in \vec{u}_1^0 axis following a circle path on a discontinuous surface

$k_p = 0.002$, $k_i = 0.01$ and $k_d = 0.000001$ selected for the force control PID parameters in \vec{u}_1^0 axis. The PID force control parameters selected for the forces in \vec{u}_2^0 axis are stated on the diagrams followed. This adjustment was necessary because during the transient state, while moving from one surface to the other, great amounts of forces are calculated with the PID parameters of the \vec{u}_1^0 axis and as a result of this great overshoots in position trajectories observed.

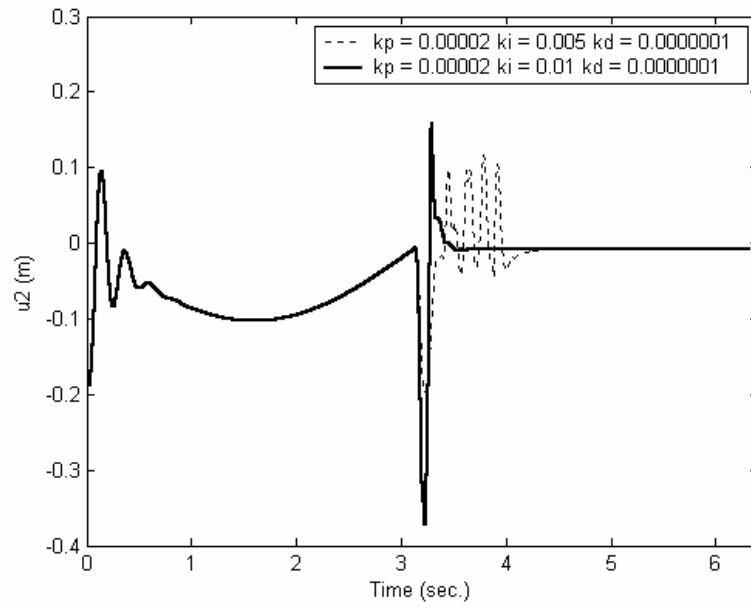


Figure 5.45 End-effector position in \bar{u}_2^0 axis following a circle path on a discontinuous surface

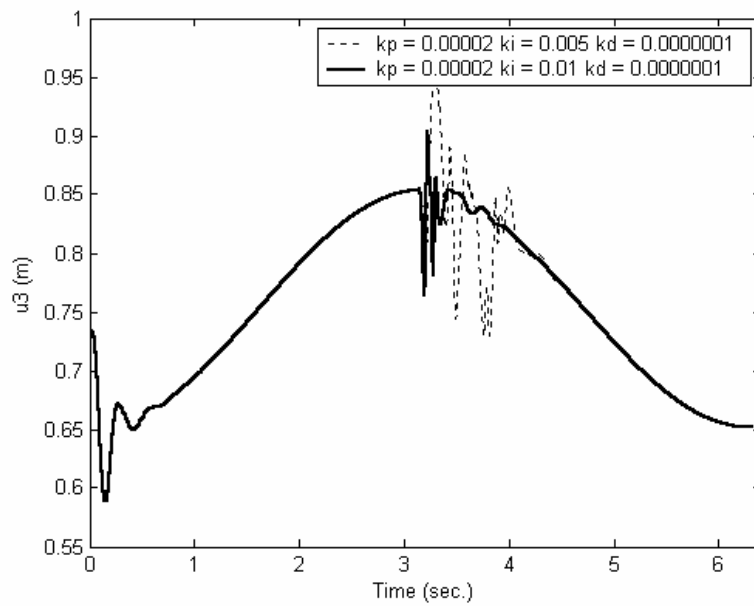


Figure 5.46 End-effector position in \bar{u}_3^0 axis following a circle path on a discontinuous surface

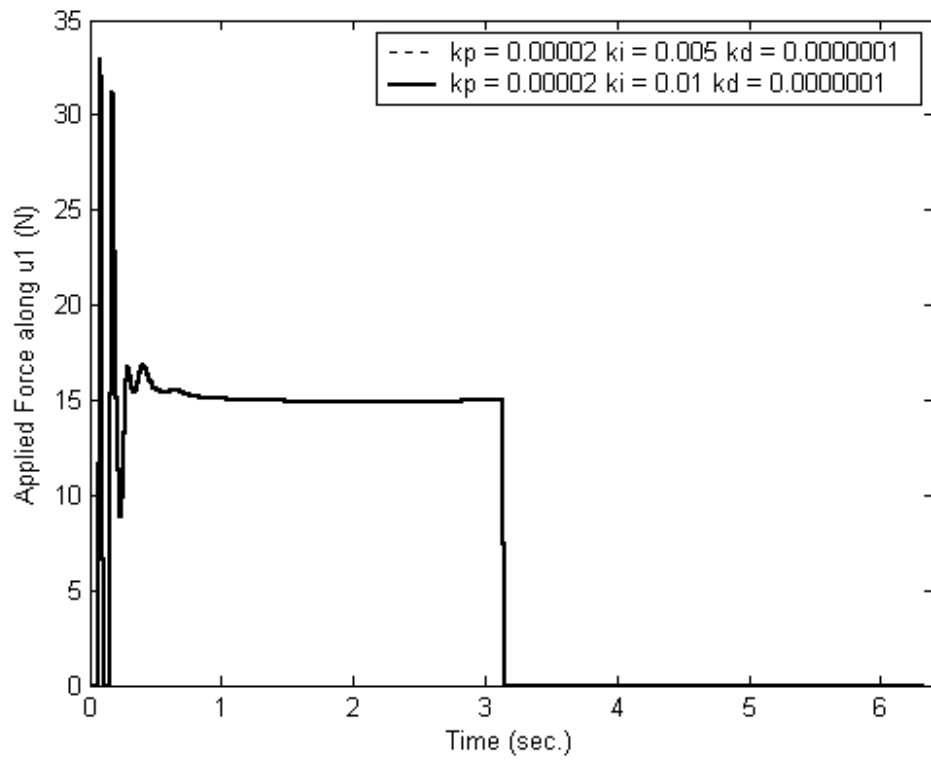


Figure 5.47 Force applied by the end-effector to the environment along \vec{u}_1^0 axis following a circle on a discontinuous surface

The applied force responses in \vec{u}_1^0 axis came out to be the same because the same PID force control parameters are used for the force control in \vec{u}_1^0 axis.

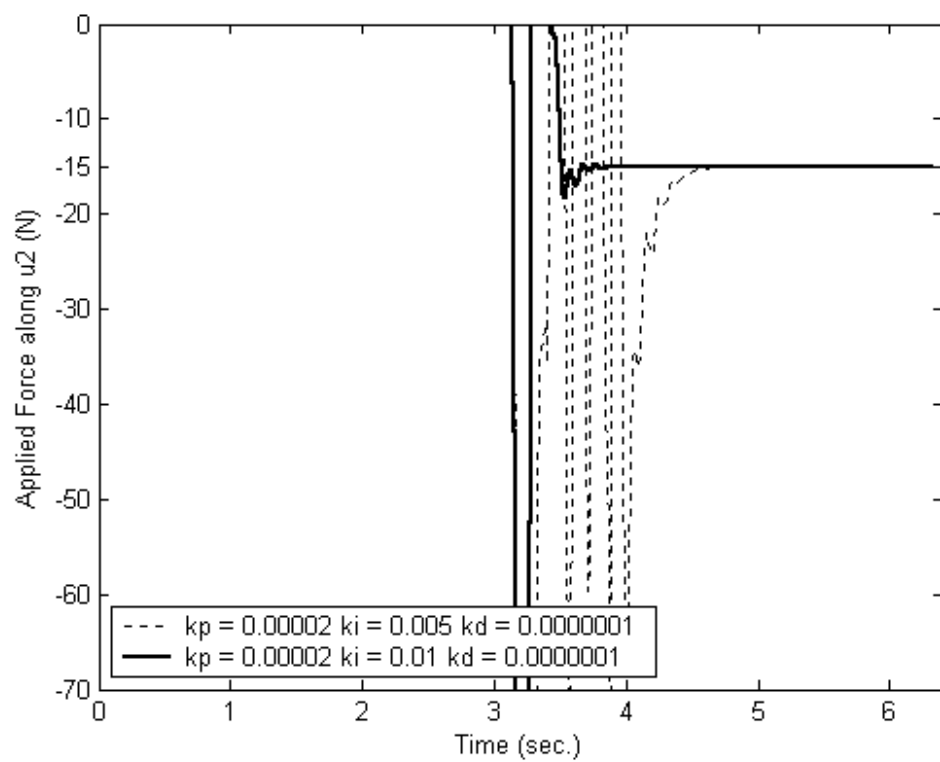


Figure 5.48 Force applied by the end-effector to the environment along \vec{u}_2^0 axis following a circle path on a discontinuous surface

5.4 HYBRID POSITION/FORCE CONTROL SIMULATION RESULTS

Hybrid control algorithm is also modified to make the necessary comparisons in the Joint Space and not in the Cartesian Space as shown in Figure 5.49.

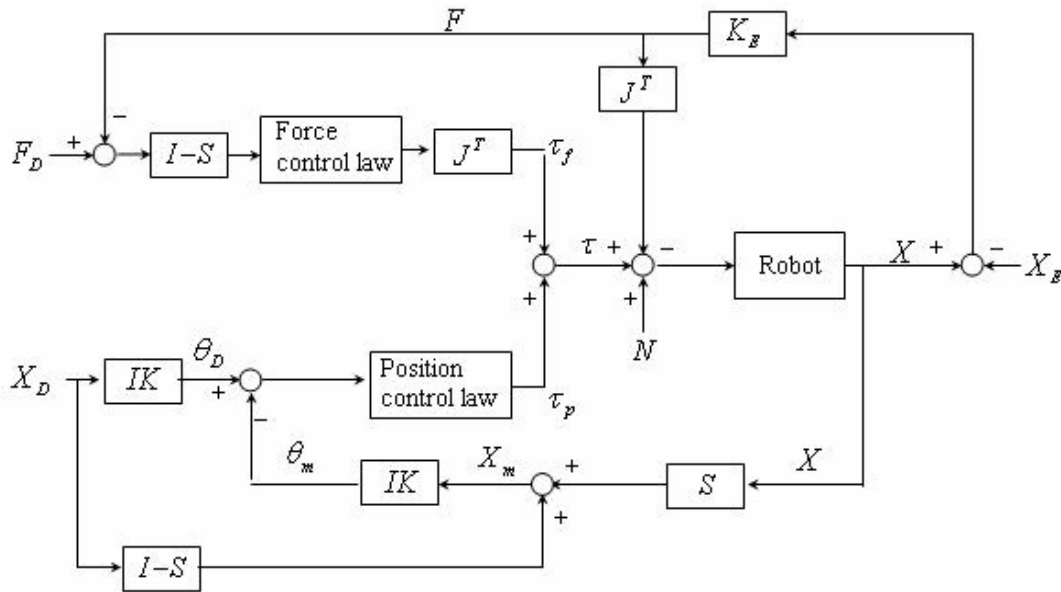


Figure 5.49 Modified hybrid position/force control algorithm

This modified version of the Hybrid Control does not use the selection matrix, “ S ” after the comparison is made in the Cartesian Space for the position control subspace. The selection matrix is used to take the measured positions along the directions to be position controlled as they are and modify the measured position along the direction to be force controlled to the desired position along that direction. This makes the position error along the direction to be force controlled equal to zero which means the position control subspace will not try to monitor the position along that direction.

After these modification on the measured position, “ X ”, modified measured position, “ X_m ”, is transform to Joint Space to calculate modified measured joint angles, “ θ_m ”, using the inverse kinematics equations. Desired position is also transformed to the Joint Space using the inverse kinematics equations. As a result of this the comparison is made in the Joint Space and the outcome is fed into the position controller. PD control is selected as the position controller like for the other position controllers used in the past simulations. Also the PD parameters are selected as they are selected in the past simulations of Stiffness, Impedance and Admittance Controls.

The force controller is used before the force error is transformed to Joint Space from the Cartesian space as a modification to the conventional force controlled subspace. The modification is made to choose only the parameters of one PI controller and not to choose PI parameters for each joint.

The slope of the motion along \vec{u}_1^0 changes and becomes steeper as the manipulator hits the surface and the control switches to Hybrid Control from a simple position control in the Figure 5.50. When the position control is active, it tries to move the end-effector to the surface and when the end-effector is near the surface the slope of the motion to the surface decreases. As soon as the end-effector hits the surface, the control is switched to Hybrid Control and the force control subspace of this control increases the slope of the motion into the surface to reach the desired force.

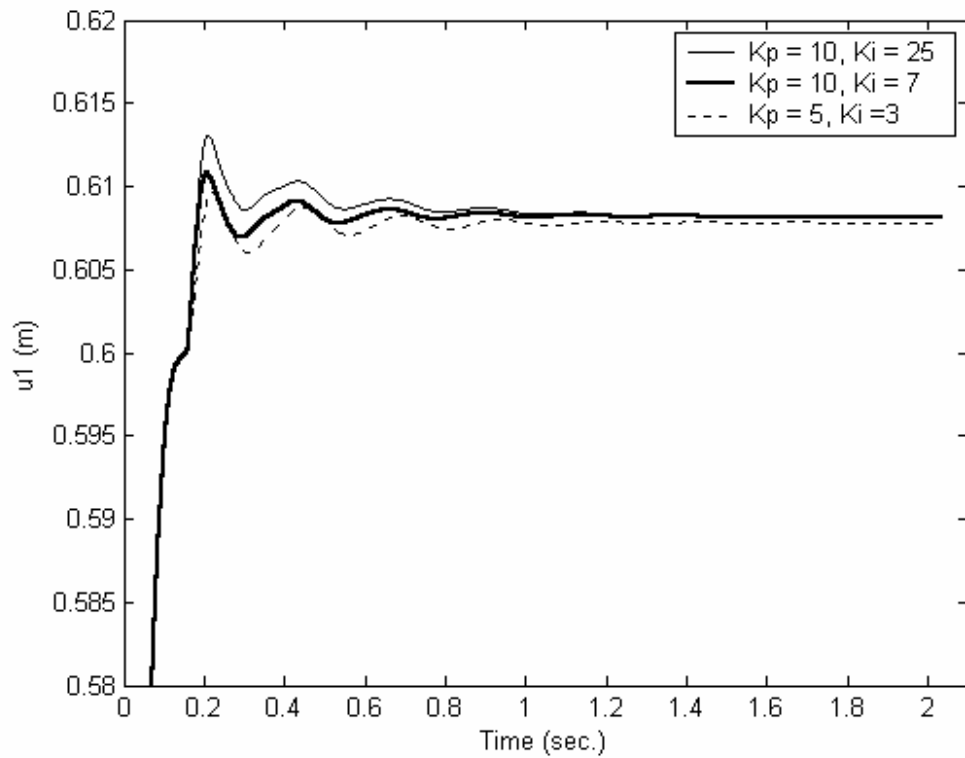


Figure 5.50 End-effector position in \vec{u}_1^0 axis following a straight line on a planar surface

PI type of control is used for the force controller. As it can be observed from the Figures 5.50 and 5.53, when the integral gain, k_i , rises the overshoot becomes bigger and when small values are selected for the integral gain, overshoot becomes smaller but a steady state error arises. Change in the proportional gain, k_p , changes the time to reach the steady state as it can be seen from the Figures 5.50 and 5.53.

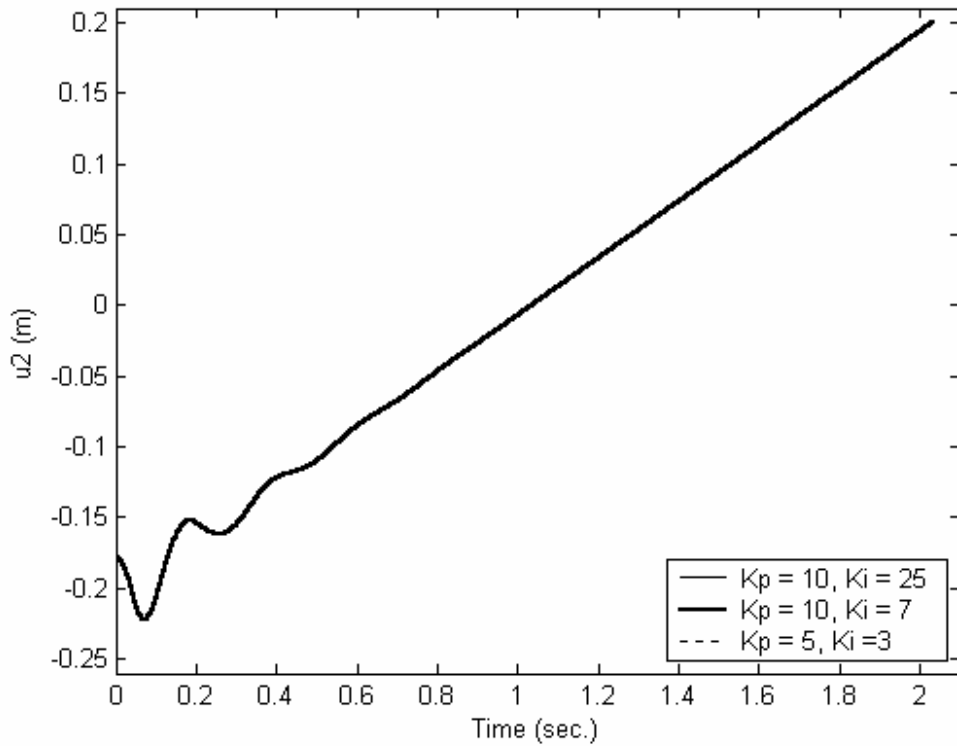


Figure 5.51 End-effector position in \vec{u}_2^0 axis following a straight line on a planar surface

The change in the force control parameters of the Hybrid Control does not affect the motions of the end-effector along the other directions as it can be seen from the Figures 5.51 and 5.52.

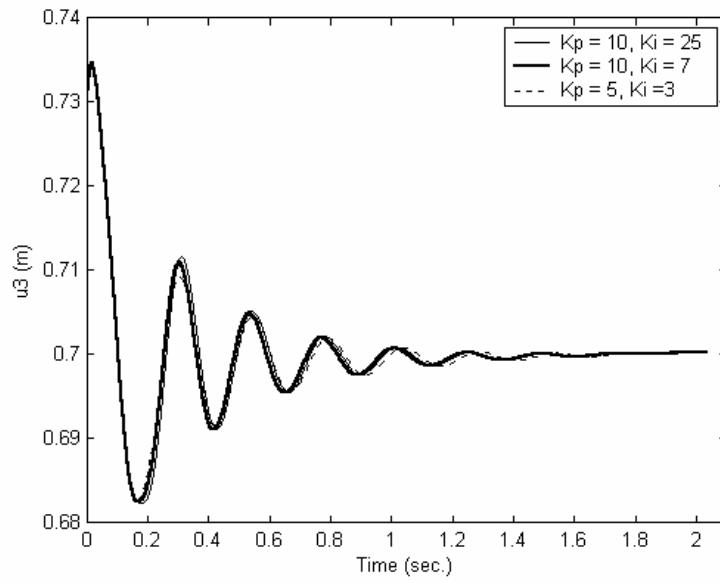


Figure 5.52 End-effector position in \vec{u}_3^0 axis following a straight line on a planar surface

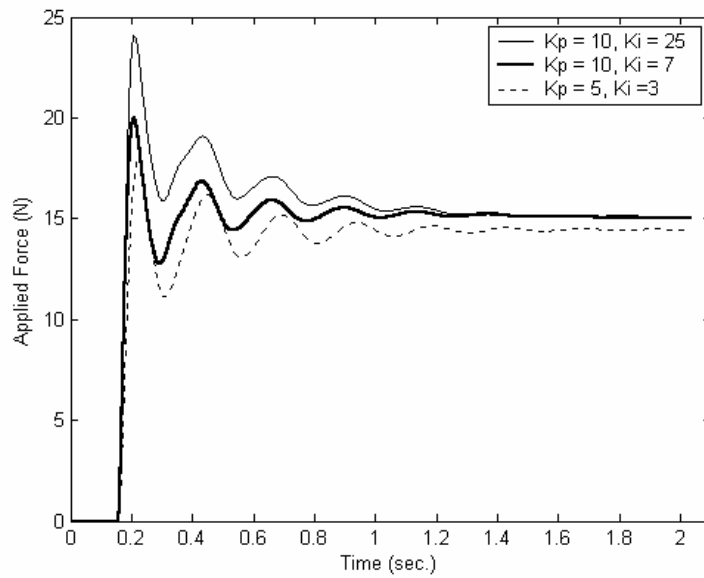


Figure 5.53 Force applied by the end-effector to the environment along \vec{u}_1^0 axis following a straight line on a planar surface

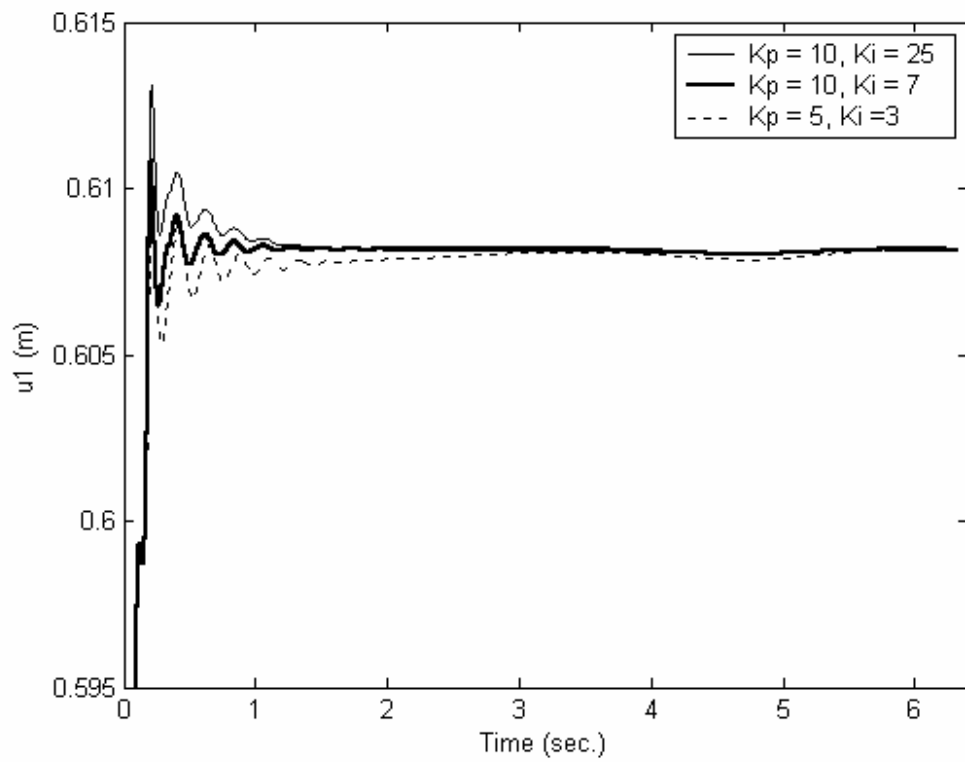


Figure 5.54 End-effector position in \bar{u}_1^0 axis following a circle path on a planar surface

Same kinds of responses are measured for the circle drawing on a planar surface task.

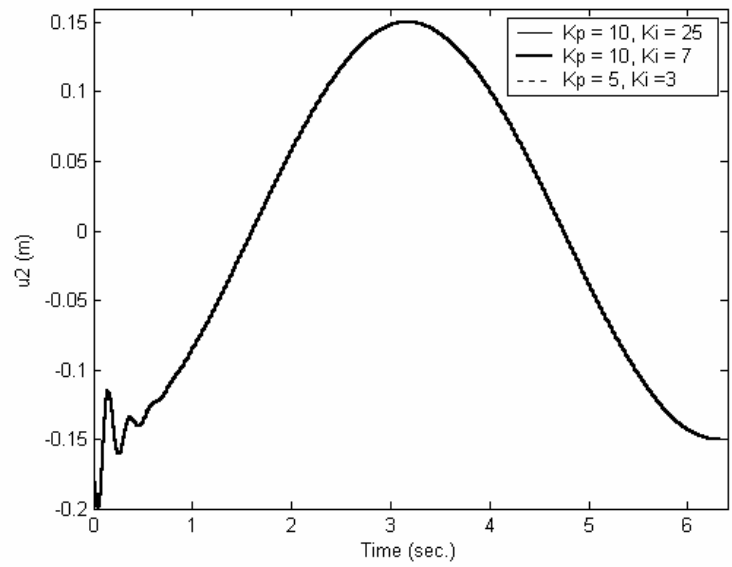


Figure 5.55 End-effector position in \bar{u}_2^0 axis following a circle path on a planar surface

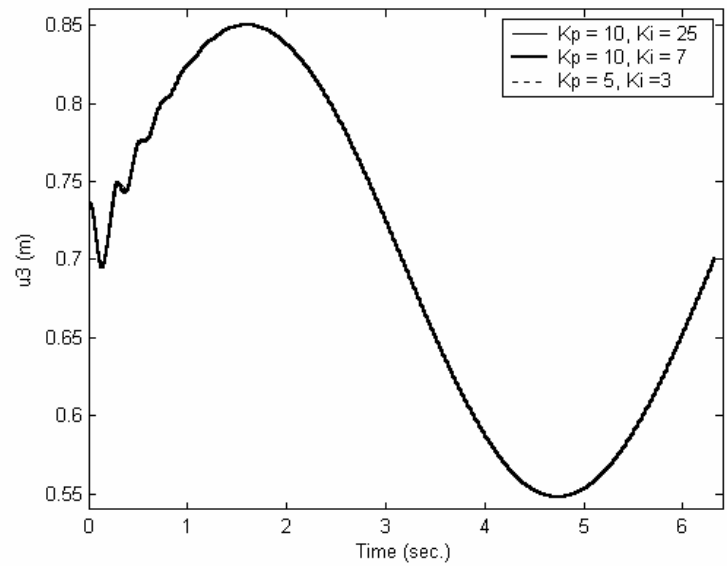


Figure 5.56 End-effector position in \bar{u}_3^0 axis following a circle path on a planar surface

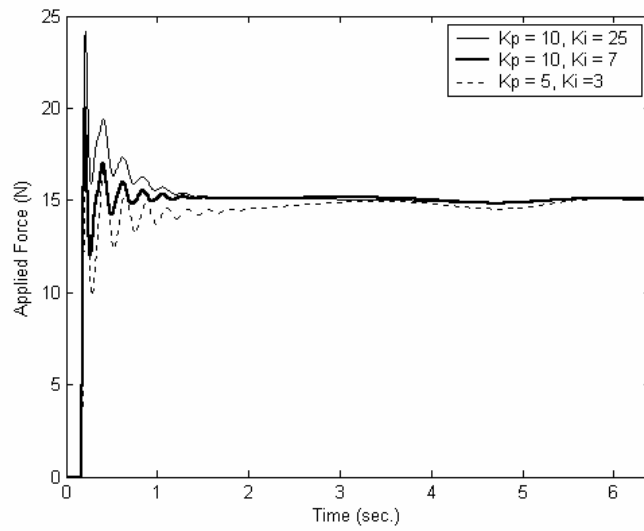


Figure 5.57 Force applied by the end-effector to the environment along \vec{u}_1^0 axis following a circle path on a planar surface

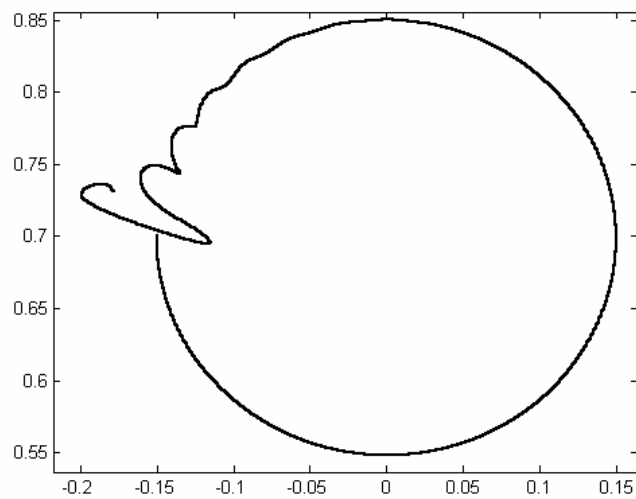


Figure 5.58 Circle path followed by the end-effector on the surface ($k_p = 10$, $k_i = 7$)

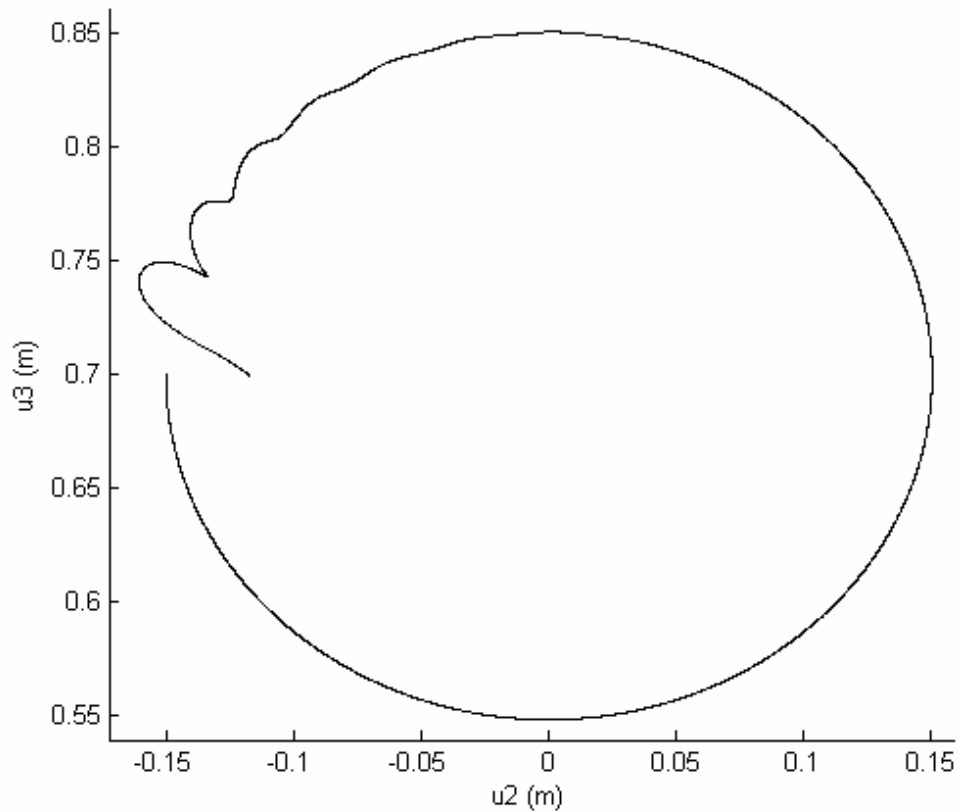


Figure 5.59 Circle drawn by the end-effector on the surface ($k_p = 10$, $k_i = 7$)

As it can be observed from the circle drawn on the surface, in Hybrid Control, it takes more time to reach the surface with the same control parameters of the Admittance Control. This is the case because, in the Admittance Control, force control is always active and as the measured force is zero before hitting the surface, it creates more torque on the joints to move into the surface before hitting it.

CHAPTER 6

DISCUSSIONS AND CONCLUSIONS

Evaluating the simulation results and investigating the control algorithms, the control algorithms considered in this thesis can be divided into two main groups as; position/force controllers and position controllers/force compensators. The first group is composed of admittance and hybrid controls where there is a desired force trajectory specified. The second group is composed of stiffness and impedance controls where there is no desired force trajectory specified, instead the control algorithms are designed to make the contact forces converge to zero.

When a task is specified so as to have the contact forces at minimum, stiffness or impedance control can be used. The biggest problem that will occur with these controls is when the contact is lost in transient state or by position control errors during the manipulation, the end-effector bounces off the contact surfaces with a higher speed than it goes into the surface. This is the case because force controller does not apply any additional damping in free motion of the manipulator. To make this bouncing off smaller, stiffness and impedance controls can be made to work for both sides. Which means force controller will apply damping whether there is contact or not. Knowing the stiffness of the sensor and the environment this could be done. The only problem that may rise is the excessive amount of force exerted on the surface when the first contact is achieved, with respect to the conventional

control's output. This kind of modified stiffness and impedance control can be a subject in future works on the topic of position/force control.

Stiffness and impedance control can be used in assembly tasks where excessive contact forces are required to be monitored and decreased. Also using very stiff sensors that can not detect the contact force that mud would achieve, automatic excavators could be controlled by impedance or stiffness controls to avoid excessive contact forces when the excavator may hit a rock.

Admittance and hybrid controls can be used for applications where a steady or varying force is required to be exerted on the working surface while following a path such as deburring, writing, polishing, carving, etc.

Taking the advantages and disadvantages of admittance and hybrid controls in the consideration, the biggest disadvantage of the hybrid control arises which is the control should be switched to a position controller when the contact is lost either because of the desired task or because of the errors in manipulation. This can cause chattering and instability. Also the control architecture of the hybrid controls is more complex than of the admittance control. Admittance control's disadvantage arises when the stiffness of the environment is close to the stiffness of the force sensor. Manipulating in such an unknown environment, where the environment stiffness is close to the force sensor stiffness, preset PID parameters of the admittance controller could fail and may cause destabilization of the contact force, which can be stabilized by applying an adaptive algorithm. As a result, hybrid controls and admittance control can be used in all tasks where desired force trajectory is required to be followed, taking the facts mentioned above into consideration.

For all the control algorithms discussed in this thesis, although all the comparisons are defined in the Cartesian Space in the control algorithm architectures found in the literature, the necessary comparisons are made in the Joint Space using inverse kinematics separately for the reference and actual Cartesian Space positions. This modification in the control architectures prevented the possible instability that may arise using the Jacobian's inverse to transform the errors calculated in Cartesian Space to the Joint Space when the error in the Cartesian Space is large. Thus, it has been possible to apply all the control algorithms more efficiently. Of course, this can be done if the manipulator (such as the one considered in this thesis) has an analytically obtainable and quickly computable inverse kinematics solution.

The robot and the environment can be modeled with more precision for future work. This includes the modeling of the motors, flexible bodies, roughness and friction of the surface. Control algorithms can be used and tested for real-time applications using a force/moment sensor on the wrist of a manipulator as a future work. Also, the control algorithms that are discussed in this thesis can be optimized for certain criteria as; minimum energy, minimum joint torques, minimum time, etc.

REFERENCES

1. G. Zeng and A. Hemami, 1997. "An Overview of Robot Force Control", Robotica, Vol. 15, pp. 473-482.
2. M. Vukobratovic and D. Stokic, 1989. "Applied Control of Manipulation Robots", Springer-Verlag, Berlin, pp. 353-358.
3. N. Hogan, March 1985. "Impedance Control: Approach to Manipulation: Part I-Theory", Journal of Dynamic Systems, Measurements, and Control, Vol. 107, pp. 1-7.
4. H. Seraji, 1994. "Adaptive Admittance Control: An Approach to Explicit Force Control in Compliant Motion", IEEE Int. Conf. On Robotics and Automation, pp. 2705-2712.
5. M. H. Raibert and J. J. Craig, 1981. "Hybrid Position/Force Control of Manipulators", ASME Journal of Dynamic Systems, Measurements, and Control, Vol. 102, pp. 126-133.

6. R. Anderson and M. W. Spong, October 1988. "Hybrid Impedance Control of Robotic Manipulators", IEEE Journal of Robotics and Automation, Vol. 4, No. 5, pp. 549-556.
7. R. Colbaugh and A. Engelmann, 1994. "Adaptive Compliant Motion of Manipulators: Theory and Experiments", IEEE Int. Conf. On Robotics and Automation, pp. 2719-2725.
8. C. J. Tsaprounis and N. A. Aspragathos, 1999. "Sliding Mode With Adaptive Estimation Force Control of Robot Manipulators Interacting With An Unknown Passive Environment", Robotica, Vol. 17, pp, 447-458.
9. N. Saadia, Y. Amirat, J. Pontnau and N. K. M'Sirdi, 2001. "Neural Hybrid Control of Manipulators, Stability Analysis", Robotica, Vol. 19, pp. 41-51.
10. Q. P. Ha, H. Q. Nguyen, D. C. Rye and H. F. Durrant-Whyte. "Robust Impedance Control of Excavator Dynamics", Australian Centre for Field Robotics, Department of Mechanical & Mechatronic Engineering, The University of Sydney.
11. R. Volpe and P. Khosla, 1993. "The Equivalence of Second Order Impedance Control and Proportional Gain Explicit Force Control: Theory and Experiments", Experimental Robotics II, pp. 3-24.

12. M. Pelletier and M. Doyon, 1994. "On the Implementation and Performance of Impedance Control on Position Controlled Robots", IEEE Int. Conf. On Robotics and Automation, pp. 1228-1233.

13. W. D. Fisher and M. S. Mutjaba, October 1991. "Hybrid Position/force Control: A Correct Formulation", Hewlett-Packard Company.

14. G. Fodor and G. Tevesz, 1999. "Hybrid Position and Force Control Algorithm Expansion of a Robot Control System", Periodica Polytechnica Ser. El. Eng., Vol. 43, No. 4, pp. 251-261.

15. İ. Başçuhadar, February 1989. "Design and Construction of a Robotic Manipulator with Six Revolute Joints", a Master's Thesis, METU, Ankara.

16. T. Balkan, M. K. Özgören, M. A. S. Arıkan and H. M. Baykurt, 2001. "A Kinematic Structure-Based Classification and Compact Kinematic Equations for Six-DOF Industrial Robotic Manipulators", Mechanism and Machine Theory, Vol. 36, pp. 817-832.

17. M. K. Özgören, 1999. "Kinematic Analysis of a Manipulator With Its Position and Velocity Related Singular Configurations", Mechanism and Machine Theory, Vol. 34, pp. 1075-1101.

18. M. K. Özgören, 2002. "Topological Analysis of 6-Joint Serial Manipulators and Their Inverse Kinematics Solutions", Mechanism and Machine Theory, Vol. 37, pp. 551-547

19. K. S. Fu, R. C. Gonzalez and C. S. G. Lee, 1987. "Robotics: Control, Sensing, Vision, and Intelligence", McGraw-Hill Book Co., Singapore.

APPENDIX A

DYNAMIC PROPERTIES OF THE LINKS

Table A.1 Dynamic properties of the Link 1

Mass	I_{xx}	I_{yy}	I_{zz}	I_{xy}	I_{yz}	I_{xz}
5.146	60933.08	29610.15	49565.34	5727.84	4985.18	1415.95

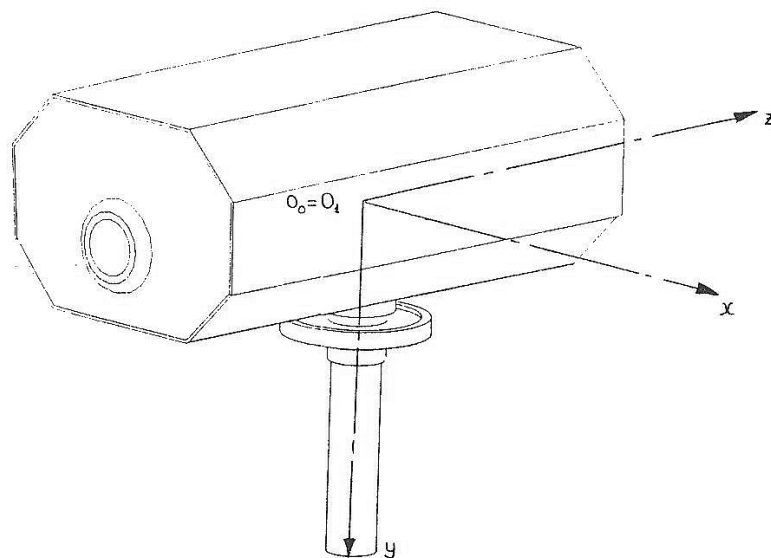


Figure A.1 3D representation of the Link 1

Table A.2 Dynamic properties of the Link 2

Mass	I_{xx}	I_{yy}	I_{zz}	I_{xy}	I_{yz}	I_{xz}
4.327	27076.77	95648.93	118618.30	-6443.52	-218.09	266.00

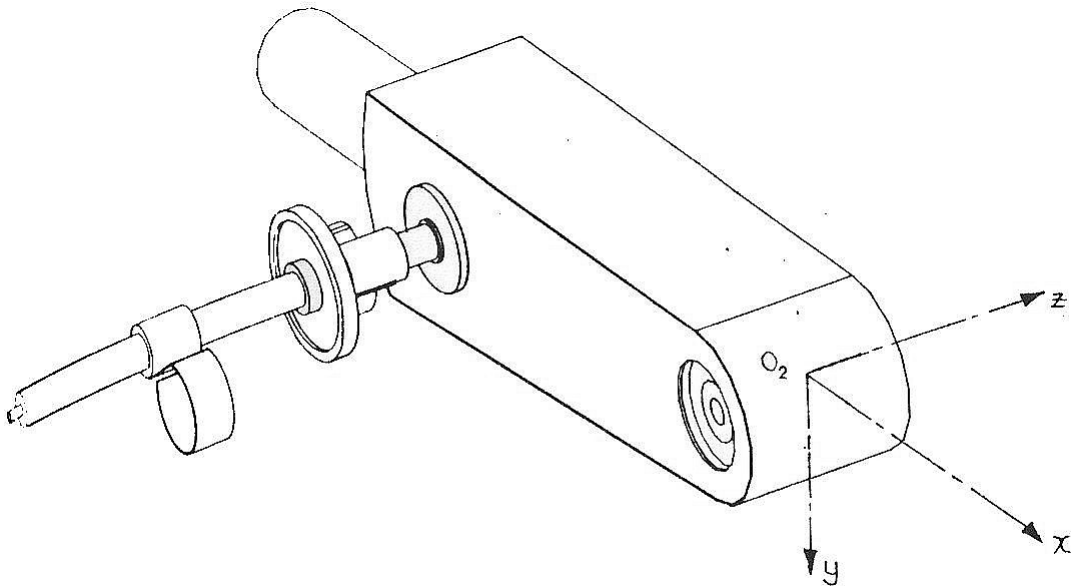


Figure A.2 3D representation of the Link 2

Table A.3 Dynamic properties of the Link 3

Mass	I_{xx}	I_{yy}	I_{zz}	I_{xy}	I_{yz}	I_{xz}
3.296	5713.91	45005.99	45668.94	170.86	93.90	685.60

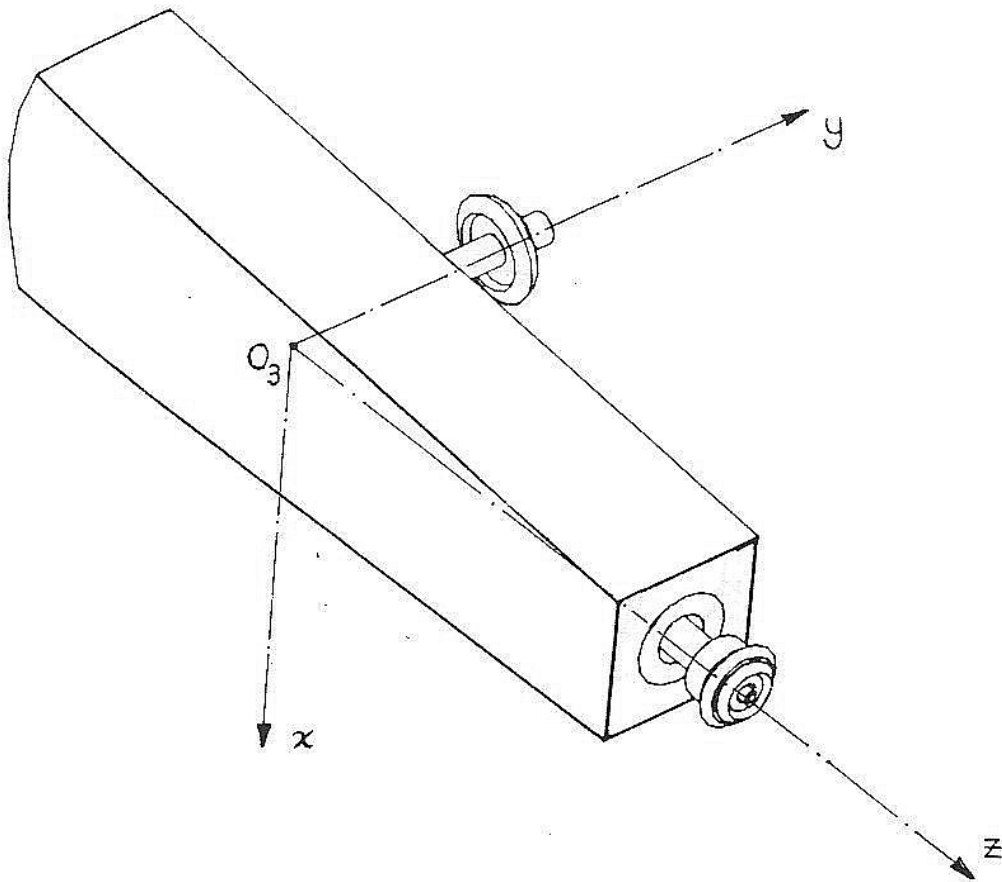


Figure A.3 3D representation of the Link 3

Table A.4 Dynamic properties of the Link 4

Mass	I_{xx}	I_{yy}	I_{zz}	I_{xy}	I_{yz}	I_{xz}
0.297	233.98	796.61	829.95	0.00	0.00	-0.02

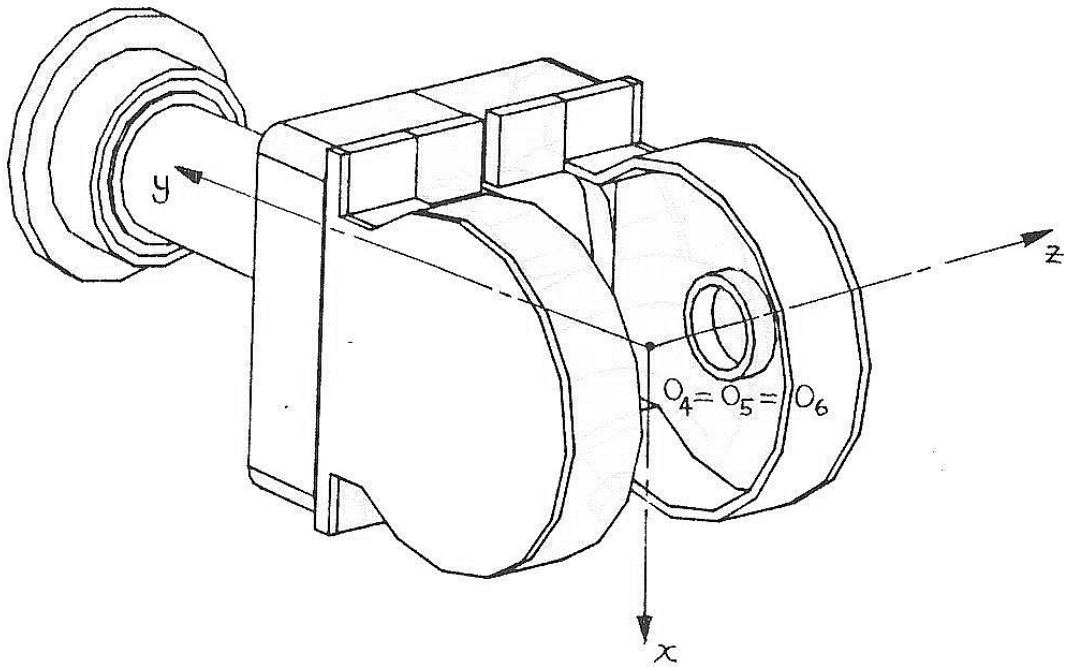


Figure A.4 3D representation of the Link 4

Table A.5 Dynamic properties of the Link 5

Mass	I_{xx}	I_{yy}	I_{zz}	I_{xy}	I_{yz}	I_{xz}
0.111	33.33	13.14	39.55	-0.45	0.00	0.00

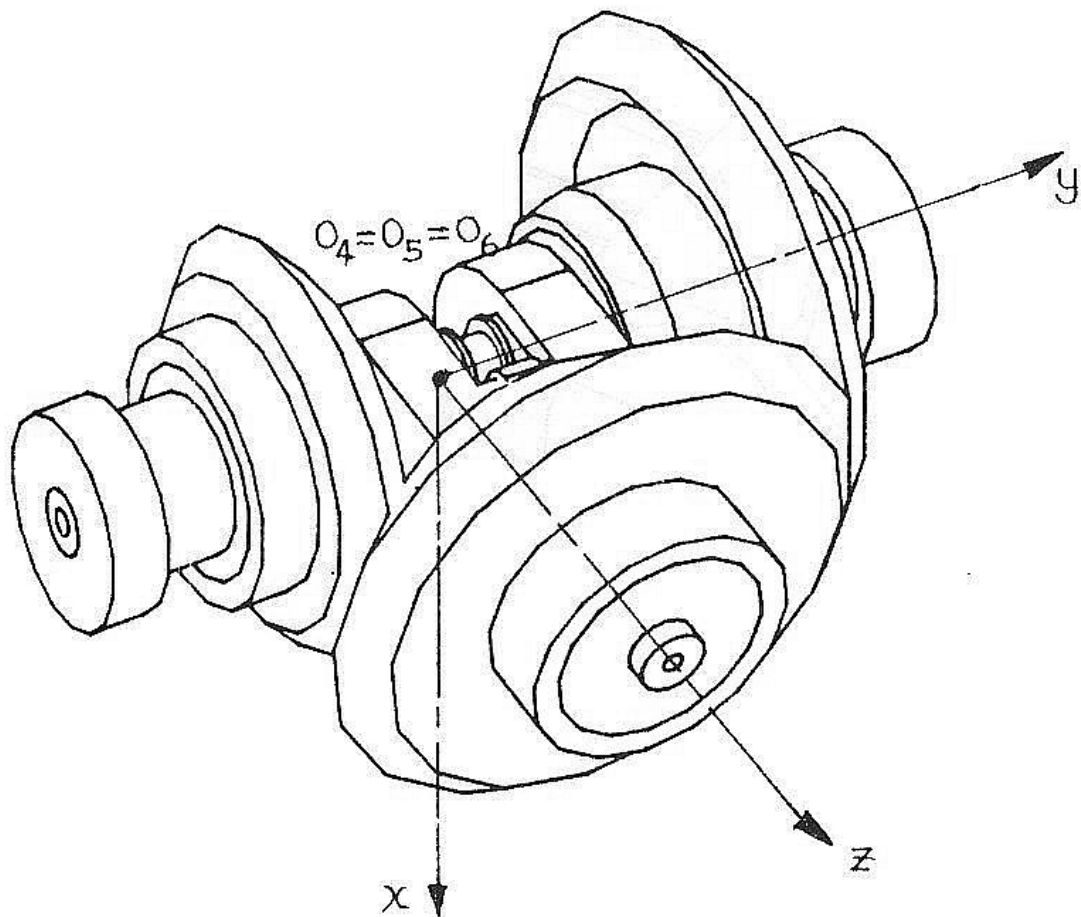


Figure A.5 3D representation of the Link 5

Table A.6 Dynamic properties of the Link 6 (Tool load of 1 kg. is included.)

Mass	I_{xx}	I_{yy}	I_{zz}	I_{xy}	I_{yz}	I_{xz}
1.086	94.51	353.39	395.34	0.00	0.00	0.06

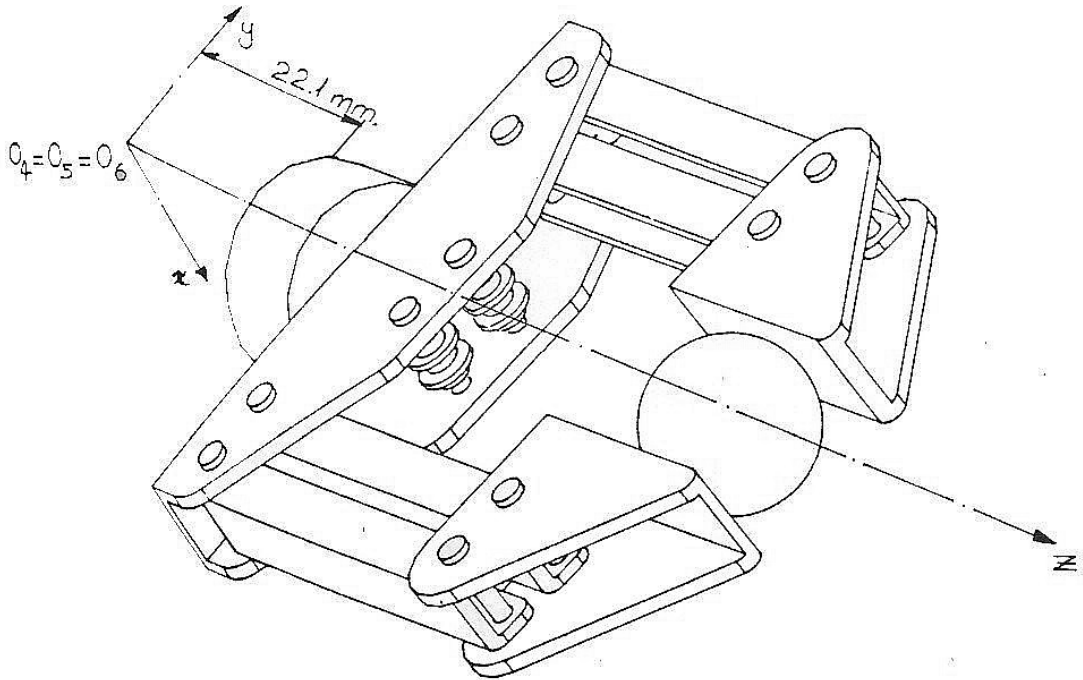


Figure A.6 3D representation of the Link 5

APPENDIX B

FEEDFORWARD COMPENSATION AND MASS MATRIX EQUATIONS

The following equations are obtained from [19]. Compensation term for gravitational effect, $c(q)$ can be formulated as,

$$c(q) = (c_1, c_2, c_3, c_4, c_5, c_6)^T \quad \text{B.1}$$

$$c_i = \sum_{j=i}^6 (-m_j g U_{ji} {}^j \bar{r}_j) \quad \text{B.2}$$

In the equation B.2, m_j is the mass of the link j , g is the gravity term, U_{ji} represents the effect of the joint j on all the other joints as shown in the equation below;

$$U_{ij} = \begin{cases} {}^0 A_{j-1} Q_j^{j-1} A_i & \text{for } j \leq i \\ 0 & \text{for } j > i \end{cases} \quad \text{B.3}$$

where A is the homogenous transformation matrix and Q is,

$$Q = \begin{bmatrix} 0 & -1 & 0 & 0 \\ 1 & 0 & 0 & 0 \\ 0 & 0 & 0 & 0 \\ 0 & 0 & 0 & 0 \end{bmatrix} \quad \text{B.4}$$

for the revolute joints of the manipulator. In the Equation B.2, ${}^j\bar{r}_j$ is the vector that represents the distance from the mass center of the link j to the coordinate frame of the joint j .

$${}^i\bar{r}_i = (x_i, y_i, z_i, 1)^T \quad \text{B.5}$$

Compensation term for the coriolis and the centrifugal forces, $h(q, \dot{q})$, is formulated as,

$$h(q, \dot{q}) = (h_1, h_2, h_3, h_4, h_5, h_6)^T \quad \text{B.6}$$

where

$$h_i = \sum_{k=1}^6 \sum_{m=1}^6 h_{ikm} \dot{q}_k \dot{q}_m \quad \text{B.7}$$

$$h_{ikm} = \sum_{j=\max(i,k,m)}^6 \text{Tr}(U_{jkm} J_j U_{ji}^T) \quad \text{B.8}$$

In the Equation B.7, \dot{q} is the angular velocities of the joints. U_{jkm} in the Equation B.8 is the interaction effects between the joints and formulated as,

$$U_{ijk} = \begin{cases} {}^0 A_{j-1} Q_j^{j-1} A_{k-1} Q_k^{k-1} A_i & i \geq k \geq j \\ {}^0 A_{k-1} Q_k^{k-1} A_{j-1} Q_j^{j-1} A_i & i \geq j \geq k \\ 0 & i < j \text{ or } i < k \end{cases} \quad \text{B.9}$$

J_j is the link inertia matrix and formulated as below,

$$J_i = \begin{bmatrix} \frac{-I_{xx} + I_{yy} + I_{zz}}{2} & I_{xy} & I_{xz} & m_i x_i \\ I_{xy} & \frac{I_{xx} - I_{yy} + I_{zz}}{2} & I_{yz} & m_i y_i \\ I_{xz} & I_{yz} & \frac{I_{xx} + I_{yy} - I_{zz}}{2} & m_i z_i \\ m_i x_i & m_i y_i & m_i z_i & m_i \end{bmatrix} \quad \text{B.10}$$

$I_{xx}, I_{yy}, I_{zz}, I_{xz}, I_{yz}, I_{xy}$ are the elements of the moments of inertia tensor about the center of mass.

Mass matrix is formulized as below,

$$M_{ik} = \sum_{j=\max(i,k)}^6 \text{Tr}(U_{jk} J_j U_{ji}^T) \quad \text{B.11}$$